Effects of Surface Conditions on Endwall Film-Cooling

Narayan Sundaram

Dissertation submitted to the Faculty of
Virginia Polytechnic Institute and State University
in partial fulfillment of the requirements for the degree of

Doctor of Philosophy
in
Mechanical Engineering

Dr. Karen A. Thole, Advisor and Chair
Dr. Wing Fai Ng
Dr. Walter F. O'Brien
Dr. Joseph Schetz
Dr. Uri Vandsburger

April 18, 2007
Blacksburg, Virginia

Keywords: Gas Turbine, Film-Cooling, Endwall, Trench

Effects of Surface Conditions on Endwall Film-Cooling

Narayan Sundaram

(Abstract)

A higher demand in power output from modern land based gas turbines has resulted in an increase in combustor exit temperatures. High temperatures in turn have resulted in flatter profiles at the combustor exit warranting the need for sufficient cooling of the endwall region. Endwall cooling is affected by the coolant flow through certain design features. A typical endwall design includes a leakage slot at the interface between the combustor and the vane, a leakage slot at the vane-to-vane interface and film-cooling holes. In addition, with the increase in energy demands and depletion of natural gas resources, alternate fuels such as coal derived synthetic gas are being used in gas turbines. Coal derived fuels, however, contain traces of ash and other contaminants that deposit on endwall surfaces, thereby altering its surface conditions.

The purpose of this study was to investigate the effects of realistic endwall features and surface conditions on leading edge endwall cooling. Endwall designs like placing film-cooling holes in a trench, which provide an effective means of improving cooling were also studied at the leading edge. An infrared camera was used to obtain measurements of adiabatic effectiveness levels and a laser Doppler velocimeter was used for flowfield measurements.

This study was done on a large scale, low-speed, recirculating wind tunnel operating at a Reynolds number of 2.1×10^5 and an inlet mainstream turbulence level of 1%. Endwall measurements were taken for coolant flow through varying slot width at the combustor-vane interface. A constant coolant mass flow and a narrower combustor-turbine interface slot caused the coolant to exit uniformly whereas increasing the slot width had an opposite effect. Measurements were also taken with hole blockage and spallation, which showed a 10-25% decrease in the effectiveness levels whereas near hole deposition showed a 20% increase in effectiveness levels.

A comparison of the cooling effectiveness due to placement of film-cooling holes in a trench was made to film-cooling holes not placed in a trench. Measurements indicated a superior performance of trenched holes to holes without a trench. Trenched holes showed a 60% increase in effectiveness levels due to decreased coolant jet separation.

Preface

This dissertation is composed of five papers, which were written to understand the effects of realistic design features and surface conditions on vane endwall cooling. These papers focused on measuring the adiabatic effectiveness levels and the flowfield on a stator vane endwall. In this research, a number of areas lacking in the literature were addressed especially with regard to the vane leading edge-endwall junction. High resolution adiabatic effectiveness measurements were made on an endwall to include the effects of: leakage flow through the slot at the interface between the combustor and vane and through the slot between the vane-to-vane interface, film-cooling hole blockage, near hole deposition and spallation of thermal barrier coating (TBC), and placing film-cooling holes in a two-dimensional transverse slot (trench). In addition, flowfield was documented at the leading edge to include the effects of combustor-turbine interface slot, film-cooling jets and placing film-cooling holes in a trench.

In the first paper, the effects of leakage flows through the interface slots in a stator vane were evaluated. The effects of varying the width of the combustor-vane interface slot were also studied. Results indicated that the endwall effectiveness levels increased with a narrower interface slot. The second paper focused on understanding the effects of realistic surface conditions like; surface deposition, film-cooling hole blockage and TBC spallation on endwall adiabatic effectiveness levels. Partial cooling hole blockage and spallation caused a reduction in adiabatic effectiveness levels, whereas near hole deposition improved the effectiveness levels at smaller deposit heights. The third paper, documents the effect of surface deposits on endwall adiabatic effectiveness levels along the pressure side film-cooling holes. Depositions along the pressure side lowered the effectiveness levels by deflecting the coolant jets towards the vane-endwall junction. The fourth paper focuses on modifying the cooling hole exits and its effects on the leading edge endwall effectiveness levels. In this paper, the adiabatic effectiveness levels were measured at the leading edge by placing film-cooling holes in a trench and in between semi-elliptical bumps. Cooling holes in trenches and in between bumps provided better cooling relative to the case with just the film-cooling holes. The fifth and final paper documents the flowfield at the leading edge-endwall junction for a stator vane and

compares the effects of trenched holes relative to no trench. Most studies in literature have documented the presence of a horseshoe vortex at the leading edge but this is the only study to have documented the flowfield with a slot at the combustor-turbine interface and film-cooling jets. Trenched holes showed decreased coolant jet separation relative to the no trench case.

A summary of significant results from this research and recommendations for future work are included at the end of this dissertation.

Granting Institution

The research supported by the US Department of Energy, Office of Fossil energy, National Energy Laboratory. Any opinions, findings, conclusions or recommendations expressed herein are those of the author and do not necessarily reflect the views of the DOE.

To Dad, Mom, Uncle Krish, Aunt Leela, and Gautham.

Acknowledgments

I would like to thank the almighty for everything I have achieved so far and will achieve in the future. Next on the list will be my advisor, my guru for life, Dr. Karen Thole. You have always been and will be a great source of inspiration for me. I cannot find words to thank you for keeping me motivated over the past three years while I struggled with my research and telling me to believe in myself. I owe all my past successes (well actually only 90%, I will take the remaining 10%) and my future successes to you. I thank my lucky stars that I got to work with an advisor who cares so much about her students and supports them for anything and everything. You are the BEST and I am glad that I got drunk on May 8, 2003! I would also like to thank Dean Karen DePauw for her encouragement and giving me an opportunity to work alongside her. You are the best thing to have happened to the Grad School at Virginia Tech and it was truly a pleasure being part of GSA executive board with you as the graduate advisor.

I would also like to thank my committee members, Dr. Ng, Dr. O'Brien, Dr. Schetz, and Dr. Vandsburger for your suggestions and comments during my prelim that helped me submit a final work of high quality. The staff in the Mechanical Engineering department, especially, Jamie, Ben, Lynn, Lisa, Peggy, Kathy, Cathy, and Mellissa for helping me with all the mundane problems I faced. My lab members and friends over the last three years: Jeff Prausa, Paul Sanders, Erin Elder, Angela Morris, Scott Walsh, Will Colban, Mike Lawson, Seth Lawson, Alan Thrift, Cam Land, Steve Lynch, Eric Lyall, Joe Scrittore, Scott B, Nick Cardwell, Mike Barringer, Markus Schwaenen, Andrew Duggleby, Daniel Knost, and the other VTExCCLers I have known in the last five years of my stay in Blacksburg, it was a pleasure working with you all. My roommates; Will Colban, Kevin Pline, Nick & Wes Cardwell, and Joe Scrittore for being my family in Blacksburg. Also my good friends who weren't part of VTExCCL, Sarah Manoogian, Kate & Jared Kavlock, Courtney Haynes, Katie Bieryla, Andrew Kemper, Eric Kennedy, and Doug Gaubauer. You all have been a great source of strength and support. I don't think without you all I could have ever recovered in a such a short time after my accident. I love you all. A special thanks to my very good friend Will Colban who never let me get bogged down with my research and for being a true friend. You are one amazing person

Will! Also, my friends from undergrad, Gautham, Sharath, Rajeev K P, Narendra and Bops who have always been proud of me and stood behind me in my difficult times. I would also like to thank everyone at the Roanoke Memorial Hospital for taking great care of me and helping me recover in such a short period.

My cousin Chitra, her husband Raja and their kids Nikita and Natasha; you have always brought a smile on my face and for being there when I needed you the most. My uncle Krish and Aunt Leela for being my parents away from home and taking care of me and pampering me with all the luxuries, which I never dreamt off. My cousins Vik and Aasha who I have become really close with in a very short time and you guys are as great as your parents. Also my cousin Janu for treating me like her own little younger brother, her husband Sridhar for the pep talks when I stayed at their place in the summer of 99 and my favorite Athreya for being the cute little KK. Last but not the least, my Dad who I have missed every minute in the last nine years. I am sure that had he been there this day, it would have been the happiest day of his life. My Mom for encouraging me to go and pursue my goals and dreams and not letting me worry about anything. My big brother Gautham, who has played a dual role of being my father and brother and never letting me feel that my Dad wasn't around. I love you all and I could have never asked for a more caring and loving family.

Table of Contents

List of Tables

List of Figures

Paper 1: The Effects of Varying the Combustor-Turbine Gap

Paper 2: Effects of Surface Deposition, Hole Blockage, and TBC Spallation on Vane Endwall Film-Cooling

Paper 3: Effects of Deposits on Film-Cooling of a Vane Endwall Along the Pressure Side

Paper 1:
THE EFFECTS OF VARYING THE COMBUSTOR-TURBINE GAP

Accepted for publication in the *ASME Journal of Turbomachinery* *

Abstract

To protect hot turbine components, cooler air is bled from the high pressure section of the compressor and routed around the combustor where it is then injected through the turbine surfaces. Some of this high pressure air also leaks through the mating gaps formed between assembled turbine components where these components experience expansions and contractions as the turbine goes through operational cycles.

This study presents endwall adiabatic effectiveness levels measured using a scaled up, two-passage turbine vane cascade. The focus of this study is evaluating the effects of thermal expansion and contraction for the combustor-turbine interface. Increasing the mass flow rate for the slot leakage between the combustor and turbine showed increased local adiabatic effectiveness levels while increasing the momentum flux ratio for the slot leakage dictated the coverage area for the cooling. With the mass flow held constant, decreasing the combustor-turbine interface width caused an increase in uniformity of coolant exiting the slot, particularly across the pressure side endwall surface. Increasing the width of the interface had the opposite effect thereby reducing coolant coverage on the endwall surface.

* Co-author: Nicholas D. Cardwell and Dr. Karen A. Thole, Mechanical Engineering Department, Virginia Tech

Introduction

Core flow temperatures within the hot section of a gas turbine commonly exceed the metal melting temperature. Cooling techniques are needed to protect turbine components from the harsh environment. To accomplish this cooling, high pressure air is bled from the compressor, bypassed around the combustor, and then routed into the turbine where it is used for internal and external cooling purposes.

Since the entire turbine is not manufactured as a single component, there exist numerous gaps between mating parts allowing leakage of high pressure coolant. Thermal expansion and mechanical stresses within the turbine make it especially difficult to seal these interfaces. One such interface is the slot between the combustor and the first stage of the turbine since the combustor and turbine are not rigidly connected. The gap between adjacent vane sections is another area that allows leakage of high pressure coolant. Leakages result in a significant loss in overall efficiency.

Turbine components are typically cast with high nickel super alloys because of their high strength at elevated temperatures. While the exact materials are proprietary, these alloys are similar in composition to Inconel 625. The average coefficient of thermal expansion for Inconel 625 is equal to 0.138 mm per cm of unrestrained metal over the standard to operating temperature range of 1075°C [1]. If one considers an unrestrained 30 cm combustor, it would result in an expansion of 4 mm. This 4 mm is on the order of the change in slot width we are modeling for this paper.

The work presented in this paper evaluates the effects of expansion and contraction of the combustor-turbine interface on endwall cooling performance. Also compared in this paper is the effect of leakage flowrates from a mid-passage gap between two mating vanes on the overall endwall cooling performance.

Relevant Past Studies

Significant work has been performed documenting the effects of leakage from the slot at the combustor-turbine interface. There have also been studies in the literature analyzing the combined effects of a combustor-turbine slot leakage and film-cooling. Very few studies exist on either the effect of a realistic mid-passage gap or the effect of changes in the combustor-turbine slot width on endwall cooling effectiveness for an

actual airfoil passage.

The majority of studies concerned with leakage flow have focused on a slot upstream of the first stage vane meant to simulate the leakage flow that occurs between the combustor and the turbine. One of the earliest works was presented by Blair [2]. Blair's study included a two-dimensional slot upstream of the vane. An enhanced cooling benefit was observed for increases in leakage flow. In a similar study, Burd et al. [3] studied the effects of coolant leaking from an upstream slot. As with Blair, Burd et al. reported better endwall cooling for leakage flows as high as 6% of the total passage flow. Colban et al. [4, 5] studied the effects of changing the combustor liner film-cooling and upstream slot leakage flows on endwall effectiveness levels for a first vane cascade. Their results, like others, showed that the upstream slot flow does not evenly distribute along the endwall, with the majority of the cooling benefit along the suction side of the vane. Pasinato et. al [6] studied the effects of injecting air upstream of the vane stagnation through a series of discrete slots. These slots were oriented in the slot in such a manner that the coolant was injected tangentially to the leading edge of their contoured endwall. Pasinato et. al [6] found that this secondary air injection strongly distorted the flowfield upstream of the vane stagnation.

Some studies have combined the effects of upstream slot leakage with endwall film-cooling. The main studies performed are those of Zhang and Jaiswal [7], Kost and Nicklas [8], Nicklas [9], and Knost and Thole [10, 11]. Kost and Nicklas [8] and Nicklas [9] reported that coolant ejection from an upstream slot causes radical changes in the near wall flowfield signifying an intensification of the horseshoe vortex, which was observable in their flow angle diagrams. This increase in intensity resulted in the slot coolant being moved off the endwall surface and heat transfer coefficients that were over three times that measured for no slot flow injection. Endwall studies by Knost and Thole [10, 11] investigated endwall effectiveness levels for a vane passage with both film-cooling and upstream slot injection. For increasing slot mass flow, Knost and Thole reported higher local effectiveness levels with the same coolant coverage area on the endwall

Several studies have documented the effect of flow from a gap between two adjacent airfoils. Aunapu et al. [12] showed that blowing through a passage gap could be

used to reduce the negative effects of the passage vortex, but with significant aerodynamic losses. Another study done by Ranson and Thole [13] used a mid-passage gap between two blades for their experimental and computational studies. Their results showed that the flow through the gap was initially directed toward the blade pressure side, due to the incoming velocity vectors, and then convected towards the suction side of the adjacent airfoil. Yamao et al. [14] reported changes in film-cooling effectiveness levels due to leakage air injected from both an upstream slot and mid-passage gap. Their study indicated that film-cooling effectiveness was enhanced with an increase in sealing flow through both leakage interfaces.

Piggush and Simon [15, 16] analyzed the effect of leakage flows on aerodynamic losses for a vane cascade. It was concluded that the mid-passage gap blowing caused both an increase in passage losses and the creation of a second smaller passage vortex which was located below the primary passage vortex. Piggush and Simon [15, 16] also concluded that the majority of mid-passage gap blowing became entrained in the formation of a second vortex within the passage. Reid et al. [17] studied the effect of interplatform leakage on overall efficiency for an axial flow turbine stage. They determined that the largest drop in efficiency associated with interplatform leakage was 1.5% when compared to the stage efficiency with no slot present. The main difference in interplatform gap geometry between these two studies is that Reid et al. [17] modeled the internal seal strip of the interplatform gap and Piggush and Simon [15, 16] did not.

Cardwell et al. [18] analyzed the effect of a mid-passage gap with a seal strip and platform misalignment on endwall cooling effectiveness. They determined that misalignment between adjacent vanes and between the combustor-turbine interface can significantly affect upstream slot coolant trajectory and effectiveness. Cardwell et al. [18] reported that a backward facing step (cascade configuration) between the combustor-turbine interface greatly reduced the need for suction side endwall film-cooling due to an increased utilization of upstream slot leakage.

The effect of a step in hub diameter just ahead of a blade row on aerodynamic blade performance was evaluated by de la Rosa Blanco et al. [19]. They also determined that a backward facing step at this location can lead to a reduction in endwall and mixing losses when compared to a flat endwall while a forward facing step produces higher

losses than a flat endwall. Piggush and Simon [15,16] also agreed with the pressure loss results of de la Rosa Blanco et al. [19] for a turbine vane indicating increased losses with a forward and decreased losses with a backward facing step upstream of the vane stagnation.

To date there has been significant research on the effect of upstream slot flow on the passage fluid dynamics and endwall heat transfer, but no study on the effects of varied upstream slot widths. This study improves upon previous works by studying the realistic effect of combustor-turbine slot expansion and contraction on endwall adiabatic effectiveness levels given a vane passage with other realistic features such as a mid-passage gap and film-cooling.

Vane and Endwall Geometry

The flat endwall used in the linear cascade has three cooling features: a combustor-turbine slot, a mid-passage vane-to-vane gap with accompanying seal strip, and discrete film cooling holes. The same film cooling pattern as shown in Figure 1.1, which was originally designed and tested by Knost and Thole [10, 11], was used in this study. Figure 1.1 shows the film cooling hole injection angles, the upstream slot, and the mid-passage gap discussed above. All film cooling holes were cylindrical and inclined at an angle of 30° with respect to the endwall surface. Table 1.1 provides a brief description of the turbine vane geometry and operating conditions. Significant studies were performed on this particular vane geometry with a more detailed description given in

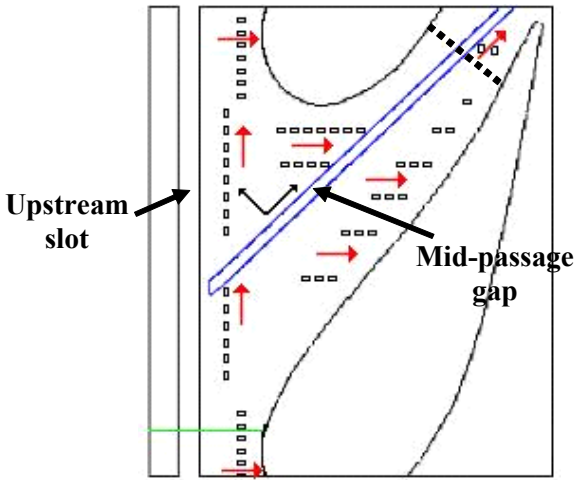

Figure1.1. Endwall geometry with film-cooling holes, an upstream slot, and a mid-passage gap.

Table 1.1. Geometric and Flow Conditions

Scaling factor	9
Scaled up chord length (C)	59.4 cm
Scaled up axial chord length (C_a)	29.3 cm
Pitch/Chord (P/C)	0.77
Span/Chord	0.93
Re_{in}	2.1×10^5
Inlet and exit angles	0° & 72°
Inlet, exit Mach number	0.017, 0.085
Inlet mainstream velocity	6.3 m/s

Table 1.2. Summary of Endwall Geometry

	Parameter	Experimental
Upstream Slot	Nominal slot width	0.024 C
	Double slot flow length to width	0.94
	Nominal slot flow length to width	1.9
	Half slot flow length to width	3.8
	Upstream slot surface angle	45°
Film Cooling	FC hole diameter (cm)	0.46
	FC Hole L/D	8.3
	Film-cooling surface angle	30°

Radomsky and Thole [20].

Figure 1.1 also shows a two-dimensional slot upstream of the vane leading edge, which represents the mating interface of the turbine and combustor. This slot had an injection angle of 45° and was located 30% of the axial chord upstream of the vane stagnation location. This leakage interface will be referred to as the upstream slot. Table 1.2 provides a summary of parameters relevant to the film-cooling holes and upstream slot geometries.

As discussed in the introduction, the primary focus of this work was to analyze the endwall cooling effect of upstream slot expansion and contraction. For this study the metering slot width was expanded by 50% and contracted by 50%, which will be referred to as double width and half width, respectively. As with the nominal slot, both the double width and half width slots had a 45° surface injection angle. For these studies, the upstream slot was expanded and contracted while keeping the slot centerline fixed

relative to the vane stagnation.

The gap between adjacent vane sections will be referred to as the mid-passage gap. A cross-section of the mid-passage gap is shown in Figure 1.2. Unlike the upstream slot, the mid-passage gap had a recessed seal strip as found in many engine designs, which influenced its interaction with the coolant and mainstream flow. To allow flow control, the mid-passage gap had a separate supply plenum which did not open into the upstream slot. The cross section of the mid-passage gap is also shown in Figure 1.2. This gap, which was described in the previous study be Cardwell et al. [18], had a 90° surface injection angle, a width of 0.635 cm, and a gap flow length to width ratio of 5. For this study, the mid-passage gap width was not varied.

Similar to the previous study reported by Cardwell et al. [18], the endwall surface was covered with a uniform roughness. To simulate a random array of a uniform roughness level, wide-belt industrial sandpaper was used to cover the entire endwall. The sandpaper had a closed coat 36 grit surface and a grade Y cloth backing. A closed coat surface had roughness elements arranged in a random array over 100% of its surface. The 36 grit sandpaper had an average particle size of 538 microns [21] which was roughly twice that observed by Bons et. al. [22] for in service turbine endwalls. A custom construction technique was used to guarantee a uniform and uniform fit around each film-cooling hole. This technique ensured a uniform interaction between the rough surface and coolant jets for the entire endwall.

Experimental Methodology

The experimental facility used for this study consisted of a linear cascade test section placed in a closed loop wind tunnel, as shown in Figure 1.3. Flow within the wind tunnel was driven by a 50 hp axial vane fan, which was controlled by a variable frequency inverter. After being accelerated by the fan, the flow turned 90° and then passed through a primary finned-tube heat exchanger. This heat exchanger was used to precool the bulk flow. After passing through the primary heat exchanger, the flow encountered another 90° turn before entering a three way split. This split simulated the primary core flow through the combustor and the bypass flow around the combustor. The flow split was achieved by using a porous plate with a 25% open area to act as a valve

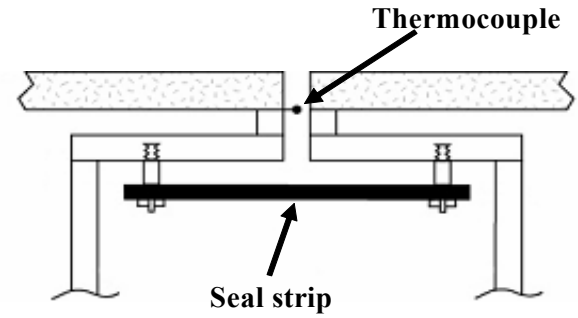

Figure 1.2. Cross section view of the mid-passage gap geometry with accompanying seal strip.

thereby directing a portion of the flow into the upper channel. The primary core flow passed through a resistance heater bank where its temperature was increased to 60°C. The secondary flow in the top channel passed through a secondary finned-tube heat exchanger where the flow temperature was lowered to 10°C. The mainstream flow continued through the middle channel into the test section. The cooler bypass flow was pulled into a 2 HP blower where it then flowed into the test section for the coolant supplies.

The test section consisted of a vane cascade comprised of two full passages with one center vane and two half vanes, an endwall with film cooling holes, an upstream slot, and mid-passage gap geometries, which were scaled up by a factor of nine. A detailed account of its construction has been previously described by Cardwell et al. [18]. The two main differences between the current test section and the one described by Cardwell et al. [18] were a change in the upstream approach flow and the ability to vary the

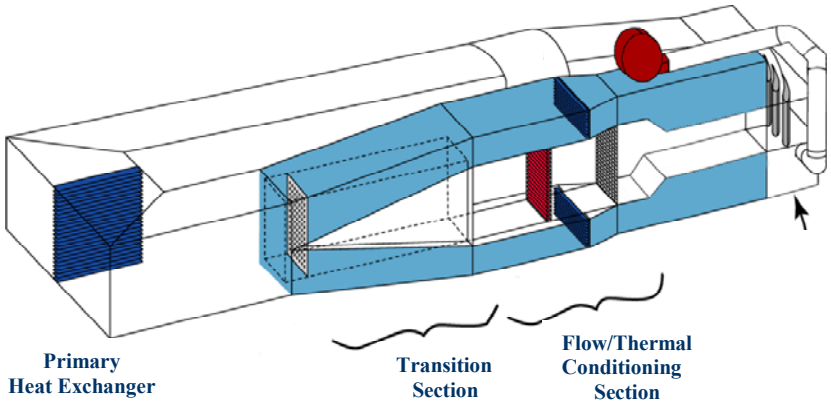

Figure 1.3. Illustration of the wind tunnel facility.

upstream slot metering width. The previous upstream approach flow had a 15.6° contraction directly upstream of the test section while the upstream flow path used in this study had a 45° contraction that was 2.9 chords upstream of the vane giving a longer constant flow area into the test section. The upstream slot was interchangeable so that the flow metering width could be adjusted. The endwall, which was the main focus of the study, was constructed of low thermal conductivity foam (0.033 W/m.K). The endwall foam was 1.9 cm thick and was mounted on a 1.2 cm thick Lexan plate. The cooling hole pattern was cut using a five-axis water jet machine to ensure proper hole placement and tight dimensional tolerances. The upstream slot, which needed to be stiffer, was constructed of hard wood which also has a low thermal conductivity value (0.16 W/m.K).

Adiabatic endwall temperatures were taken for the different slot geometries and flowrates and also for different gap flowrates. Each coolant path had its own separate plenum for independent control of the flow through the film-cooling holes, upstream slot, and mid-passage gap as shown in Figure 1.4. For the studies reported in this paper, film cooling was not varied so a nominal value was set for all cases. The mid-passage gap was maintained even when no coolant was supplied to its plenum. Experiments were conducted for both a sealed and leaking mid-passage gap. Sealing of the mid-passage gap plenum was accomplished by closing the appropriate coolant feed pipe.

The inlet turbulence was measured to be 1.3%. The turbulent inlet boundary layer thickness was measured as 22% of span at a location 15 slot widths upstream of the

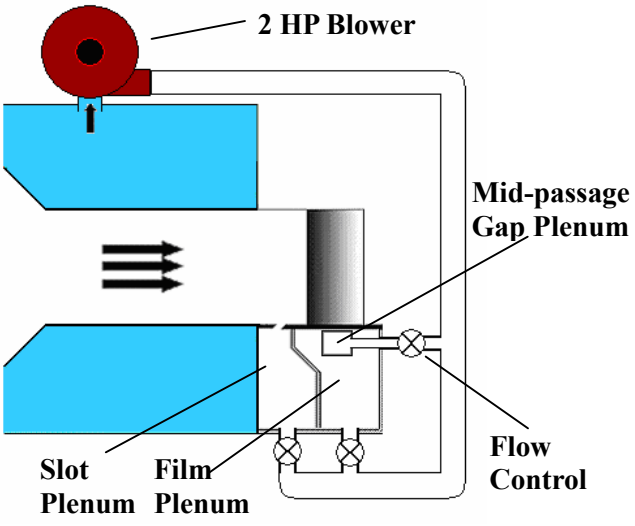

Figure 1.4. Separate plenums for film-cooling, upstream slot, and mid-passage gap provided independent flow control.

center vane stagnation location. During steady state operation, a temperature difference of 40 °C was maintained between the mainstream and the coolant. From a room temperature start, the typical time to achieve steady state conditions was 3 hours.

Coolant Flow Settings

As stated earlier, all three coolant plenums were sealed with respect to each other and had independent flow control. CFD studies reported by Knost and Thole [10] were used to set the coolant massflows through the film-cooling holes through the use of a predicted discharge coefficient. The method previously described by Knost and Thole and Cardwell et al. [18] was used whereby a global discharge coefficient was found through CFD analysis. Only one film-cooling flowrate was used for these studies, which was 0.5% of the core flow.

A discharge coefficient of 0.6 was chosen for the upstream slot. This is a typically assumed value for a flow through a sharp-edged orifice. No assumed discharge coefficient was needed for the mid-passage gap as the coolant flow rate was measured directly using a laminar flow element placed downstream of the coolant control valve. Feeding this plenum differently was necessary due to the high amounts of ingestion seen in the mid-passage gap, which will be explained later in the paper.

Instrumentation and Measurement Methods

Spatially-resolved adiabatic endwall temperature contours were recorded using an FLIR P20 infrared camera. The test section had multiple viewing ports on the top end wall through which measurements were taken until the entire endwall surface was mapped. At each viewing location the camera was placed perpendicular to the endwall surface at a distance of 55 cm. Given the camera's viewing angle, each picture covered an area of 24 cm by 18 cm, with the resolution being 320 by 240 pixels. The camera's spatial integration was 0.16 hole diameters (0.71 mm). Post calibration of the images was accomplished using actual temperature values taken by thermocouples placed on the endwall surface. The surface emissivity was assumed to be 0.92, which is a commonly reported value for the material type and surface structure associated with coarse grit sandpaper [23]. During post calibration, the image background temperature was adjusted

until the thermocouple data and infrared image data were within 0.01 °C. Typical values of background temperature were 55 °C (note the freestream temperature was typically 60 °C). Six images were taken at each viewing location, of which five were used to obtain an average image using an in-house Matlab program. The same program then scales, rotates, and assembles the averaged images at all locations. This fully assembled contour gives a complete temperature distribution for the endwall surface.

Freestream temperature values were measured at 25%, 50%, and 75% of the vane span at four locations across the passage pitch. Maximum variations along the pitch and span were less than 0.5 °C and 1.0 °C, respectively. Three thermocouples were attached in the upstream slot plenum and two thermocouples were attached in the film cooling plenum to measure the respective coolant temperatures. Differences in temperature between the plenums were typically less than 1 °C. Eleven thermocouples were placed within the mid-passage gap to measure the air temperature profile. These thermocouples were located six seal strip thicknesses beneath the endwall surface (see Figure 1.2). A 32 channel data acquisition module by National Instruments was used with a 12-bit digitizing card to measure and record the thermocouple voltage data. All temperature data was recorded and compiled after the system had reached steady state.

A one-dimensional conduction correction as described by Ethridge et. al. [24] was applied to all adiabatic effectiveness measurements. This correction involved measuring the endwall surface effectiveness with no coolant flow. This was accomplished by blocking off the film-cooling holes within the passage. The resulting η correction was 0.16 at the entrance for a η value of 0.9 and 0.02 at the exit region at a measured η value of 0.5.

An uncertainty analysis was performed on the measurements of adiabatic effectiveness using the partial derivative method described at length by Moffat [25]. The precision uncertainty was determined by taking the standard deviation of six measurement sets of IR camera images with each set consisting of five images. The precision uncertainty of the IR camera measurements was ±0.0143°C and the bias uncertainty was ±1.02°C, based on the calibration of the image. The precision uncertainty and bias uncertainty of the thermocouples was ±0.1°C and ±0.5°C, respectively. The total uncertainty was then calculated as ±1.02°C for the IR images and

±0.51°C for the thermocouples. Uncertainty in effectiveness, η, was found based on the partial derivative of η with respect to each temperature in its definition and the total uncertainty in the measurements. Uncertainties of $\partial\eta = \pm 0.028$ at $\eta = 0.1$ and $\partial\eta = \pm 0.028$ at $\eta = 0.8$ were calculated.

Discussion of Results

A number of tests were conducted for this study with the most representative results being given in this paper, as described in the next section on the test matrix. First, the effect of varying upstream slot width will be discussed for constant mass flow rate and a constant momentum flux ratio. Second, the effect of a fixed slot width for varying upstream slot mass flow rate will be discussed. Last, a mid-passage gap comparison with and without flow width will be discussed.

Derivation of Test Matrix

Significant consideration was given to the creation of a test matrix (shown in Table 1.3), which would be of particular use to the turbine designer. Mass flowrates are reported on a percent basis with respect to the total mass flowrate through the passage. For all cases, the film-cooling mass flow was set at 0.5% and, unless specified, the mid-passage gap was at 0%.

The first comparison done was for a 0.85% matched mass flow for expanding and contracting the slot width by 50%. The mass flow was kept constant by increasing or decreasing the plenum pressure accordingly, which resulted in a matched mass flow but

Table 1.3. Upstream Slot Coolant Settings

	% mass flow	M	I
Double Width Slot	0.85	0.22	0.04
	1.13	0.29	0.08
Nominal Slot Width	0.75	0.29	0.08
	0.85	0.33	0.10
Half Width Slot	0.38	0.29	0.08
	0.85	0.66	0.39

varying momentum flux and mass flux ratios. While a sensible choice from an experimental point of view, this does not necessarily correlate to that of an actual engine.

Within the engine, the pressure difference between the coolant and exit static pressure typically remains constant resulting in a matched momentum flux ratio (given that $\Delta p \sim U^2$). The second comparison was for an average slot I = 0.08 while expanding and contracting the slot width 50%. Total coolant pressure to static gas pressure was held at a constant value, which resulted in nominally the same average slot velocity (and momentum flux ratio) but differing slot mass flows as the slot metering width was contracted or expanded. Next, the effect of varying slot mass flow was analyzed for the nominal slot width. The last effect to be analyzed was the mid-passage gap leakage. The mid-passage gap mass flow was set at 0.1%, 0.2%, and 0.3% of core passage flow.

Matched Mass Flow Ratios for Differing Slot Widths

For nominal slot flow rate of 0.85%, Figure 1.5 compares adiabatic effectiveness for different slot widths. It is important to note that while the slot mass flow remained constant for all slot widths, the average slot momentum flux ratio changed by a factor of ten between the half and double width slots.

The effect of expanding the slot is shown in Figure 1.5a. No coolant was observed exiting the upstream slot on the pressure side of the mid-passage gap. The hot ring observed on the vane's leading edge was apparent and effectiveness levels on the entire pressure side and suction side had decreased substantially relative to Figure 1.5b. The effect of contracting the slot is shown in Figure 1.5c. Figures 1.5a and 1.5b show the upstream slot coolant had been primarily confined to the suction side surface by the presence of the mid-passage gap. In Figure 1.5c for the half width slot the leakage flow seems evenly distributed over the entire slot pitch with a substantial increase in cooling on the pressure side of the mid-passage gap. Film-cooling holes upstream of the vane stagnation are redundant and the hot ring around the vane pressure side shown in other cases which extends from the leading edge into the passage is no longer apparent. More even cooling was observed on the mid-passage gap suction side as well in Figure 1.5c, while the locally high values of effectiveness seen using the nominal upstream slot width (Figure 1.5b) were less apparent.

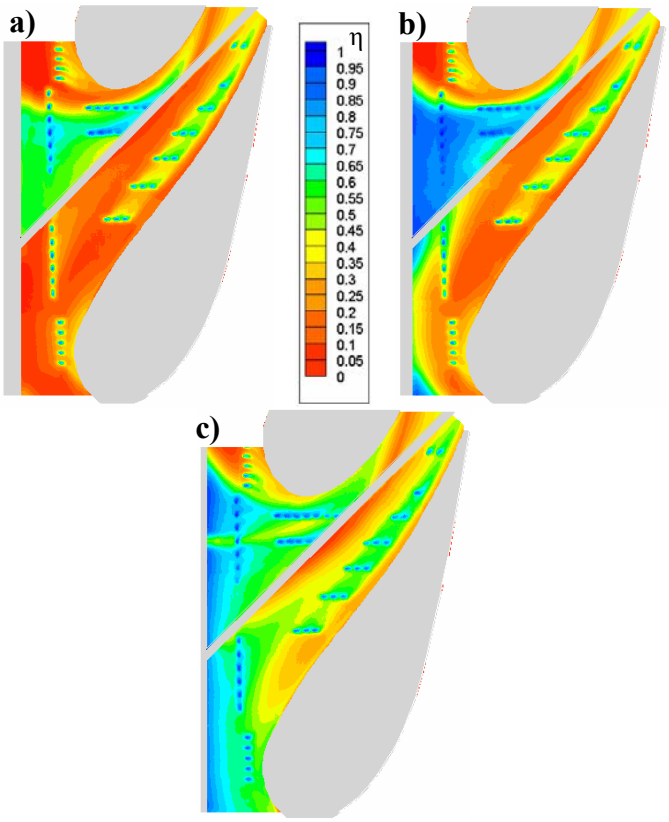

Figure 1.5. Contours of adiabatic effectiveness for a) double, b) nominal c) half width upstream slot with 0.85% slot mass flow ratio.

Pitchwise averaged values of effectiveness for varied slot width with matched mass flow ratios are shown in Figure 1.6. Expanding the slot shows a decrease in averaged effectiveness levels along much of the platform while contracting the slot increases the averaged effectiveness. This can be explained by the contours shown in Figure 1.5 where the coverage area was greater in Figure 1.5c and more localized in 1.5a. The contracted slot shows better coolant coverage than nominal with higher averaged effectiveness levels than both the nominal and double-width slot. This result is expected based on the viewpoints of coolant momentum and mass flow (see Table 1.3). The higher plenum pressure required to supply 0.85% from the contracted slot has resulted in an increase in the coverage uniformity. This improvement in uniformity can be explained by considering that with a higher plenum pressure there is less sensitivity to the exit static pressure variation due to the presence of the vane. For the expanded slot, lower plenum pressures are required to supply 0.85% mass flow thereby resulting in more sensitivity to the exit static pressure.

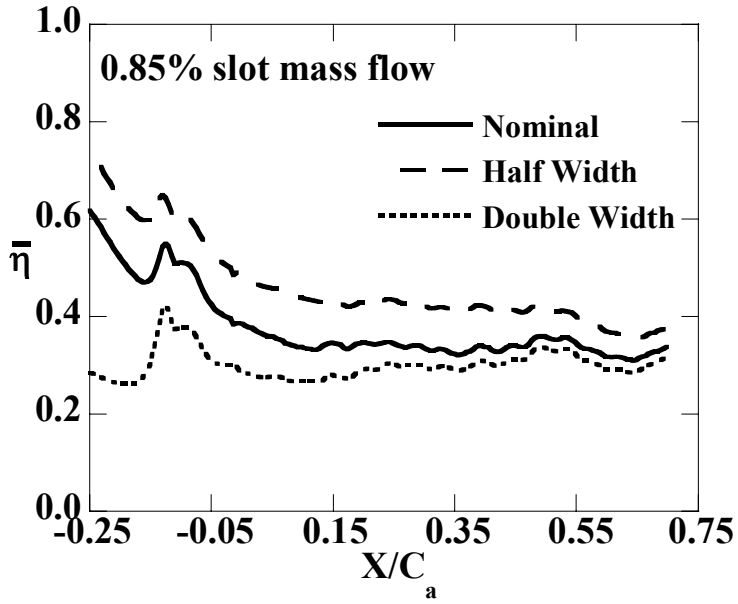

Figure 1.6. Pitchwise averaged adiabatic effectiveness for the entire passage with varied upstream slot widths.

Through observation of Figure 1.5a it was concluded that a portion of the slot was ingesting hot mainstream air since no coolant was observed exiting the slot on the mid-passage gap pressure side. Therefore, the ejected coolant on the suction side was already premixed with hot main gas within the upstream slot, which explains the strong reduction in averaged effectiveness levels for the expanded slot.

Mid-passage gap temperature profiles are shown in Figure 1.7. This information is important as turbines are typically designed so that ingestion of hot mainstream gas into the gaps is minimized. The nondimensional gap temperature, θ, was based on the mainstream and the coolant temperatures where θ values of zero and one signify maximum and minimum gap temperatures, respectively. Again, Figure 1.2 illustrates the thermocouple location for the mid-passage gap. Also shown in Figure 1.7 are the calculated inviscid gap velocities based on the local static pressure at the gap exit, which was known from previous studies [26]. Note that this calculation assumed a constant total plenum pressure difference between the mainstream and the gap plenum. An iterative procedure was used to calculate the pressure difference which resulted in zero net mass flow from the slot (ingested flow equals ejected flow). For zero net mass flow through the mid-passage gap, negative velocity values (signifying ingestion) were predicted for $X/L < 0.45$ and positive velocity values (signifying ejection) were predicted

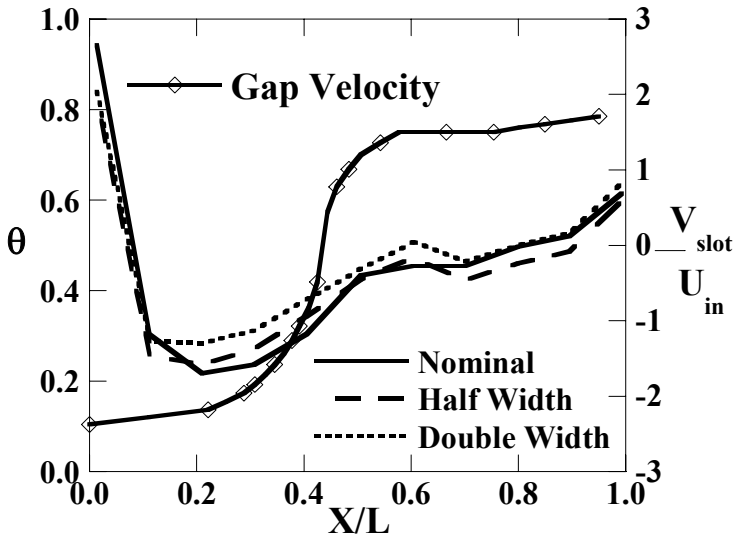

Figure 1.7. Non-dimensionalized mid-passage gap temperature profiles with varied upstream slot widths.

for X/L > 0.45.

The gap leading edge ingested a substantial amount of coolant from the upstream slot. In the location 0 < X/L < 0.2, this ingested coolant resulted in cooler temperatures with the amount of coolant being ingested decreasing with increasing X/L. There was also increased ingestion of the hot mainstream flow which caused a rapid increase in the gap air temperature. Temperature in the gap increased dramatically as hot mainstream flow was ingested X/L < 0.2. The increase in θ observed at X/L = 0.2 was most likely caused by ingestion of fresh coolant from film-cooling holes in the vicinity of X/L=0.2 as well as continued mixing of previously ingested upstream slot coolant and main gas. This mixture of coolant and hot mainstream gas convects inside the mid-passage gap until the exit static pressure is low enough for it to exit the gap. Up to X/L = 0.45, the inviscid velocity is indicated to be into the slot (static endwall pressure is higher than the plenum pressure), which is consistent with the fact that flow is ingesting into the gap. Beyond X/L = 0.45, Figure 1.7 shows that flow is exiting the mid-passage gap.

All θ profiles for varying slot width in Figure 1.7 are very similar with values slightly lower for both the double and half width upstream slots. Since the coolant exiting the half-width slot has a relatively high momentum compared with the nominal, it is less likely that it will be ingested into the mid-passage gap than for the double-width slot.

Matched Momentum Flux Ratios for Differing Slot Widths

Upstream slot momentum flux ratios were matched to a average value of I = 0.08, which corresponded to a nominal width upstream slot flow of 0.75%. As previously, the upstream slot width was contracted and expanded by 50%. There was 0% flow in the mid-passage gap.

Figure 1.8 shows contours of adiabatic effectiveness and Figure 1.9 shows pitchwise averaged values of adiabatic effectiveness on the endwall for an average upstream slot momentum flux ratio of 0.08. The coolant coverage area is very similar for all three slot widths, illustrating that coverage area is a function of the coolant to mainstream momentum flux ratios rather than the coolant mass flow rate. By contracting the slot and keeping the plenum-to-mainstream pressure difference the same, the mass flow of coolant exiting the upstream slot was reduced (see Table 1.3). This reduction in coolant flow explains the observed reduction in effectiveness on the suction side platform and the lower values of averaged effectiveness. By the same reasoning, the coolant mass

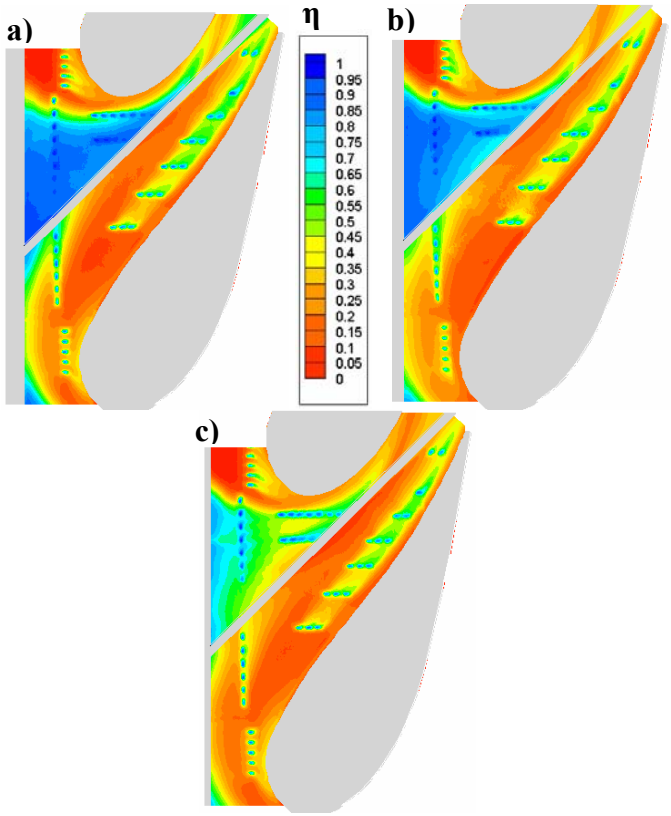

Figure 1.8. Contours of adiabatic effectiveness for a) double, b) nominal c) half-width upstream slot with I = 0.08 average slot momentum flux ratio.

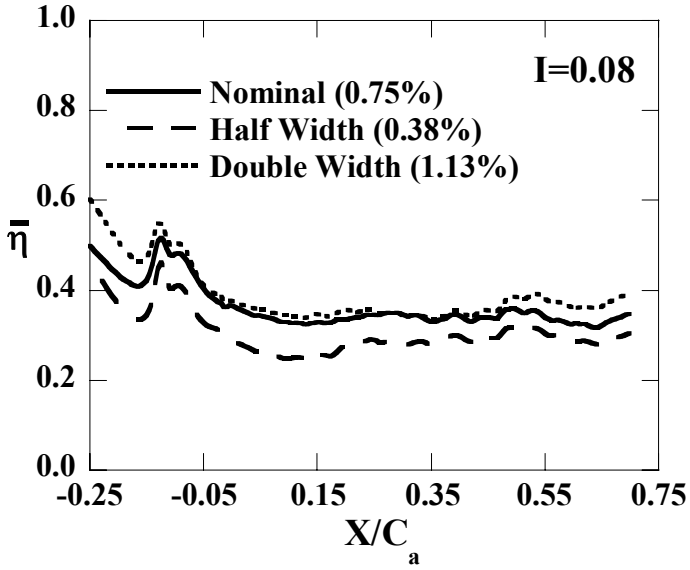

Figure 1.9. Plots of pitchwise averaged adiabatic effectiveness for the entire passage with varied slot widths.

flow would be higher for the expanded slot, thus explaining the increase in averaged coolant effectiveness on the suction side platform.

Figure 1.8 shows there is also an effect of slot width on the mid-passage gap trailing edge. In this region, the mid-passage gap ejects a mixture of the coolant and main gas, which was ingested in the leading edge region. A slight increase in effectiveness levels for the nominal and double slot cases relative to the half slot width were observed on the suction side of the mid-passage gap trailing edge. The cooler region near the trailing edge indicates different amounts of coolant were being ingested into the mid-passage gap near the leading edge and then ejected near the trailing edge. Upstream slot momentum flux was the same for all cases, but coolant mass flow was higher for the double slot and lower for the half slot.

By examining the mid-passage gap temperature profiles in Figure 1.10, we see that by matching the upstream slot coolant momentum flux ratios the amount of coolant being ingested into the mid-passage gap changed with slot width. Expanding the slot width dramatically decreased gap temperature, sometime by as much as 70% from nominal. The effect of contracting the slot is not observed until X/L = 0.45, where ejecting mid-passage gap temperatures were observed to be 10-20% lower.

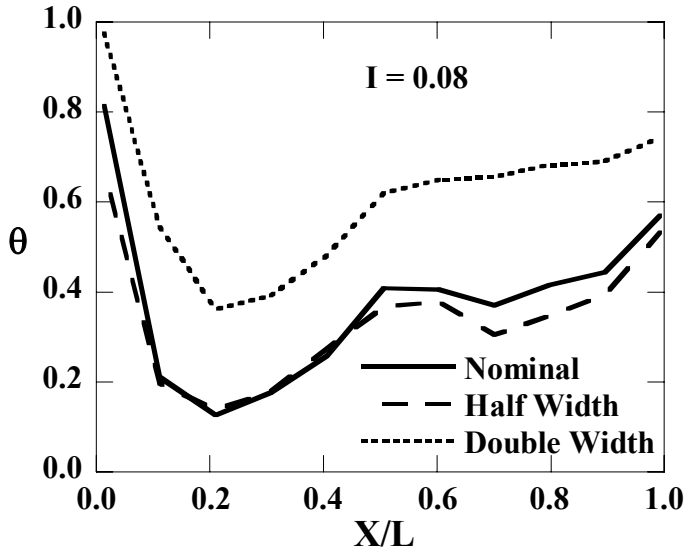

Figure 1.10. Non-dimensionalized mid-passage gap temperature profiles with varied upstream slot widths at a given nominal slot momentum flux ratio.

Adiabatic Effectiveness with Varying Slot Leakage Flows

For a constant upstream slot width and a varying difference between the coolant and the mainstream static pressures, the coolant flow rate exiting the slot varies. To determine this effect, tests were conducted, as before, with no mid-passage gap flow and upstream slot mass flow rates were set to 0.75%, 0.85%, and 1.0%. The effect of varying upstream slot flowrate was analyzed for a nominal slot width. Contours of adiabatic effectiveness for the effect of coolant mass flux ratio are shown in Figure 1.11.

The primary result was that for all three cases the coverage area had not changed significantly but the cooling benefit had increased. It is important to note that upstream slot momentum flux ratio increased with slot mass flow by a factor of 1.6 from the lowest to highest slot flowrate studied. This increase was much smaller than the factor of ten discussed in the previous section. For each case, there was very little coolant flow from the upstream slot crossing over the mid-passage gap as shown before by Cardwell et al. [18]. As the coolant convected along the gap until the end of the vane passage where it exited the gap. The effect of film-cooling was also nominally the same for all upstream slot flows. As the slot mass flow rate was increased, the amount of coolant observed on the pressure side of the slot increased slightly. The suction side of the gap, which was well cooled for all flow rates, showed higher adiabatic effectiveness levels when the slot flow rate was increased. Although the coolant mass flow rate through the slot was

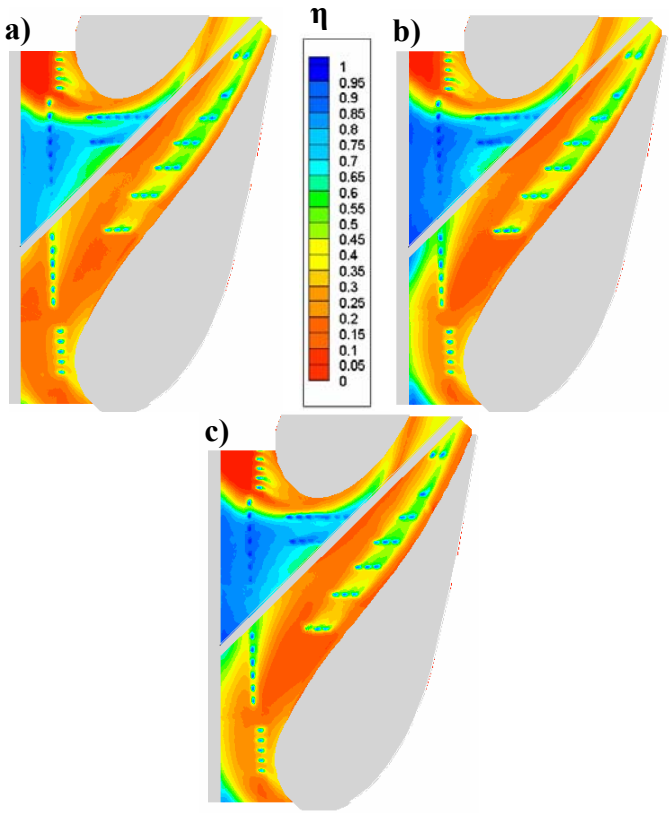

Figure 1.11. Contours of adiabatic effectiveness for a) 0.75%, b) 0.85% c) 1.0% upstream slot mass flow rate for a nominal slot width.

increased substantially, much of the pressure side endwall continued to show lower values of adiabatic effectiveness. To quantify the effect of increasing slot flow at these levels, the adiabatic effectiveness values were pitchwise averaged for all flow rates, as shown in Figure 1.12. Increasing the upstream slot cooling showed increased values of pitchwise averaged adiabatic effectiveness.

Since there was more coolant on the endwall for increased upstream slot leakage, it was hypothesized that more coolant was being ingested into the mid-passage gap. The measured non-dimensional gap temperature profiles for the above mentioned cases are shown in Figure 1.13. Note that again, no coolant mass flow was provided to the gap. The increase in slot flow rate from 0.75% to 0.85% showed a substantial decrease in gap temperatures. The ratio of ingested coolant to hot gas was higher, thus explaining the decrease in ejected gap temperatures beyond X/L = 0.45. In contrast, negligible changes in gap temperatures were recorded for the increase to 1% upstream slot flow. Most likely the gap was saturated with coolant from the upstream slot at the 1% case.

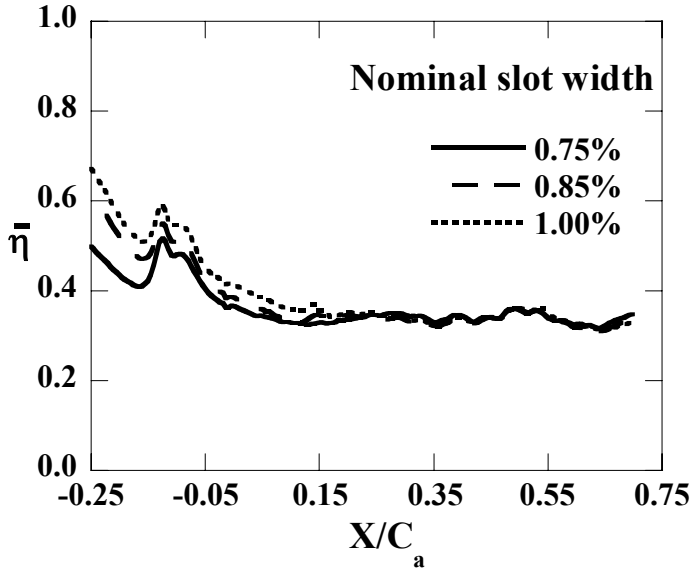

Figure 1.12. Plots of laterally averaged adiabatic effectiveness for the entire passage with varied upstream slot mass flow.

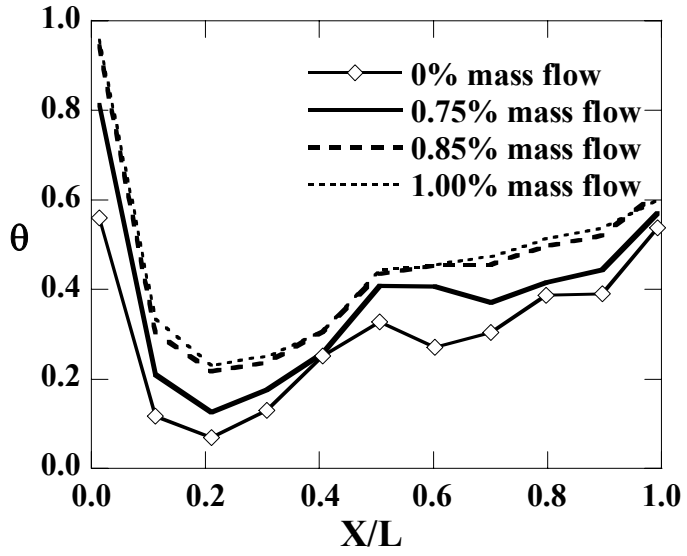

Figure 1.13. Non-dimensionalized mid-passage gap temperature profiles varied upstream slot mass flow.

Adiabatic Effectiveness Varying Mid-Passage Gap Flows

The last comparison completed for this study was for a variation in the mid-passage gap leakage. These experiments were conducted with a nominal upstream slot width and a 0.75% upstream slot mass flow rate (I = 0.08). Mid-passage gap mass flow rates were set to 0.1%, 0.2%, and 0.3%.

The contours of adiabatic effectiveness for the varying gap flows are shown in

Figure 1.14. These contours are very similar to each other with no large effect due to varied mid-passage gap flow. As before, the contours were pitchwise averaged, which is shown in Figure 1.15. No effect is observed in the leading edge region of the slot. It appears that the mid-passage gap flow has little to no effect on the endwall surface for the entire passage in this flowrate range. The presence of the gap, however, does affect the endwall effectiveness patterns relative to a continuous endwall as previously described by Cardwell et al. [18].

There was a slight effect of the coolant flow rate on the non-dimensional temperature distribution within the gap. Figure 1.16 shows the non-dimensional gap temperature profiles for the three cases as compared to the no flow case. As compared to the no gap flow condition, the gap temperature was lower relative to all values of coolant mass flow. Increasing the mid-passage gap flow rate reduced the temperature measured within the gap for $0.45 < X/L < 1$. For between $0.45 < X/L < 1$, decreases in gap temperatures were observed for increases in mid-passage gap flow. Note that the ejected

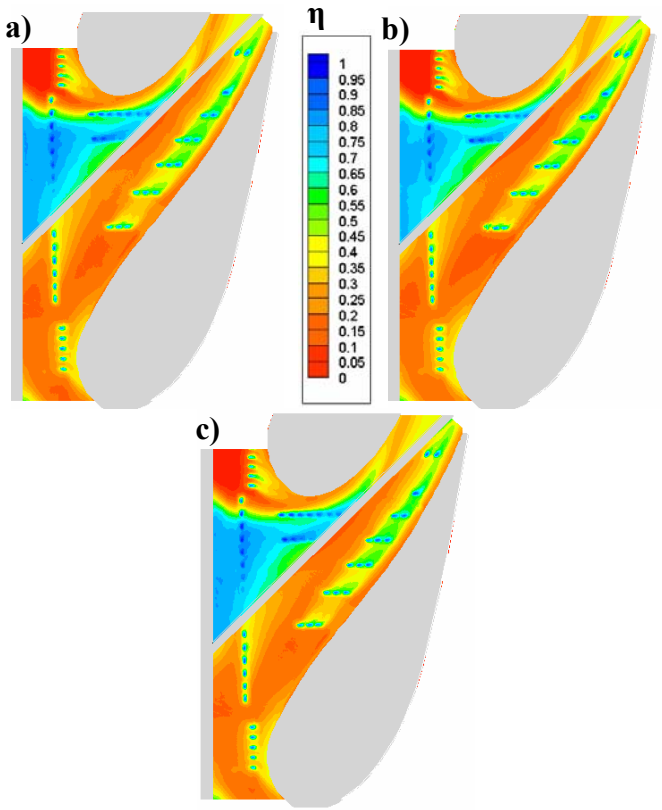

Figure 1.14. Contours of adiabatic effectiveness for a) 0.1%, b) 0.2%, and c) 0.3% mid-passage gap mass flow with nominal upstream slot width.

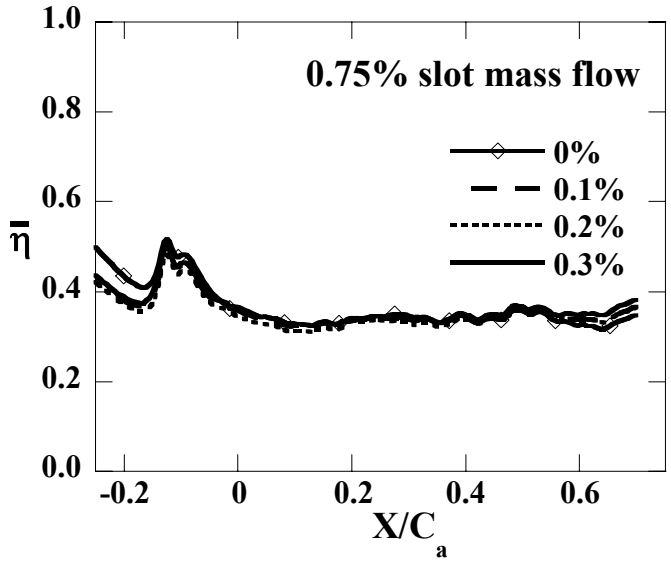

Figure 1.15. Plots of laterally averaged adiabatic effectiveness for the entire passage with varied mid-passage gap cooling.

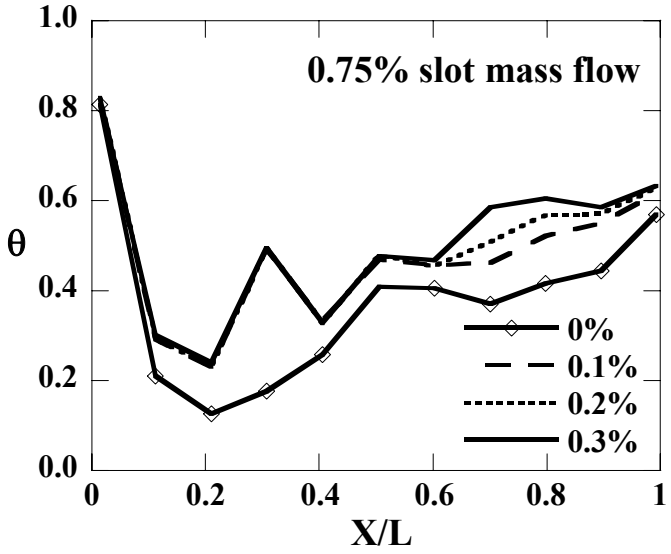

Figure 1.16. Non-dimensionalized mid-passage gap temperature profiles with varied mid-passage gap cooling.

fluid was a mixture of ingested upstream slot coolant, ingested main gas, and mid-passage gap coolant.

Figure 1.17 shows thermal field profiles which were taken within the passage for 0% and 0.3% mid-passage gap flow. The measurement plane was located at s/C=0.5, which is illustrated by the dashed on Figure 1.1. There was little change in the passage temperature profiles indicating little change in the secondary flows. Again as previously noted when comparing gap temperature profiles, the interaction of the mid-passage gap

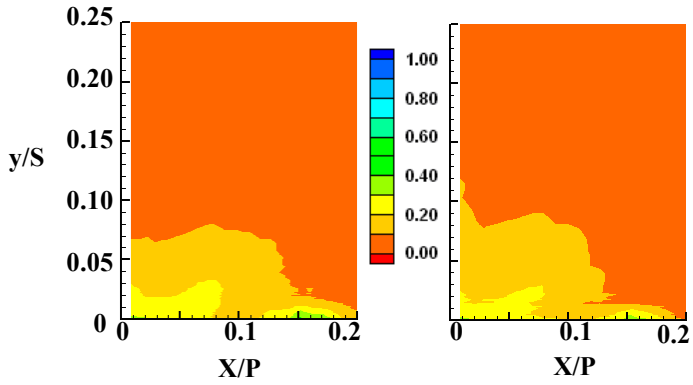

Figure 1.17. Plots of thermal field data for a). 0% flow and b) 0.3% flow within the mid-passage gap.

was only slightly affected by changes in leakage flow and was primarily driven by the endwall static pressure distribution throughout the passage.

Conclusions

Measurements of endwall adiabatic effectiveness and non-dimensional mid-passage gap temperature profiles were presented for a double, nominal, and half-width combustor to turbine interface. Two parameters were used to compare the different configurations: mass flow and momentum flux ratios.

When comparing varying slot width while matching mass flow, it was observed that decreasing the slot width caused the coolant to be more evenly distributed on the endwall. Increasing the slot width while matching mass flow indicated a reduced coverage with no coolant observed on the pressure side of the passage. Moreover, the effectiveness values on the suction side were lower that those observed at the same flow rate for a nominal slot width. This decrease was caused by ingesting hot mainstream gas. Averaged effectiveness values were found to be the lowest for the double slot relative to the nominal and half width.

Matching the slot momentum flux ratios for the three slot widths resulted in endwall contours that looked nominally the same in terms of upstream slot coolant coverage. These results indicated that the upstream coolant coverage area was a function of momentum flux ratio, not mass flow rate. The cooling from the upstream slot had a beneficial effect only along the suction side endwall surface. Doubling the slot width resulted in better endwall cooling on the suction side platform and significantly lowered

temperatures within the mid-passage gap. Given the same slot momentum flux ratio, halving the slot resulted in less coolant mass flow and higher temperatures within the gap. With a nominal width, increasing upstream slot cooling resulted in improved endwall adiabatic effectiveness values and lower gap temperatures. Even at 1.0% mass flow, the upstream coolant momentum was still too low to adequately cool the pressure side platform due to the presence of the ingesting mid-passage gap.

Mid-passage gap leakage flows proved to have little effect on endwall adiabatic effectiveness levels, though gap temperatures were lower for increased leakage flows. Since the gap plenum was ingesting, it was at an equilibrium pressure somewhere between the passage inlet static wall pressure, which was higher, and the passage exit static wall pressure, which was lower. By introducing coolant flow to the gap plenum, the temperature of the gap fluid was effectively lowered while the equilibrium pressure stayed nominally the same. Thus it would require much higher coolant pressure to significantly affect the mid-passage gap velocity distribution.

These results indicate that the leakage through the combustor-turbine interface can provide cooling to the endwall. Since this interface width changes as the turbine and combustor heat up, it is important to account for the associated changes in coolant coverage area and local coolant levels thereby reducing the need for film-cooling on certain areas of the vane-endwall surface.

Acknowledgments

This publication was prepared with the support of the US Department of Energy, Office of Fossil Fuel, and National Energy Technology Laboratory and the South Carolina Institute for Energy Studies (SCIES) University Turbine Systems Research program (UTSR). However, any opinions, findings, conclusions, or recommendations expressed herein are solely those of the authors and do not necessarily reflect the views of the DOE, SCIES, or the UTSR program. The authors would also like to thank Mike Blair (Pratt & Whitney), Ron Bunker (General Electric), and John Weaver (Rolls-Royce) for their input on the modeling of realistic turbine features.

Attribution

This paper was co-authored with Nick Cardwell and Dr. Karen Thole. They had the following roles in the paper

Co-author 1 – paper 1

Name - Nick Cardwell

Department – Mechanical Engineering

Degree – MS

Relationship – fellow graduate student

Role - Nick helped in taking part of the adiabatic effectiveness measurements and helped in building the test section and instrumenting the vane and endwall.

Co-author 2 – paper 1

Name – Dr. Karen A. Thole

Department – Mechanical Engineering

Degree – Ph.D

Relationship – Chair and primary advisor

Role - Dr. Thole served as my dissertation chair and advised me through my Ph.D and on all the work presented in this dissertation.

Nomenclature

C	true chord of stator vane
C_a	axial chord of stator vane
D	diameter of film-cooling hole
I	average momentum flux ratio, $I = \frac{\rho_c U_c^2}{\rho_\infty U_\infty^2} = \frac{\rho_s (\dot{m}/\rho_s A_s)^2}{\rho_\infty U_\infty^2}$
L	length of mid-passage gap
$\dot{m}$	mass flowrate
M	average blowing ratio
p	static pressure
P	vane pitch; hole pitch
Re_{in}	Reynolds number, $Re_{in} = CU_{in}/\nu$

S span of stator vane

T temperature

X local coordinate

U velocity

s distance along vane from flow stagnation

Greek

η adiabatic effectiveness, $\eta = (T_\infty - T_{aw})/(T_\infty - T_c)$

ρ density

ν kinematic viscosity

θ non-dimensional gap effectiveness,

$\theta = (T_\infty - T_G)/(T_\infty - T_c)$

Subscripts

aw adiabatic wall

c coolant conditions

G gap air temperature

in inlet conditions

s upstream slot

∞ freestream conditions

Overbar

– lateral average

= area average

References

[1] Electronic Space Products International "Inconel 625," http://www.espimetals.com/tech/Tech%20Inconel%20625.htm, (Ashland, OR).

[2] Blair, M.F., 1974, "An Experimental Study of Heat Transfer and Film-cooling on Large-Scale Turbine Endwall," *ASME J. of Heat Transfer*, vol. 96, pp. 524-529.

[3] Burd, S.W., Satterness, C.J., and Simon, T.W., 2000, "Effects of Slot Bleed Injection Over a Contoured Endwall On Nozzle Guide Vane Cooling Performance: Part II - Thermal Measurements," 2000-GT-200.

[4] Colban, W. F., Thole, K. A., and Zess, G., 2002, "Combustor-Turbine Interface Studies: Part 1: Endwall Measurements," *J of Turbomachinery*, vol. 125, pp.193-202.

[5] Colban, W. F., Lethander, A. T., Thole, K. A., and Zess, G., 2002, "Combustor-Turbine Interface Studies: Part 2: Flow and Thermal Field Measurements," *J of Turbomachinery,* vol. 125, pp.203-209.

[6] Pasinato, H. D., Squires, K. D., and Roy, R. P., 2004, "Measurement and modeling of the flow and heat transfer in a contoured vane-endwall passage," *Int. J. of Heat and Mass Transfer,* 47 (2004) 5685-5702.

[7] Zhang, L.J., and Jaiswal, R.S., 2001, "Turbine Nozzle Endwall Film-cooling Study Using Pressure Sensitive Paint," *J of Turbomachinery*, **123**, pp. 730-738.

[8] Kost, F. and Nicklas, M., 2001, "Film-Cooled Turbine Endwall in a Transonic Flow Field: Part I – Aerodynamic Measurements,"ASME Paper Number 2001-GT-0145.

[9] Nicklas, M., 2001, "Film-Cooled Turbine Endwall in a Transonic Flow Field: Part II – Heat Transfer and Film-Cooling Effectiveness," *J of Turbomachinery*, **123**, pp.720-729.

[10] Knost, D.G., and Thole, K.A., 2003, "Computational Predictions of Endwall Film-Cooling for a First Stage Vane," GT2003-38252.

[11] Knost, D. G., and Thole, K. A., 2005, "Adiabatic Effectiveness Measurements of

Endwall Film- Cooling for a First Stage Vane," *J. of Turbomachinery*, vol. 127, pp. 297-305.

[12] Aunapu, N.V., Volino, R.J., Flack, K.A., and Stoddard, R.M., 2000, "Secondary Flow Measurements in a Turbine Passage with Endwall Flow Modification," *J. of Turbomachinery*, **122**, pp. 651-658.

[13] Ranson, W., Thole, K. A., and Cunha, F., 2005, "Adiabatic Effectiveness Measurements and Predictions of Leakage Flows along a Blade Endwall," *J. of Turbomachinery*, vol. 127, pp. 609-618.

[14] Yamao, H., Aoki, K., Takeishi, K., and Takeda, K., 1987, "An Experimental Study for endwall Cooling Design of Turbine Vanes," IGTC-1987, Tokyo, Japan.

[15] Piggush, J.D., and Simon, T.W., "Flow Measurements in a First Stage Nozzle Cascade having Endwall Contouring, Leakage, and Assembly Features," GT2005-68340.

[16] Piggush, J. D., and Simon, T. W., 2005, "Flow Measurements in a First Stage Nozzle Cascade having Leakage and Assembly Features: Effects of Endwall Steps and Leakage on Aerodynamic Losses," IMCE2005-83032.

[17] Reid, K., Denton, J., Pullan, G., Curtis, E., and Longley, J., "The Interaction of Turbine Inter-Platform Leakage Flow with the Mainstream Flow," GT2005-68151.

[18] Cardwell, N. D., Sundaram, N., and Thole, K. A., "Effects of Mid-Passage Gap, Endwall Misalignment and Roughness on Endwall Film-Cooling," *Journal of Turbomachinery*, vol. 128, pp. 62-70.

[19] de la Rosa Blanco, E., Hodson, H. P., and Vazquez, R., "Effect of Upstream Platform Geometry on the Endwall Flows of a Turbine Cascade," GT2005-

68938.

[20] Radomsky, R. and Thole, K. A., 2002, "Detailed Boundary Layer Measurements on a Turbine Stator Vane at Elevated Freestream Turbulence Levels," *Journal of Turbomachinery*, vol. 124, pp. 107-118.

[21] "Sandpaper – coated abrasives," www.sizes.com/tools/ sandpaper.htm, (11 August 2004).

[22] Bons, J.P., Taylor, R.P., McClain, S.T., and Rivir, R.B., 2001, "The Many Faces of Turbine Surface Roughness," *J. of Turbomachinery*, vol. 123, pp.739-748.

[23] Modest, M. F., 2003, *Radiative Heat Transfer*, 2nd Edition, pp. 743-758.

[24] Ethridge, M. I., Cutbirth, J. M., and Bogard, D. G., 2000, "Scaling of Performance for Varying Density Ratio Coolants on an Airfoil with Strong Curvature and Pressure Gradients," *J. of Turbomachinery*, vol. 123, pp. 231-237.

[25] Moffat, R. J., 1988, "Describing the Uncertainties in Experimental Results," *Experimental Thermal and Fluid Science*, Vol.1, pp. 3-17.

[26] Kang, M., Kohli, A., and Thole, K. A., 1999, "Heat Transfer and Flowfield Measurements In The Leading Edge Region of A Stator Vane Endwall," *J. of Turbomachinery*, vol. 121, no. 3, pp. 558-568 (ASME Paper 98-GT-173).

Paper 2:
Effects of Surface Deposition, Hole Blockage, and TBC Spallation on Vane Endwall Film-Cooling

Accepted for publication in the *ASME Journal of Turbomachinery* *

Abstract

With the increase in usage of gas turbines for power generation and given that natural gas resources continue to be depleted, it has become increasingly important to search for alternate fuels. One source of alternate fuels is coal derived synthetic fuels. Coal derived fuels, however, contain traces of ash and other contaminants that can deposit on vane and turbine surfaces affecting their heat transfer through reduced film-cooling. The endwall of a first stage vane is one such region that can be susceptible to depositions from these contaminants.

This study uses a large-scale turbine vane cascade in which the following effects on film-cooling adiabatic effectiveness were investigated in the endwall region: the effect of near-hole deposition, the effect of partial film-cooling hole blockage, and the effect of spallation of a thermal barrier coating. The results indicated that deposits near the hole exit can sometimes improve the cooling effectiveness at the leading edge, but with increased deposition heights the cooling deteriorates. Partial hole blockage studies revealed that the cooling effectiveness deteriorates with increases in the number of blocked holes. Spallation studies showed that for a spalled endwall surface downstream of the leading edge cooling row, cooling effectiveness worsened with an increase in blowing ratio.

* Co-author: Dr. Karen A. Thole, Mechanical Engineering Department, Virginia Tech

Introduction

In a typical gas turbine, components in the hot gas path operate under conditions of very high temperature, pressure, and velocity. These hostile conditions cause thermal oxidation and surface deterioration leading to reduced component life. Surface deteriorations are caused from deposits formed by various contaminants present in the combustion gases. With depleting natural gas resources, the focus now is on using alternate fuels like coal derived synthetic gas for gas turbine operation. These alternate fuels are not as clean as natural gas resulting in deposition, erosion, and/or corrosion on turbine airfoils. Hence, it is important to understand how surface distortions can affect the performance of film-cooling.

During engine operation, contaminants in the hot gas path are in a molten state resulting in surface deposition that leads to film-cooling hole blockage and oxidation of the metal surface as a result of spallation. The dominant delivery mechanism of the contaminants on to the surface depends on the size or state of the contaminant [1]. Since the region around the film-cooling holes are at a relatively lower temperature, deposits tend to adhere to surfaces near the holes. In some cases the deposits on the surface extend into the film-cooling holes and end up partially or completely blocking the holes. Also, deposits can detach from the surface peeling the thermal barrier coating (TBC) resulting in spallation.

Higher power outputs from the turbine require higher turbine inlet temperatures and increasing gas temperatures in turn increase the rate of deposition. This study is aimed at understanding which of these effects is more detrimental to film-cooling adiabatic effectiveness levels. With the knowledge of which of these effects are more detrimental, cooling designs can be made to combat those effects. The work presented in this paper compares three different surface distortions on film-cooling effectiveness including; surface deposition, film-cooling hole blockage, and TBC spallation.

Relevant Past Studies

A number of studies in the literature have documented the effect of using alternate fuels on turbine surfaces. There are also studies showing the effect of surface roughness on film-cooling. Only a few studies exist on the effect of blocked holes on film-cooling

effectiveness. In addition, there have been few studies simulating the effect of TBC spallation on film-cooling effectiveness.

Studies concerning the effect of using coal and other solid fuels have focused on ash and other contaminant levels on deposition, corrosion, or erosion. A study by Wenglarz et al. [2] showed that high levels of ash, up to 40 tons/yr, can enter a turbine. DeCorso et al. [3] found that most coal derived fuels after conversion and purification had greater levels of impurity levels than those found in natural gas. They found that in natural gas sulfur levels are about 10 ppm, but a coal derived fuel after liquefaction and separation had about 1000 ppm of sulfur. Studies have also been carried out to see the effect of small amounts of ash flowing through a turbine. Moses and Bernstein [4] found that a fuel burning with 0.5 percent ash results in about 1.5 tons/day of ash flowing through a turbine. A study by Wenglarz [5] yielded that the mass fraction of the ash particles adhering to surface and contributing to deposit build up was 0.06 with an average particle diameter of 10 μm. Recent studies by Bons et al. [6] were carried out to study the effect of ash deposits present in coal fuels in an accelerated deposition test facility. They carried out their tests with ash particles at a slightly higher mean mass diameter of 13.3 μm than those found in coal fuels. For a test duration of three hours, they found the net particle loading to be 165 ppmw-hr (parts per million by weight per hour) resulting in an average deposit thickness of 1.3mm.

Bonding of ash and other contaminants to turbine component surfaces is dependent on their surface properties [3]. Deposition of contaminants and other particulate matter present in the mainstream gas takes place through impingement onto the surface. Typically in a gas turbine, the first rows of vanes are subjected to direct impingement resulting in particulate deposition [7]. The mechanism for this could be attributed to the fact that the particles are broken up and redistributed by impact [8]. Also, the leading edge film-cooling regions on a vane endwall are more prone to deposition. Because this is the first cold surface the hot mainstream gas encounters before it enters a turbine and as mentioned before the molten contaminants would quench and adhere near the relatively colder regions. Bons et al. [9] showed through their turbine surface measurements that the leading edge region will have the greatest degradation. Also, actual turbine component measurements by Bons et al. [9], Taylor [10], and Tarada and

Suzuki [11] revealed that all the regions of a turbine blade and vane are prone to deposition and roughness with varying levels.

A number of studies have been reported showing the effect of surface roughness on film-cooling. Goldstein et al. [12] placed cylindrical roughness elements at the upstream and downstream location of film-cooling holes on a flat plate. They observed that at low blowing rates, there is a decrease in adiabatic wall effectiveness by 10 to 20 percent over a smooth surface. However, at higher blowing rates they observed an enhancement of 40 to 50 percent in cooling performance. Schmidt et al. [13] did a similar study using conical roughness elements. They also found a higher degradation of film-cooling effectiveness at lower momentum flux ratios than at higher momentum flux ratios. Barlow and Kim [14] studied the effect of staggered row of roughness elements on adiabatic effectiveness. They found that roughness degraded cooling effectiveness compared to a smooth surface and the smaller elements caused a greater reduction than the larger elements.

There have been very few studies on the effect of roughness on endwall film-cooling. In the study by Cardwell et al. [15], they showed that a uniformly rough endwall surface decreased cooling effectiveness at higher blowing ratios but at lower blowing ratios there was no significant change.

Not many studies are available in the literature showing the effect of blockage on film-cooling effectiveness. The study done by Bunker [16] showed that for a partially blocked row of cylindrical holes there was significant degradation of local adiabatic effectiveness near the hole exit regions. The partial hole blockage was simulated by applying air-plasma sprayed TBC over the holes without any protection. Bogard et al. [17] showed a cross-section of a film-cooling hole for an actual turbine part which depicted partial blockage of the hole downstream with the deposition extending outside of the hole.

Ekkad and Han [18, 19] carried out heat transfer and film-cooling measurements on a cylindrical model simulating TBC spallation. Ekkad and Han [18] found that spallation enhances heat transfer up to two times compared to a smooth surface. They also found that local heat transfer distributions were greatly affected by spallation depth and location. Ekkad and Han [19] found that higher freestream turbulence coupled with

spallation greatly reduced film effectiveness. They found that spallation reduced film effectiveness inside the spallation cavity but increased it downstream of the spallation cavity.

In summary it is important to understand the effects of surface distortion due to contaminants present in fuel and combustion air. Though there have been many studies addressing the issue of surface deposition and surface distortion as a whole, there have been very few studies showing the effect of these distortions on a film-cooled endwall.

Experimental Methodology

The experimental section was placed in a closed loop wind tunnel facility, as shown in Figure 2.1. The flow encounters an elbow downstream of the fan and passes through a primary heat exchanger used to cool the bulk flow. The flow is then divided into three channels including the center passage and two cooled secondary passages located above and below the test section. Note that only the top secondary passage was used for this study. The primary core flow, located in the center passage, convects through a heater bank where the air temperature is increased to about 60°C. The secondary flow, in the outer passage, was cooled to about 20°C, thereby maintaining a temperature difference of 40°C between the primary and secondary flows. The secondary flow provided the coolant through the film-cooling holes and through the leakage paths. Also, for all the tests carried out in this study a density ratio of 1.1 was maintained between the coolant and mainstream flows. Due to the fact that density ratios are not being matched to that of the engine, velocity ratios for the cooling holes will be

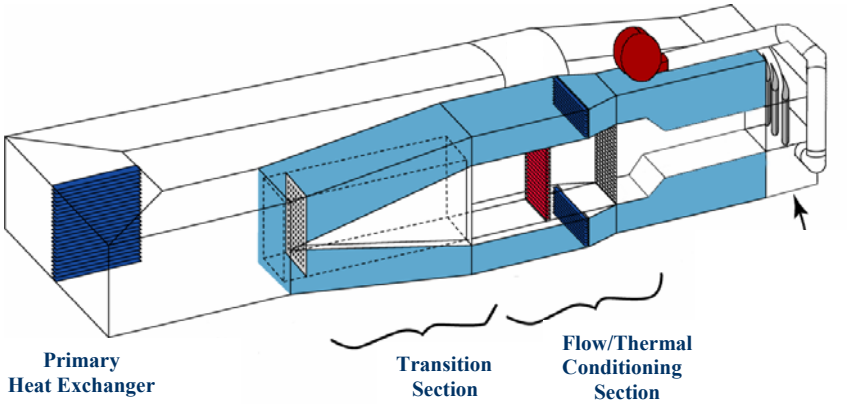

Figure 2.1. Illustration of the wind tunnel facility.

significantly higher than those found in an engine for the same mass flux or momentum flux ratios. While there have been studies indicating that momentum flux scales jet lift-off for flat plate film-cooling, it is unknown as to whether it best scales lift-off for endwall film-cooling

Downstream of the flow/thermal conditioning section, is the test section that consists of two full passages with one center vane and two half vanes. Table 2.1 provides a description of turbine vane geometry and operating conditions. The vane geometry used in the current study is a commercial first-stage vane previously described by Colban et al. [20, 21]. The passage under study consisted of an endwall surface with film-cooling holes and leakage paths simulating the combustor-vane interface and vane-to-vane interface.

A detailed description of the endwall construction has been previously described by Knost and Thole [22] and Cardwell et al. [15], who used exactly the same film-cooling and slot geometries as we used for this study. The endwall of the vane was constructed of foam because of its low thermal conductivity (0.033 W/m.K). The endwall foam was 1.9 cm thick and was mounted on a 1.2 cm thick Lexan plate. The cooling hole pattern on the endwall was cut with a five-axis water jet to ensure precision and integrity. The upstream slot was constructed with poplar wood as it had a low conductivity and was stiffer. The endwall surface was also covered with a 36 grit sandpaper to simulate a uniform surface roughness. Adiabatic endwall temperatures were measured for different flowrates through film-cooling holes, through the combustor-to-turbine interface slot (referred to as upstream slot), and a constant flowrate through the

Table 2.1. Geometric and Flow Conditions

Scaling factor	9
Scaled up chord length (C)	59.4cm
Pitch/Chord (P/C)	0.77
Span/Chord	0.93
Hole L/D	8.3
Re_{in}	2.1×10^5
Inlet and exit angles	0° & 72°
Inlet, exit Mach number	0.017, 0.085
Inlet mainstream velocity	6.3 m/s
Upstream slot width	0.024C
Mid-passage gap width	0.01C

vane-to-vane interface gap (referred to as mid-passage gap).

The inlet turbulence intensity and length scales were measured to be 1.3 percent and 4 cm respectively. For every test condition the dimensionless pressure coefficient distribution was verified to ensure periodic flow through the passages. Three separate plenums were used to control the flowrate through the film-cooling holes, through the upstream slot, and through the mid-passage gap. A global blowing ratio was calculated using an inviscid blowing ratio along with a global discharge coefficient, C_D, that was obtained from CFD studies (as reported by Knost and Thole [23]).

The upstream slot flow was assumed to have a discharge coefficient of 0.6 which is the assumed value for a flow through a sharp-edged orifice and the flowrate was calculated accordingly. Flow through the mid-passage gap was measured directly using a laminar flow element (LFE). In this study coolant flow rates are reported in terms of percent coolant mass flow rate per total passage mass flow rate for one vane pitch. Typical times to achieve steady state conditions were three hours.

Instrumentation and Measurement Methods

A FLIR P20 infrared camera was used to spatially-resolve adiabatic wall temperatures on the endwall. Measurements were taken at six different viewing locations to ensure that the entire endwall surface was mapped. The camera was placed perpendicular to the endwall surface at a distance 55 cm from the endwall. Each picture covered an area 24 cm by 18 cm with the area being divided into 320 by 240 pixel locations. The spatial integration of the camera was 0.715 mm (0.16 hole diameters). Thermocouples were also placed on the endwall surface at different locations to directly measure the temperature to post calibrate the infrared images. For the post calibration the emissivity was set at a constant value of 0.92 and the background temperature (~ 45ºC) was adjusted until the temperatures from the infrared camera images were within 0.05ºC of the corresponding thermocouple data. Six images were taken at each of the viewing locations to obtain an averaged picture using an in-house Matlab program. The same program was also used to assemble the averaged pictures at all locations to give a complete temperature distribution along the passage endwall.

Freestream temperatures were measured at multiple locations along the pitch and

the average was determined by using a thermocouple rake consisting of three thermocouples along the span. It was found that the variations along the pitch were less than 0.2ºC and that along the span were less than 1.5ºC. Voltage outputs from the thermocouples were acquired by a 32 channel data acquisition module that was used with a 12-bit digitizing card. The temperature data was compiled after the system reached steady state.

A 1D conduction correction as described by Ethridge et al. [24] was applied to all adiabatic effectiveness measurements. This correction involved measuring the endwall surface effectiveness with no blowing through the film-cooling holes. This was done by blocking the film-cooling holes on the endwall passage under study while maintaining similar flowrates through the adjacent passage to insure the correct boundary condition under the endwall. The resulting η correction was found to be 0.16 at the entrance for a η value of 0.9 and 0.02 at the exit region at a measured η value of 0.5.

Experimental Uncertainty

An uncertainty analysis was performed on the measurements of adiabatic effectiveness using the partial derivative method described at length by Moffat [25]. The precision uncertainty was determined by taking the standard deviation of six measurement sets of IR camera images with each set consisting of six images. The precision uncertainty of the measurements was ±0.014°C. The bias uncertainty was ±1.0°C based on the uncertainty in the IR camera measurements specified by the manufacturer. The bias uncertainty of the thermocouples was ±0.5°C. The total uncertainty was then calculated as ±1.02°C for the images and ±0.51°C for the thermocouples. Uncertainty in effectiveness, η, was found based on the partial derivative of η with respect to each temperature in the definition and the total uncertainty in the measurements. Uncertainties in adiabatic effectiveness were calculated to be $\partial\eta = \pm 0.0303$ at a η value of 0.2 and $\partial\eta = \pm 0.0307$ at a η value of 0.9.

Simulations of Surface Distortions

Direct surface measurements on turbine engine hardware reported by Bons et al. [9], Taylor [10], and Tarada and Suzuki [11] all indicate an increase in surface roughness

with an increase in turbine operational hours. Measurements by Taylor [10] were made on a blade with rms roughness heights varying from 30 μm to 50 μm. His measurements also revealed that the maximum peak-to-valley height of 79 μm at the leading edge was higher than at other regions of the blade. Tarada and Suzuki [11] did measurements on industrial and aero-engine blades. They also found that the specimens measured a higher distortion at the leading edge areas with a roughness center line average as high as 85 μm.

Most surface roughness measurements were done on engine blades with very little data available in literature on measurements done on a vane and no data available for hardware used with synfuels. Bons et al. [9] performed measurements on vanes and blades of an actual land based gas turbine engine. Their findings also reported that on an average the roughness on the leading edge is greater than at the trailing edge. Their maximum roughness height (R_t) at different locations varied from 20 μm to as high at 440 μm.

For this simulation, the measurements completed by Bons et al. [9] were referenced and scaled up to match realistic vane endwall distortions. All the measurements done by Bons et al. [9] were represented in terms of center-line average roughness (R_a), rms roughness (R_q), and maximum peak to valley distance (R_t). Studies by Bogard et al. [17] showed that it is appropriate to represent uniform surface roughness in terms of equivalent sand grain roughness (k_s) instead of R_a. As this study primarily focuses on the effects of localized distortions on endwall film-cooling effectiveness the authors thought that it to be more appropriate to represent the deposit heights in terms of R_t. Bons et al. [9] measured an R_t value of 258 μm on the endwall surface and the simulated deposit heights on our endwall corresponded to 253 μm, 406 μm and 609 μm at engine scale.

Even though deposits on an actual vane endwall do not have a characteristic shape and size, a methodical approach was taken to simulate cooling hole distortions by molding specific deposits with definable shapes and sizes. The endwall deposits (shown in Figure 2.2a) were all semi-elliptical with varying minor radii (in the wall-normal direction) of 0.5D, 0.8D and 1.2D. As mentioned before, the heights at engine scale corresponded to 253 μm, 406 μm, and 609 μm respectively. The streamwise length of all deposits was 2D.

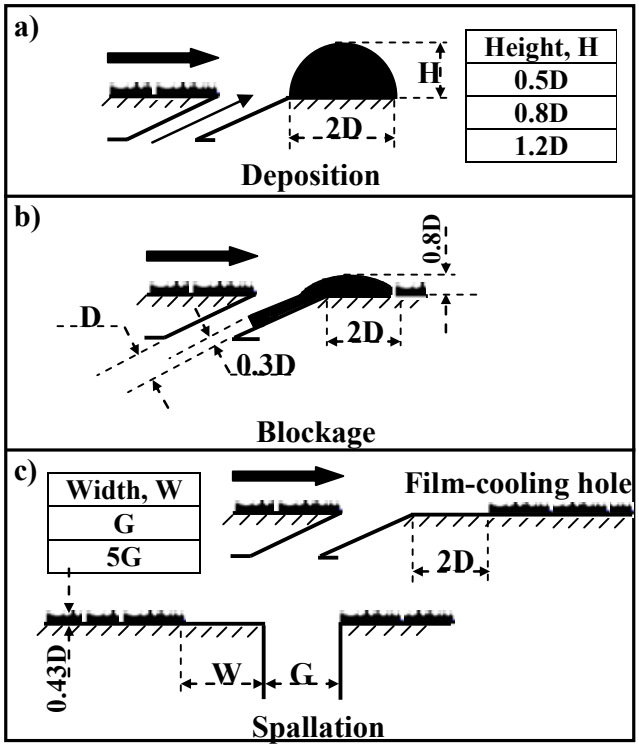

Figure 2.2. Schematic of the surface distortions simulated on the endwall surface.

The deposits were manufactured by injecting epoxy gel into a mold made of aluminum. The epoxy was allowed to dry in the mold for about 10 minutes before it was peeled out of the mold and left to dry until it was rigid enough to be placed on to the endwall. The dried epoxy was sprayed with adhesive to provide a sticky surface whereby sand was sprinkled on top of the deposit to make the surface rough. As mentioned previously the endwall surface was covered with a 36 grit sand paper [15] with an equivalent sand grain roughness (k_s) value of 0.42 mm at engine scale. Finally, the deposit was painted black and secured onto the sandpaper using a double sided tape.

The cooling hole blockages were manufactured similar to the deposits conforming to the required dimensions. Figure 2.2b shows the cross-sectional view of a blocked film-cooling hole. The holes were blocked in such a manner as to reduce the exit hole area by 25 percent. The deposit extended one hole diameter into the hole and extended two hole diameters downstream of the cooling hole exit.

The sandpaper on the endwall simulating the uniform roughness corresponded to a thickness of 0.43D or 220 μm at engine scale. In most land based gas turbine vanes and blades the TBC thickness is on the order of about 300 μm. As such, to simulate a spalled

endwall the sand paper was removed from the surface to the specified width as shown in Figure 2.2c.

Because the mainstream gas flows from the pressure side to the suction side, heavy particles in the flow deposit along the pressure side surface and in the stagnation region. Considering these findings, the film-cooling row at the leading edge region of the vane endwall was chosen to carry out deposition, blockage, and spallation studies, as shown in Figure 2.3a. In addition, deposition was also studied along the pressure side cooling holes and spallation was studied along the length of the mid-passage gap.

Discussion of Results

Two baseline cases were measured whereby these included one with upstream slot coolant and one without upstream slot coolant. For the deposition and spallation studies, the upstream slot leakage flow was present. Blockage studies were done for the case without any upstream slot coolant flow. Figures 2.3a-e show the surface distortions, the complete endwall contour and the two baseline cases for this study. Figure 2.3c-e compares lateral average effectiveness and contours of the two baseline cases only at the leading edge region. Adiabatic effectiveness levels were laterally averaged across the pitch (boxed region) from upstream of the cooling holes at a location X/C = -0.05, to a downstream location at X/C = 0.05. It is important to note that for the baseline cases the endwall surface did not have localized surface distortions but did have a uniform surface roughness covering the entire endwall surface [15]. The coolant mass flow rate for the baseline cases was set at 0.5 percent of the core flow through the film-cooling holes and 0.2 percent through the mid-passage gap. For the baseline case with the upstream slot flow, 0.75 percent of the core flow passed through the upstream slot.

There are some clear differences between the cases with and without upstream slot flow in terms of jet penetration towards the leading edge-endwall juncture as shown in Figures 2.3d and 2.3e. In the case where the slot flow is present, the cooling jets convect closer to the stagnation region. This may be due to the fact that just upstream of the holes, the endwall boundary layer is most likely ingested into the upstream slot giving only a thin boundary layer thickness approaching the holes. The thinner boundary layer minimizes any horseshoe vortex formation, which causes the coolant to be swept away

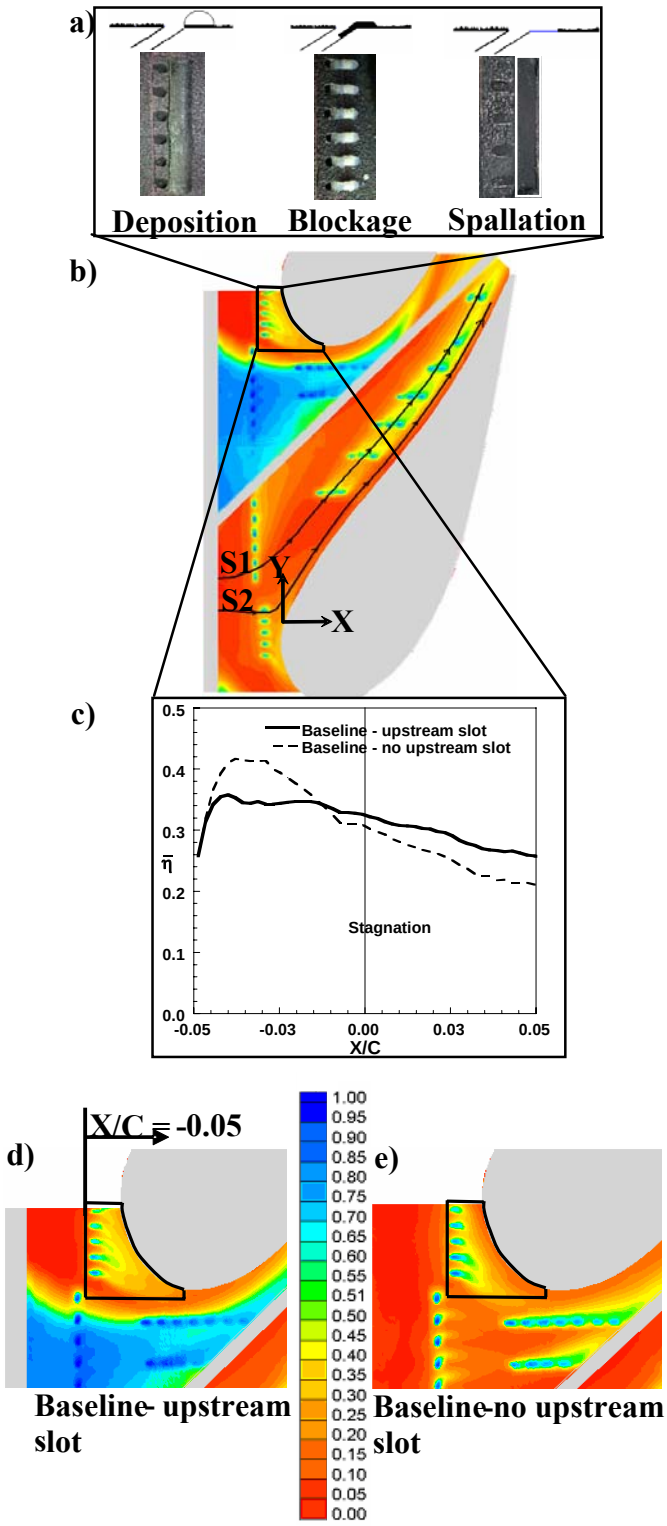

Figure 2.3. Illustrates a) surface distortions simulated at leading edge, b) baseline case with upstream slot flow, c), d), e) lateral average and effectiveness contours of the two baseline cases.

from the endwall. It can be seen in Figure 2.3e, that without the upstream slot flow, the horseshoe vortex effect is more dominant resulting in the formation of a hot band around the stagnation region.

Deposition Studies

Figures 2.4a-c show the local adiabatic effectiveness for different deposit heights at the leading edge region. For these cases, the coolant mass flowrates were 0.75 percent (M_{in}=0.3) through the upstream slot, 0.5 percent (M_{in}=1.5) through the film-cooling holes and 0.2 percent (M_{in}=0.1) through the mid-passage gap.

Figure 2.3d shows that for the baseline case without any deposition downstream, the coolant from the leading edge holes was swept around the endwall junction from the stagnation region to the suction side. By placing a deposit that is 0.5D in height (refer Figure 2.4a) downstream of the cooling row, the coolant levels were much improved. The reason for this improved cooling is attributed to the fact that the coolant impacts the raised deposit as the jet is slightly separated from the wall for the baseline case. Moreover, it is speculated that a Coanda effect further contributes to the improvement, causing the coolant to move towards the endwall surface. With the increase in deposit height to 0.8D (refer Figure 2.4b), the coolant flow stagnates and is then deflected from

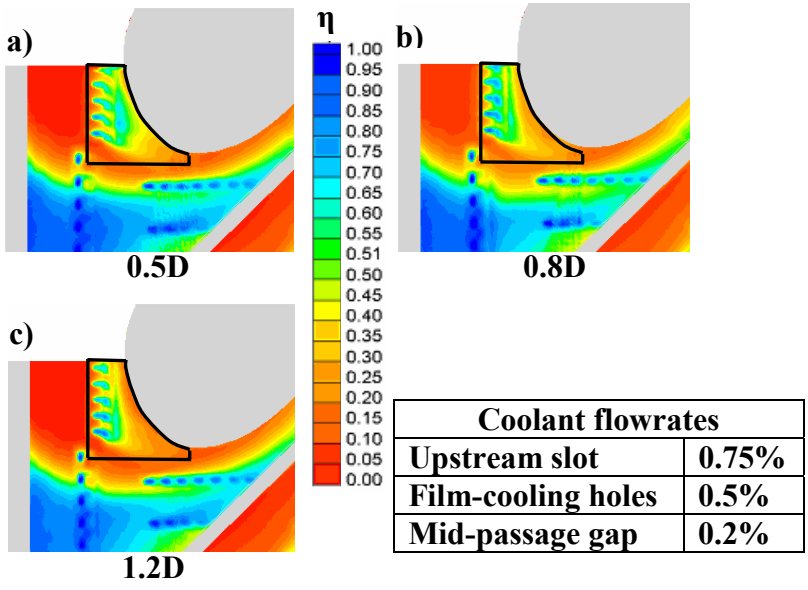

Figure 2.4. Effectiveness contours comparing the effects of different deposit heights at the leading edge region.

the surface thereby reducing the cooling effectiveness relative to that of the 0.5D case. In comparing Figures 2.4b and 2.4c it can be seen that an increase in deposit height to 1.2D brought about the same affect for both deposit heights of 0.8D and 1.2D.

The above effects can be further quantified by looking at the lateral average plots. Figure 2.5 shows the change in laterally averaged adiabatic effectiveness between the deposit cases, relative to the baseline case. Note that the values greater than one are enhancements in effectiveness levels and less than one are reductions in effectiveness levels. Effectiveness was laterally averaged across the pitch downstream of the leading edge film-cooling row as shown in Figure 2.3b and 2.3c. It can be seen that at a deposit height of 0.5D there is an overall enhancement of cooling effectiveness. The initial peak near the exit of the cooling holes is due to the obstruction and collection of the coolant flow caused by the deposit. Though there is decay in the enhancement of cooling effectiveness as the flow proceeds towards the vane-endwall junction it can be clearly seen that a deposit of height 0.5D enhances the overall cooling effectiveness. Figure 2.5 also shows that for deposits of height 0.8D and 1.2D, there is an improvement in effectiveness in the near hole region, but due to jet lift off there is a sudden decrease with reduced cooling relative to the baseline case as the coolant flows towards the vane-endwall junction.

Deposition studies were also carried out along the pressure side cooling rows. For

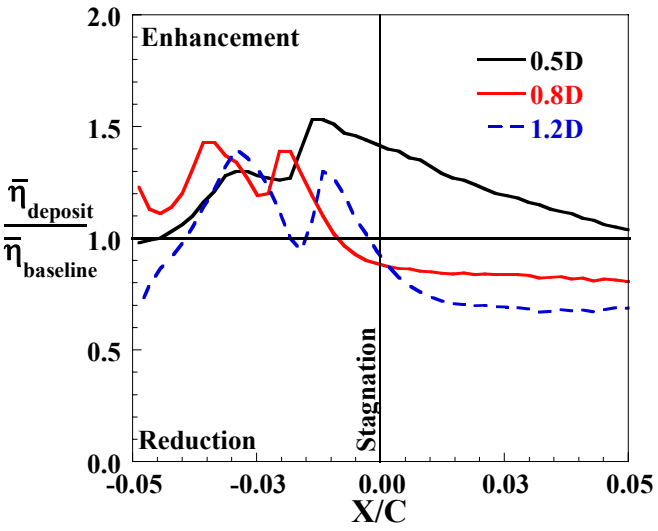

Figure 2.5. Augmentation of laterally averaged effectiveness due to different deposit heights.

these tests a constant deposit height of 0.8D was used. Figures 2.6a-c compare the adiabatic effectiveness along the pressure side cooling holes with deposits placed at the downstream, upstream and on both sides of the cooling rows (indicated in the contours with lines). Note that the upstream deposits were similar to downstream deposits (Figure 2.2a) except that the deposits were placed upstream of the cooling hole rows. Both sides refer to placing deposits on both downstream and upstream of the cooling hole rows. Downstream deposits shown in Figure 2.6a deflected the cooling jets towards the vane-endwall junction, which is the direction that the jets are directed. As the coolant is directed more towards the juncture, there is an overall reduction in the cooling downstream of each row (compare with Figure 2.3b). Upstream deposits (Figure 2.6b) tended to cause the jets to have the same trajectory, but also cause a larger reduction in film-cooling effectiveness relative to the downstream deposits. Similar to these results, placing deposits on both sides of the cooling rows (Figure 2.6c) resulted in the bulk of the coolant getting even more streamlined towards the vane-endwall junction. From Figure 2.3b it can be seen that for the baseline case, the coolant from the pressure side flowed towards the suction side increasing effectiveness levels downstream of the cooling rows. By placing deposits in this region the coolant was redirected towards the vane-endwall junction causing a reduction in the effectiveness levels downstream of the cooling rows. Though, deposits at every location deflected the coolant, upstream deposition was found to cause the most severe reduction in adiabatic effectiveness.

The above effects can be quantified by comparing the laterally averaged adiabatic effectiveness. In this region effectiveness was laterally averaged streamwise as shown in Figure 2.7. Shown in Figure 2.7 are the laterally averaged local blowing ratios for each row of holes along the pressure side. Note that CFD results were used to quantify the local coolant flows from each cooling hole and the local static pressure was used to calculate the local freestream velocity that was used in the blowing ratio definition. It was seen that deposits upstream of the holes and on both sides of the cooling holes caused similar and higher degradation than deposits placed downstream of the cooling rows. Note that the deposits were placed on the first four cooling hole rows, but the effects are present on all the rows on the pressure side. It can be concluded that upstream deposition resulted in higher degradation than deposits at the downstream of the film-

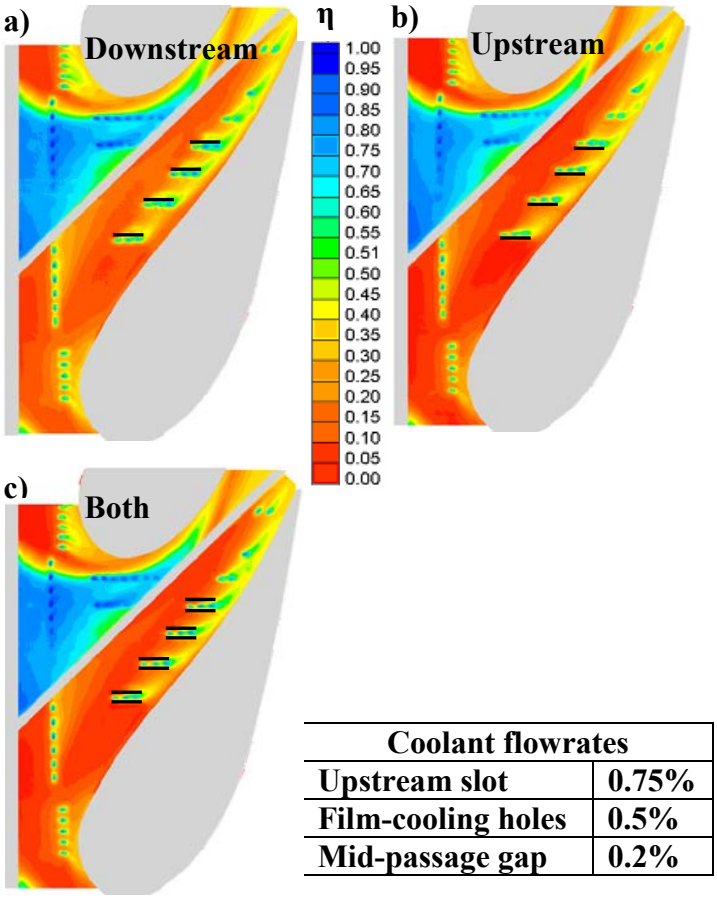

Coolant flowrates	
Upstream slot	0.75%
Film-cooling holes	0.5%
Mid-passage gap	0.2%

Figure 2.6. Contours comparing the effects of pressure side deposition a) downstream, b) upstream, and c) downstream and upstream of holes.

cooling holes. This conclusion can be generated because the deposits on both upstream and downstream have nearly the same degradation as the upstream deposits alone.

As the coolant jets were directed towards the pressure-surface endwall junction, it was important to quantify the change in adiabatic effectiveness along flow streamlines passing through the cooling holes and also along the pressure-surface endwall junction. Figures 2.8a-b show the variation of adiabatic effectiveness along the flow streamlines at different film-cooling flowrates with deposits placed on both sides of the cooling rows. Variation in adiabatic effectiveness was measured along two streamlines; S1 and S2 as shown in Figure 2.3b. The flow streamlines were computationally predicted at 2 percent span from the endwall surface using FLUENT 6.1.2. Figure 2.8a shows that by placing deposits on both upstream and downstream locations the adiabatic effectiveness levels decreased by about 50 percent along S1 for 0.5 percent film-cooling mass flowrate. A similar effect was seen for 0.75 (M_{in}=2.2) and 0.9 percent (M_{in}=2.7) flowrate through the

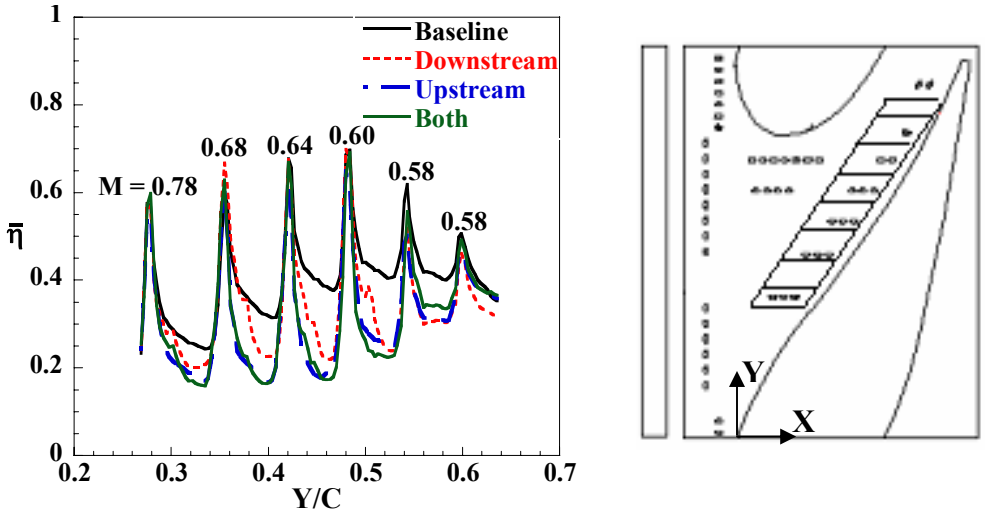

Figure 2.7. Laterally averaged effectiveness along pressure side (boxed region on the right shows the averaged area).

film-cooling holes though there was a higher reduction at a mass flowrate of 0.9 percent.

As mentioned earlier, in the presence of deposits on both sides of the cooling rows the coolant was streamlined towards the vane-endwall junction. This was further quantified by measuring the adiabatic effectiveness along streamline S2 as shown in Figure 2.8b. It was seen that there was a two-fold increase in adiabatic effectiveness levels in the presence of deposits along S2 for the nominal flow rate of 0.5 percent through the film-cooling holes. A further increase in coolant mass flowrate to 0.75 and 0.9 percent increased the effectiveness levels nominally by 25 percent. Hence, it was seen that deposition on pressure side decreased effectiveness downstream of the cooling rows, but increased the effectiveness levels along the vane-endwall junction.

Hole Blockage Studies

Partial blockages of film-cooling holes were simulated at the leading edge film-cooling row as mentioned previously. Tests were carried out by sequentially blocking each one of the five film-cooling holes in the stagnation region though results are presented only for 1 hole, 2 hole and 5 hole blockages. Similar to the other cases, the coolant mass flow-rate for the baseline case for this study was set at 0.5 percent film-cooling holes, 0.2 percent mid-passage gap, and no coolant injected through the upstream slot. There was no flow through the upstream slot as it was important to isolate any effect of the upstream flow at the leading edge cooling near stagnation region.

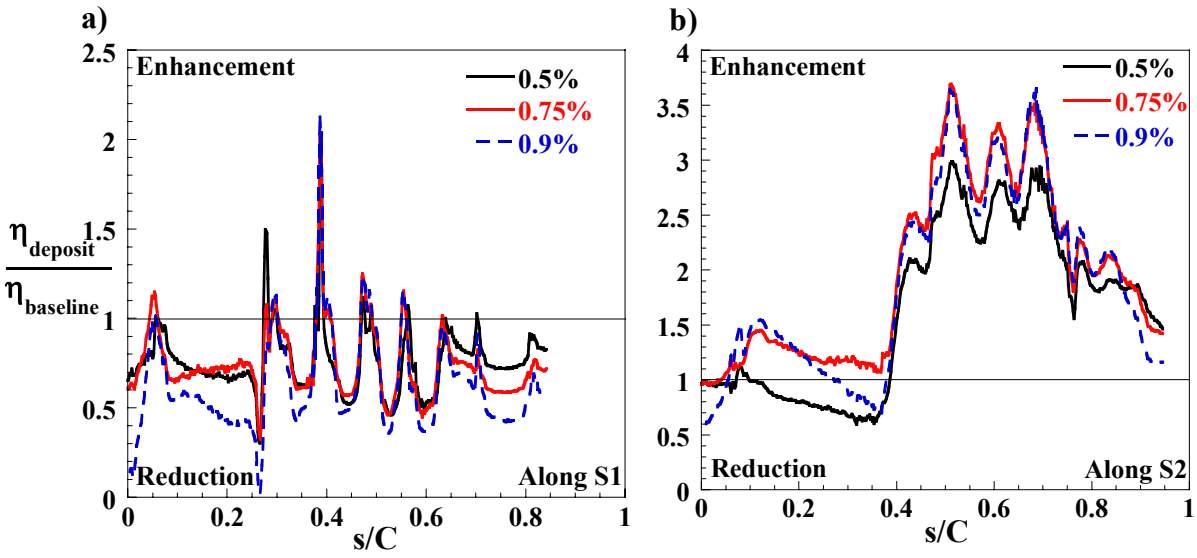

Figure 2.8. Change in adiabatic effectiveness levels along streamlines S1 and S2 (refer Figure 3b) for deposits on both sides of the cooling rows.

Figures 2.9a-c compare the adiabatic effectiveness contours with different number of holes partially blocked. The blockage extended one cooling hole diameter into the film-cooling holes with a net flow area reduction of 25 percent at the cooling hole exit. Note that the same pressure ratio was used for the baseline and for the cases with blocked holes. Indicated with boxes in Figures 2.9a-c are the holes that are blocked. It can be seen that there is a dramatic decrease in effectiveness level with the increase in the number of holes being blocked as the coolant from the holes cease to flow onto the endwall. The main reason for this is that when a hole is partially blocked, the momentum of the jet and the trajectory of the jet is increased, which causes the coolant to exit at a higher exit angle promoting separation. In this particular test the coolant from the partially blocked hole tended to flow directly into the mainstream resulting in lower adiabatic effectiveness on the endwall surfaces.

Figure 2.10 compares the degradation in laterally averaged effectiveness due to film-cooling hole blockage. It can be seen that with the increase in the number of holes being partially blocked from 1 to 5 the laterally averaged effectiveness degrades from about 20 percent to about 50 percent of the baseline, respectively. It can be also seen that at upstream of the leading edge cooling holes (at X/C = -0.05) the effectiveness levels are higher due to the change in coolant jet trajectory caused by hole blockages. The study done by Bunker [16] showed a similar reduction of about 40 percent in the centerline adiabatic effectiveness for a row of blocked film-cooling holes on a flat plate.

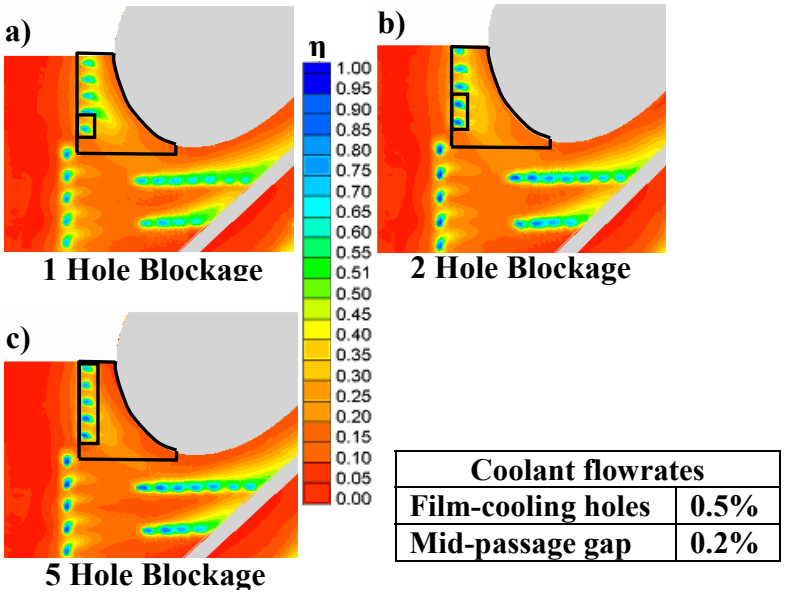

Figure 2.9. Contours showing the effect of film-cooling hole blockage on adiabatic effectiveness.

Spallation Studies

TBC spallation was simulated downstream of the leading edge film-cooling row and also along the mid-passage gap. The coolant mass flow rates for the baseline case for this study were set at 0.75 percent upstream slot, 0.5 percent film-cooling holes, and 0.2 percent mid-passage gap. Figures 2.11a-b compare the contours of adiabatic effectiveness of a spalled leading edge surface at film-cooling mass flow rates of 0.5 and 0.9 percent.

The spalled endwall surface downstream of the cooling holes caused the coolant to flow over a forward facing step. This resulted in flow recirculation and prevented the coolant from sweeping across the vane-endwall junction. It was seen that at a mass flowrate of 0.5 percent although the near hole region is sufficiently cooled, effectiveness levels along the vane-endwall junction were relatively lower than the baseline case. By increasing the coolant mass flowrate to 0.9 percent the effectiveness levels were further reduced due to the combined effect of spallation and coolant jet lift off the surface.

Figure 2.12 compares the degradation in laterally averaged effectiveness due to spallation at the leading edge region. It can be seen that at a mass flowrate of 0.5 percent, the near hole regions have similar effectiveness levels as the baseline, but effectiveness levels decrease by about 20 percent near the vane endwall region. At higher mass

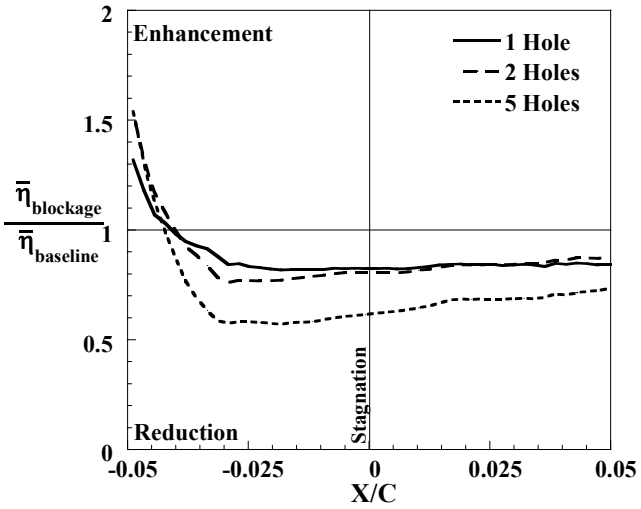

Figure 2.10. Laterally averaged effectiveness showing the effect of hole blockages at the leading edge.

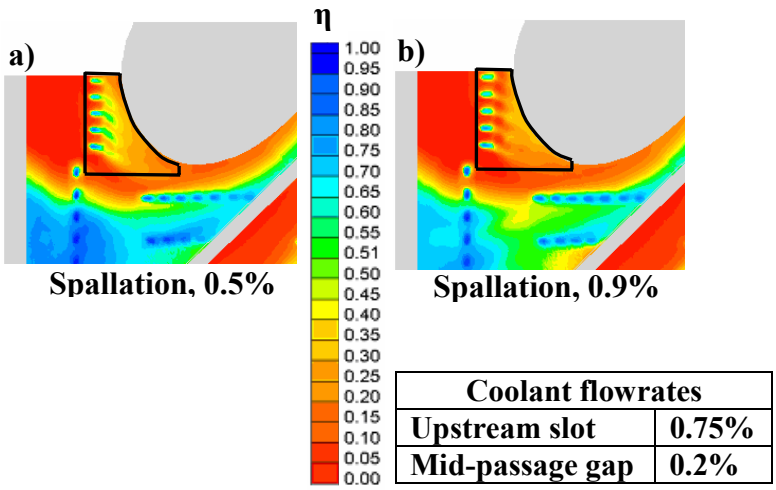

Figure 2.11. Effectiveness contours showing the effect of leading edge spallation at 0.5% and 0.9% film-cooling flowrate.

flowrate of 0.9 percent, due to jet liftoff, there is a reduction of about 50 percent downstream of cooling holes. Effectiveness levels increase near the junction due to jet reattachment, though these levels are still lower than the levels occurring in the baseline case. Note that the cooling holes lie between -0.05<X/C<-0.034 and the spalled surface extends from X/C = -0.034 to X/C = -0.02.

Figures 2.13a-b compare the adiabatic effectiveness levels of the baseline and an endwall surface spalled five gap widths (5G) along the mid-passage gap. The study by Cardwell et al. [15], showed that due to the presence of the mid-passage gap, coolant from the upstream slot flows towards the suction side negating the need for endwall

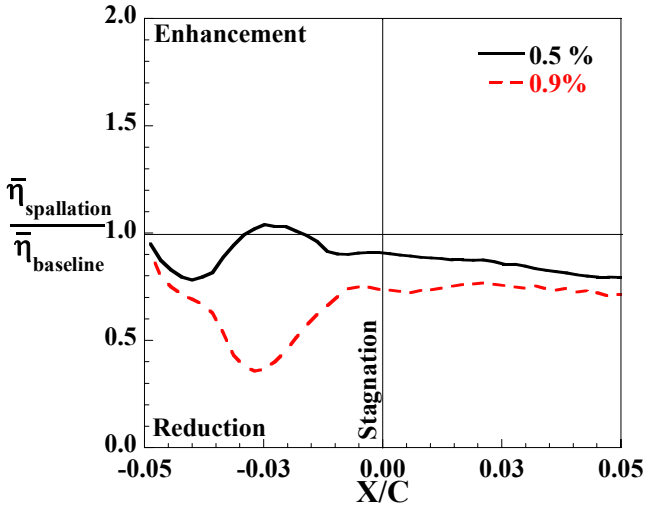

Figure 2.12. Laterally averaged effectiveness showing the effect of leading edge spallation at different film-cooling flowrates.

cooling in that region. Even though the surface was spalled along the mid-passage gap there seemed to be no effect on the overall endwall effectiveness resulting from the large coolant flow over this region. It can be seen from Figure 2.13 a-b that the coolant from the upstream slot has the same coverage area and there is no significant reduction in adiabatic effectiveness levels. For the spallation studies along mid-passage gap, tests were also carried out for smaller spalled regions. These tests also showed that spallation along mid-passage gap had little effect on endwall effectiveness.

Summary of Cooling Reductions

The two factors that are important to quantify the effects of surface distortions are the film-cooling effectiveness levels and heat transfer coefficients. This study focused primarily on film-cooling effectiveness alterations due to surface distortion factors. It is important to understand which surface distortion brought about the maximum reduction in cooling effectiveness. This was done by calculating the percent reduction in area-averaged effectiveness. Figure 2.14 shows the combined effectiveness reduction for each endwall distortion study. This plot allows one to assess which is the most degrading effect.

Deposition studies had varied results. Deposits improved effectiveness at the leading edge whereas along the pressure side deposits resulted in reducing the film-cooling effectiveness. A very interesting result was observed that deposits directly

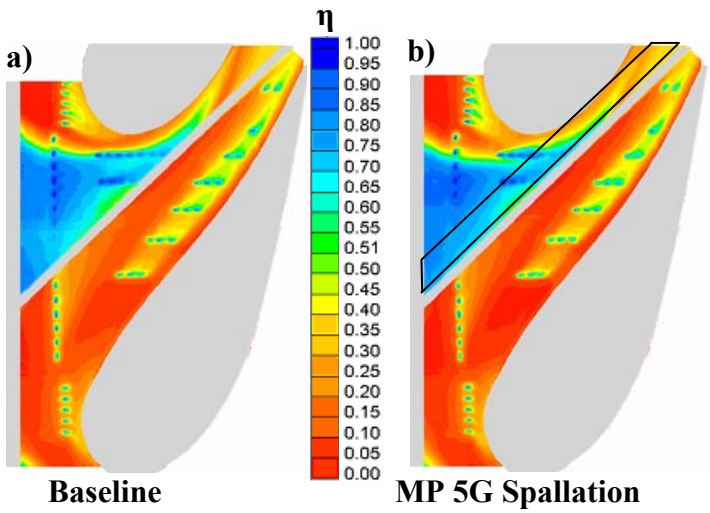

Figure 2.13. Contours showing the effect of spallation along mid-passage on endwall adiabatic effectiveness.

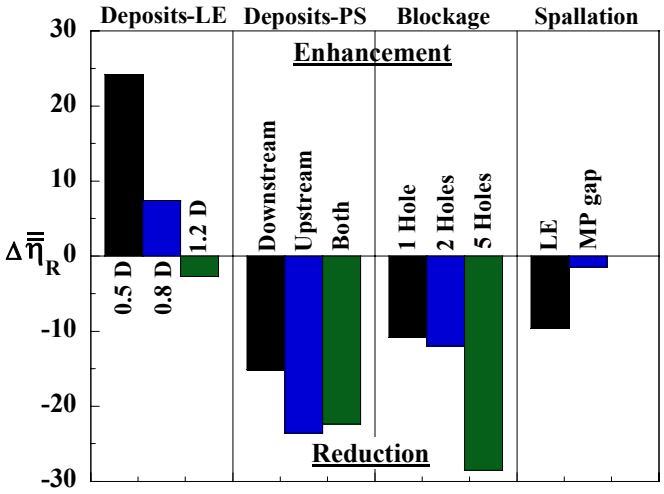

Figure 2.14. Comparison of percent reduction on area-averaged adiabatic effectiveness due to surface distortions.

downstream of the leading edge cooling row enhanced film-cooling effectiveness at lower deposit heights (0.5D and 0.8D) and caused little reduction in effectiveness levels at a deposit of height 1.2D. Along the pressure side it was seen that depositions typically degraded effectiveness levels downstream of the cooling rows by redirecting the coolant towards the vane-endwall junction. The reason for the degradation along the pressure side is because the jets are more attached to the surface and are easily deflected by deposits.

The maximum reduction in cooling effectiveness at the leading edge region was caused by film-cooling hole blockages. At a mass flowrate of 0.5 percent, with the increase in number of holes being blocked the percent reduction in cooling effectiveness

also increased. Blocking one and two holes brought similar effectiveness reductions, but with five holes blocked the effectiveness was significantly reduced by about 30 percent. This reduction in effectiveness due to blockages was expected given the lack of jet penetration.

Spallation along the mid-passage gap had little to no effect on the overall endwall effectiveness, but spallation downstream of the leading edge film-cooling row reduced the cooling effectiveness by about 10 percent.

Conclusions

Measurements of adiabatic effectiveness were presented for an endwall surface with simulated surface distortions namely, surface deposition, film-cooling hole blockage, and TBC spallation. When the effects of these distortions were compared at the leading edge region, it was found that partial hole blockage and TBC spallation caused a higher reduction in adiabatic effectiveness levels than surface deposition.

Near hole depositions were studied with varying deposit heights and it revealed very interesting results. For a smaller deposit height of 0.5D the overall film-cooling effectiveness downstream of the film-cooling row was enhanced by about 25 percent. These deposits tended to deflect the coolant towards the endwall surface. With an increase in deposit height to 1.2D the coolant jet tends to lift off lowering the film-cooling effectiveness. Deposition along the pressure side lowered the effectiveness between successive cooling rows, but enhanced the effectiveness along the vane-endwall junction.

Hole blockage studies showed that partially blocked holes have the greatest detrimental effect on degrading film-cooling effectiveness downstream of a film-cooling row. At low blowing ratios, partially blocking five film-cooling holes reduced film-cooling effectiveness by about 30 percent and blocking a single hole resulted in a reduction in effectiveness of about 10 percent. Spallation studies conducted at the leading edge film-cooling row showed a reduction in effectiveness of about 10 percent. Past studies have shown that spallation near film-cooling holes is a significant form of surface distortion and hence it is very important to consider its effect while designing endwall cooling arrangements. Spallation was also studied along the mid-passage gap

which showed very little to no effect in endwall cooling effectiveness.

This study has shown the effects that cooling hole blockages can have on reducing endwall effectiveness levels. These effects should be considered in determining improved film-cooling designs so that partial hole blockages can be avoided on turbine components.

Acknowledgments

This publication was prepared with the support of the US Department of Energy, Office of Fossil Fuel, and National Energy Technology Laboratory. However, any opinions, findings, conclusions, or recommendations expressed herein are solely those of the authors and do not necessarily reflect the views of the DOE. The authors would also like to specially thank Nick Cardwell for building and instrumenting the test section. The authors also thank Mike Blair (Pratt & Whitney), Ron Bunker (General Electric), and John Weaver (Rolls-Royce) for their input on the modeling of realistic turbine features.

Attribution

This paper was co-authored with Dr. Karen Thole. Her role was:

Co-author – paper 2

Name – Dr. Karen A. Thole

Department – Mechanical Engineering

Degree – Ph.D

Relationship – Chair and primary advisor

Role - Dr. Thole served as my dissertation chair and advised me through my Ph.D and on all the work presented in this dissertation.

Nomenclature

C	true chord of stator vane
D	diameter of film-cooling hole
G	mid-passage gap width
k_s	equivalent sand grain roughness
L	length of mid-passage gap

LE leading edge

M local mass flux/blowing ratio, $M = \rho_j U_j / \rho_\infty U_\infty$

M_{in} blowing ratio based on inlet mainstream velocity

MP mid-passage

P vane pitch; hole pitch

PS pressure side

Re_{in} Reynolds number defined as $Re_{in} = CU_{in} / \nu$

R_a center-line average roughness

R_q rms roughness

R_t maximum peak to valley distance

s distance measured along a streamline

S span of stator vane

T temperature

X,Y,Z local coordinates

U velocity

Greek

η adiabatic effectiveness, $\eta = (T_\infty - T_{aw}) / (T_\infty - T_c)$

$\overline{\eta}$ laterally averaged effectiveness

$\overline{\overline{\eta}}$ area-averaged effectiveness

$\Delta\overline{\overline{\eta}}_R$ percent reduction in area-averaged effectiveness,

$\Delta\overline{\overline{\eta}}_R = [(\overline{\overline{\eta}}_{effect} - \overline{\overline{\eta}}_{baseline}) / \overline{\overline{\eta}}_{baseline}] \times 100$

ν kinematic viscosity

Subscripts

aw adiabatic wall

c coolant conditions

in inlet conditions

j coolant flow through film-cooling holes

∞ local freestream conditions

R reduction

Overbar

– lateral average

= area average

References

[1] Wenglarz, R. A., 1985, "Deposition, Erosion, and Corrosion Protection for Coal-Fired Gas Turbines," 85-IGT-61.

[2] Wenglarz, R. A., Nirmalan, N. V., and Daehler, T. G., 1995, "Rugged ATS Turbines for Alternate Fuels," 95-GT-73.

[3] Decorso, S. M., Newby, R. A., Anson, D., Wenglarz, R. A., and Wright, I. G., 1996, "Coal/Biomass Fuels and the gas Turbine: Utilization of Solid Fuels and their Derivatives," 96-GT-76.

[4] Moses, C. A., and Bernstein, H. L., 1996, "Fuel-Specification Considerations for Biomass Pyrolysis Liquids to be used in Stationary Gas Turbines," 96-GT-406.

[5] Wenglarz, R. A., 1992, "An Approach for Evaluation of Gas Turbine Deposition," *Journal of Engineering for Gas Turbines and Power*, Vol. 114, pp. 230 – 234.

[6] Bons, J. P., Corsby, J., Wammack, J. E., Bentley, B. I., and Fletcher, T. H., 2005, "High Pressure Turbine Deposition in Land Based Gas Turbines from Various Synfuels," GT2005-68479.

[7] Bornstein, N. S., 1996, "Reviewing Sulfidation Corrosion – Yesterday and Today," *Journal of the Minerals, Metals, and Materials Society*, 48(11), 37-39.

[8] Wright, I. G., Leyens, C., and Pint, B. A., 2000, "An Analysis of the Potential for

Deposition, Erosion, or Corrosion in Gas Turbines Fueled by the Products of Biomass Gasification or Combustion," 2000-GT-0019.

[9] Bons, J. P., Taylor, R. P., McClain, S. T., and Rivir, R. B., 2001, "The Many Faces of Turbine Surface Roughness," *Journal of Turbomachinery*, Vol.123, pp. 739-748.

[10] Taylor, R. P., 1990, "Surface Roughness Measurements on Gas Turbine Blades," *Journal of Turbomachinery*, Vol.112, pp. 175-180.

[11] Tarada, F., and Suzuki, M., 1993, "External Heat Transfer Enhancement to Turbine Blading Due to Surface Roughness," 93-GT-74.

[12] Goldstein, R. J., Eckert, E. R. G., and Chiang, H. D., 1985, "Effect of Surface Roughness on Film-Cooling Performance," *Journal of Engineering for Gas Turbines and Power*, Vol. 107, pp. 111-116.

[13] Schmidt, D. L., Sen, B., and Bogard, D. G., 1996, "Effects of Surface Roughness on Film-Cooling," 96-GT-299.

[14] Barlow, D. N., and Kim. Y. W., 1995, "Effect of Surface Roughness on Local Heat Transfer and Film-Cooling Effectiveness," 95-GT-14.

[15] Cardwell N. D., Sundaram, N., and Thole, K. A., 2005, "Effects of Mid-Passage Gap, Endwall Misalignment, and Roughness on Endwall Film-Cooling," *Journal of Turbomachinery*, Vol. 128, pp. 62-70.

[16] Bunker, R. S., 2000, "Effect of Partial Coating Blockage on Film Cooling Effectiveness," 2000-GT-0244.

[17] Bogard, D. G., Schmidt, D. L., and Tabbita. M., 1998, "Characterization and

Laboratory Simulation of Turbine Airfoil Surface Roughness and Associated Heat Transfer," *Journal of Turbomachinery*, Vol. 120, pp. 337-342.

[18] Ekkad, S., and Han, J. C., 1997, "Detailed Heat Transfer Distributions on a Cylindrical Model with Simulated TBC Spallation," AIAA Paper 97-0595.

[19] Ekkad, S. V., and Han. J. C., 2000, "Film Cooling Measurements on Cylindrical Models with Simulated Thermal Barrier Coating Spallation," *Journal of Thermophysics and Heat Transfer*, 14, No. 2, pp. 194-200.

[20] Colban, W. F., Thole, K. A., and Zess, G., 2002, "Combustor-Turbine Interface Studies: Part 1: Endwall Measurements," *Journal of Turbomachinery*, Vol. 125, pp. 193-202.

[21] Colban, W. F., Thole, K. A., and Zess, G., 2002, "Combustor-Turbine Interface Studies: Part 2: Flow and Thermal Field Measurements," *Journal of Turbomachinery*, Vol. 125, pp. 203-209.

[22] Knost, D. G., and Thole, K. A., 2004, "Adiabatic Effectiveness Measurements of Endwall Film-Cooling for a First Stage Vane," *Journal of Turbomachinery*, Vol. 127, pp. 297-305.

[23] Knost, D. G., and Thole, K. A., 2003, "Computational Predictions of Endwall Film-Cooling for a First Stage Vane," GT2003-38252.

[24] Ethridge, M. I., Cutbirth, J. M., and Bogard, D. G., 2000, "Scaling of Performance for Varying Density Ratio Coolants on an Airfoil with Strong Curvature and Pressure Gradient Effects," *Journal of Turbomachinery*, Vol. 123, pp. 231-237.

[25] Moffat, R. J., 1988, "Describing the Uncertainties in Experimental Results," *Experimental Thermal and Fluid Science*, Vol.1, pp. 3-17.

Paper 3:
Effects of Deposits on Film-Cooling of a Vane Endwall Along the Pressure Side

Recommended for publication in the *ASME Journal of Turbomachinery* *

Abstract

Film-cooling is influenced by surface roughness and depositions that occur from contaminants present in the hot gas path, whether that film-cooling occurs on the vane itself or on the endwalls associated with the vanes. Secondary flows in the endwall region also affect the film-cooling performance along the endwall. An experimental investigation was conducted to study the effect of surface deposition on film-cooling along the pressure side of a first-stage turbine vane endwall. A large-scale wind tunnel with a turbine vane cascade was used to perform the experiments. The vane endwall was cooled by an array of film-cooling holes along the pressure side of the airfoil. Deposits having a semi-elliptical shape were placed along the pressure side to simulate individual row and multiple row depositions. Results indicated that the deposits lowered the average adiabatic effectiveness levels downstream of the film-cooling rows by deflecting the coolant jets towards the vane endwall junction on the pressure side. Results also indicated that there was a steady decrease in adiabatic effectiveness with a sequential increase in the number of rows with the deposits.

* Co-author: Dr. Michael Barringer, Dr. Karen A. Thole, Mechanical Engineering Department, Virginia Tech

Introduction

The flow along the endwall in a first stage turbine vane is influenced by both roughness levels present on the surface and vortices that extend from the airfoil leading edge region to the trailing edge region. These secondary flows impact the endwall film-cooling effectiveness levels by lifting coolant jets from the endwall surface and directing them towards the vane suction side. This jet lift off results in low adiabatic effectiveness levels along the pressure side of the vane endwall, which ultimately results in a weak layer of coolant shielding the metal hardware from the hot mainstream gases. Continuous exposure of the endwall to these extreme conditions reduces the operability and life of the hardware. The adiabatic effectiveness is a measure of the film-cooling potential along a surface downstream of the coolant injection location.

Film-cooling performance is also affected by surface deposits formed by small particles and unburned combustion products adhering to the turbine hardware. Modern gas turbines are being developed to have the capability of operating with fuels other than natural gas. Coal derived synthetic gas is one such alternative fuel which is comparable to natural gas in terms of performance, however, it can have contaminants. The size of the contaminant particles can vary greatly from 5-60 μm [1]. While the smaller particles tend to follow the mainstream flow path, the larger particles may not due to their larger momentum and can deposit on the pressure side of the vane and endwall surfaces [2]. These larger particles when in molten form tend to quench near cooled regions on turbine component surfaces, for example near a film-cooling hole or slot, thus leading to film-cooling depositions.

This study is aimed at understanding the effects of surface deposition and deposit location on the adiabatic effectiveness levels along the pressure side of a vane endwall. In particular, the work presented in this paper is aimed at understanding the row-by-row interaction due to depositions on the endwall surface. The effects of placing deposits upstream and downstream of single and multiple cooling hole rows were investigated.

Relevant Past Studies

A number of studies in the literature have documented the effects of using alternative fuels on the surface contamination of turbine engine components. Studies

have also specifically focused on determining the effects of surface roughness and surface depositions on film-cooling performance. The current literature includes studies that have investigated the effects of using coal and other solid fuels on ash and other contaminant levels on deposition, corrosion, and erosion.

A study by Wenglarz et al. [3] showed that high levels of ash up to 40 tons per year can enter a turbine. DeCorso et al. [4] found that most coal derived fuels, even after conversion and purification, had higher levels of impurities than natural gas. They found that sulfur levels in natural gas are about 9 ppm, while for coal derived fuels the sulfur levels are approximately 900 ppm. Moses and Bernstein [5] found that a fuel burning with 0.5% ash results in about 1.5 tons of ash per day flowing through the turbine engine. In a separate study by Wenglarz [6] it was reported that the mass fraction of the ash particles that adhere to the engine surface and contribute to deposit build up was 0.06 with an average particle diameter of 9 μm. A recent study by Bons et al. [6] investigated the effect of ash deposits present in coal fuels using an accelerated deposition test facility. Their tests were conducted with ash particles slightly higher in mean mass diameter (12.3 μm) than those found in coal fuels. For a test duration of three hours, they found the net particle loading to be 165 ppmw-hr (parts per million by weight per hour) which resulted in an average deposit thickness of 1.3 mm.

Deposition of contaminants and other particulate matter present in the mainstream gas takes place through an impingement process in which the particles make contact with and adhere to the surface. The first row of vanes is directly subjected to the combustion products that exit the combustion chamber. This direct exposure results in an elevated level of particulate deposition via impingement [7]. The mechanism for this can be attributed to particle break up and redistribution upon impacting the component wall surface [8]. More specifically, the leading edge film-cooling regions on a turbine vane endwall are most prone to this deposition phenomenon since this is the first relatively cold surface the hot mainstream flow encounters as it enters the turbine. Bons et al. [9] showed through their turbine surface measurements that the leading edge region will have the greatest degradation. Other turbine component measurements by Taylor [10] and Tarada and Suzuki [11] revealed that all regions of a turbine blade and vane are prone to deposition and surface roughening at varying levels.

Bonding of ash and other contaminants to turbine component surfaces is also dependent on the properties of the hardware. Some studies have been performed that specifically report the effects of surface roughness on film-cooling. Goldstein et al. [12] placed cylindrical roughness elements at the upstream and downstream location of film-cooling holes on a flat plate. They observed that at low blowing rates, there is a decrease in adiabatic wall effectiveness by 9-20% over a smooth surface. However, at higher blowing rates they observed an enhancement of 40-50% in cooling performance. Schmidt et al. [13] did a similar study using conical roughness elements. They found a higher degradation of film-cooling effectiveness at lower momentum flux ratios than at higher momentum flux ratios. Barlow and Kim [14] studied the effect of a staggered row of roughness elements on adiabatic effectiveness. They found that roughness degraded cooling effectiveness compared to a smooth surface and that smaller elements caused a greater reduction than larger elements.

In addition to these studies, Cardwell et al. [16] showed that an endwall surface with uniform roughness decreased cooling effectiveness at higher blowing ratios but at lower blowing ratios there was no significant change. More recently Sundaram and Thole [16] conducted a study to investigate the effect of localized deposition at the leading edge of a vane endwall. Their results indicated that deposits of smaller heights placed in the leading edge region enhanced the adiabatic effectiveness levels. They also found that the adiabatic effectiveness levels degraded with the increase in deposit height.

In summary, the current literature contains few studies that have focused on understanding how surface deposition affects the film-cooling performance along an endwall in a turbine. The results from this study shed some new light onto the flow physics associated with film-cooling along the pressure side of turbine vane endwall and thus allow improvements to be made in endwall designs.

Experimental Methodology

The cascade test section was placed in the closed loop wind tunnel facility shown in Figure 3.1. The flow encounters an elbow downstream of the fan and passes through a primary heat exchanger used to cool the bulk flow. The flow is then divided into three channels including the center passage and two cooled secondary passages located above

and below the test section. Note that only the top secondary passage was used for this study. The primary core flow, located in the center passage, passes through a heater bank where the air temperature is increased to about 60°C. The secondary flow, in the outer passage, was cooled to 20°C, thereby maintaining a temperature difference of 40°C between the primary and secondary flows. The secondary flow provided the coolant through the film-cooling holes located on the endwall within the test section. For all of the tests carried out in this study a density ratio of 1.1 was maintained between the coolant and mainstream flows. Since the density ratios were not matched to that of the engine, the velocity ratios for the cooling holes were significantly higher than those found in an engine for the same mass flux or momentum flux ratios. In this study momentum flux ratios were set relevant to engine conditions as previous studies have shown that momentum flux ratios scale the jet lift-off well for flat plate cooling.

Downstream of the flow and thermal conditioning section, is the test section that consists of two full vane passages with one center vane and two half vanes. Table 3.1 provides a description of the turbine vane geometry and operating conditions. The vane geometry used in the current study is a commercial first-stage vane previously described by Radomsky and Thole [17]. A detailed description of the endwall construction has been previously described by Knost and Thole [18] and Sundaram and Thole [16], who used the exact same film-cooling geometries that were used for this study. The endwall of the vane was constructed of 1.8 cm thick, low-density foam having a low thermal conductivity of 0.033 W/m·K, which was mounted on a 1.2 cm thick Lexan plate. The

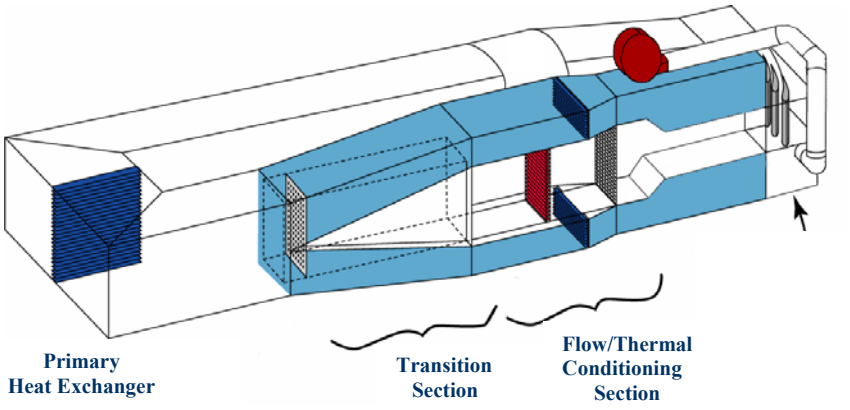

Figure 3.1. Illustration of the wind tunnel facility.

Table 3.1. Geometric and flow conditions

Scaling factor	9
Scaled up chord length (C)	59.4 cm
Pitch/Chord (P/C)	0.77
Span/Chord	0.93
Hole L/D	8.3
Re_{in}	2.1×10^5
Inlet and exit angles	0° & 72°
Inlet, exit Mach number	0.017, 0.085
Inlet mainstream velocity	6.3 m/s
Upstream slot width	0.024C

cooling hole pattern on the endwall was cut with a five-axis water jet to ensure precision and integrity. The endwall surface was covered with 36 grit sandpaper to simulate a uniform surface roughness. The sandpaper corresponded to an equivalent sand grain roughness of 420 μm at the engine scale. In addition to the surface roughness, the endwall also simulated a combustor-turbine interface gap upstream of the vane and a vane-to-vane interface gap between the vanes. In all, the endwall used in this study simulated the geometries and surface conditions of an actual engine.

The inlet turbulence intensity and length scales were measured to be 1.3 percent and 4 cm respectively. These tests were carried out at a low turbulence intensity of 1.3 percent to isolate the effects of deposits on endwall adiabatic effectiveness levels. For every test condition the dimensionless pressure coefficient distribution was verified to ensure periodic flow through the passages. To set the coolant mass flow rate through the film-cooling holes a global blowing ratio was calculated using an inviscid blowing ratio along with a global discharge coefficient, C_D, that was obtained from CFD studies reported by Knost and Thole [20].

Instrumentation and Measurement Methods

A FLIR P20 infrared camera was used to spatially resolve adiabatic wall temperatures along the vane cascade endwall. Measurements were taken at six different viewing locations to ensure that the entire endwall surface was thermally mapped. The camera was placed perpendicular to the endwall surface at a distance of 55 cm from the endwall. Each picture covered an area of 24 cm by 17 cm, with the area being divided into 320 by 240 pixel locations. The spatial integration circle of the camera had a

diameter equal to 0.614 mm (0.16 hole diameters). Thermocouples were also placed on the endwall surface at different locations to directly measure the temperature and to post calibrate the infrared images. The post calibration process involved setting the surface emissivity at a constant value of 0.92 and the background temperature (~ 45ºC) was then adjusted until the temperatures from the infrared images were within 0.05ºC of the corresponding thermocouple data. Six camera images were taken at each of the viewing locations and an in-house Matlab program was used to obtain a single averaged picture. The same program was also used to assemble the averaged pictures at all locations to give a complete temperature distribution along the passage endwall.

Freestream temperatures were measured at multiple locations along the vane pitch and the average was determined by using a thermocouple rake consisting of three thermocouples along the span. It was found that the variations along the pitch were less than 0.2ºC and along the span they were less than 1.5ºC. Voltage outputs from the thermocouples were acquired using a 32 channel National Instruments data acquisition module and a 11-bit digitizing card. All temperature data was acquired and compiled after the system reached a steady state operating condition.

The one-dimensional conduction correction method described by Ethridge et al. [21] was applied in a point-by-point manner to all adiabatic effectiveness measurements made on the endwall surface. This correction involved measuring the endwall surface effectiveness without flow passing through the film-cooling holes. This required the film-cooling holes to be blocked on the endwall in the passage under study, however similar film-cooling flow rates were maintained through the adjacent passage to insure the correct boundary condition was established under the endwall. The resulting correction in adiabatic effectiveness, η_o, was found to be 0.16 at the entrance of the vane passage for a η_{meas} value of 0.9, and 0.02 at the exit of the vane passage for a η_{meas} value of 0.2.

Experimental Uncertainty

An uncertainty analysis was performed on the adiabatic effectiveness measurements using the partial derivative method described by Moffat [22]. The precision uncertainty was determined by taking the standard deviation of six

measurement sets of IR camera images with each set consisting of six images. The precision uncertainty of the measurements was found to be ±0.013°C. The bias uncertainty was ±1.0°C based on the camera specifications supplied by the manufacturer. The bias uncertainty of the thermocouples was ±0.5°C. The total uncertainty was then calculated to be ±1.02°C for the infrared images and ±0.51°C for the thermocouples. The uncertainties in the measured adiabatic effectiveness, η_{meas}, and the correction adiabatic effectiveness, η_o, was determined based on its partial derivative with respect to each temperature in the definition and the total uncertainty in the temperature measurements. The uncertainty in the measured adiabatic effectiveness was then calculated to be $\partial\eta_{meas} = \pm 0.03$ for all values of η_{meas}. Similarly there is an uncertainty associated with the correction adiabatic effectiveness, which was estimated to be $\partial\eta_{meas} = \pm 0.03$ at all values of η_o. Hence the total uncertainty in the adiabatic effectiveness, η, was calculated to be $\partial\eta = \pm 0.04$ over the entire measured range.

Test Design

The primary aim of this study was to investigate the effects of surface deposition on the adiabatic effectiveness levels along the pressure side of the vane endwall. This study was designed to examine deposition on (1) the upstream and downstream sides of the cooling hole rows, (2) a single cooling hole row, and (3) multiple cooling hole rows. The tests were conducted for three different film-cooling mass flow rates corresponding to 0.5% (M_{in}=1.6), 0.75% (M_{in}=2.3), and 0.9% (M_{in}=2.6) of the total passage mass flow rate for one vane pitch. Note that for all cases there was a 0.5% coolant flow from the upstream slot, which simulated the combustor-turbine interface gap.

Figure 3.2 shows a schematic of a row of film-cooling holes and the location of the upstream and downstream deposition with respect to the cooling row. Figure 3.2 also illustrates the cross-sectional shape of the semi-elliptical deposits used in this study. A detailed description of the shape and construction of the deposit was previously described by Sundaram and Thole [16]. For this study a constant deposit height was used such that h/D = 0.8 and w/D = 2, where D is the film-cooling hole diameter. The deposit height was not varied in this study since Sundaram and Thole [16] showed that h/D = 0.8 is representative of most results achieved for surface depositions.

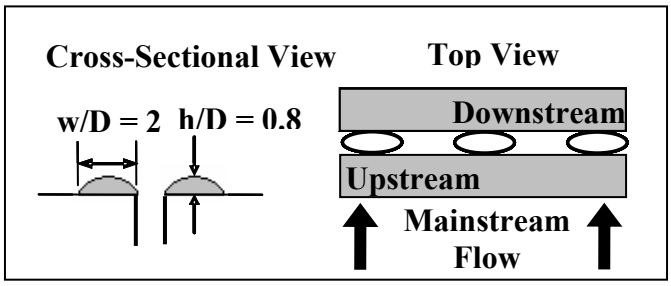

Figure 3.2. Illustrates the deposit shape and geometry tested along the pressure side of the vane endwall.

Figure 3.3a shows the film-cooling hole arrangement on the pressure side of the vane endwall. Note that these holes are aligned in the axial direction such that they inject flow directly towards the vane. Studies were conducted with single row and multiple row deposits on the first four rows of cooling holes along the vane pressure side, where each row contains three holes. The first row is located nearest to the leading edge of the vane and the fourth row is located closer to the trailing edge. The deposit on the first row will be referred to as 1R1 where the first numeral designates the number of rows that have deposits, and the second numeral designates the row in which the deposit was placed. Similarly, the single row deposit on the second film-cooling row will be referred to as 1R2, the third row as 1R3, and the fourth row as 1R4. These studies were carried out for a low film-cooling flow rate of 0.5% and a high flow rate of 0.9% through the cooling holes.

Figure 3.3b shows a schematic of the configuration for multiple row deposition study. This study was carried out by sequentially increasing the number of row deposits from row 1 to row 4 along the pressure side. Deposits placed along row 1 will be referred to as 1R which is similar to the single row 1R1 configuration. When the deposits are placed simultaneously along row 1 and row 2 it will be referred to as 2R. Similarly the configuration where deposits are placed simultaneously along three and four film-cooling rows will be referred to as 3R and 4R respectively.

Discussion of Results

Baseline tests were conducted without any deposits on the pressure side of the rough endwall surface. Figures 3.4a-c compare the contours of adiabatic effectiveness for the baseline study with varying film-cooling flowrates. It was found that with an

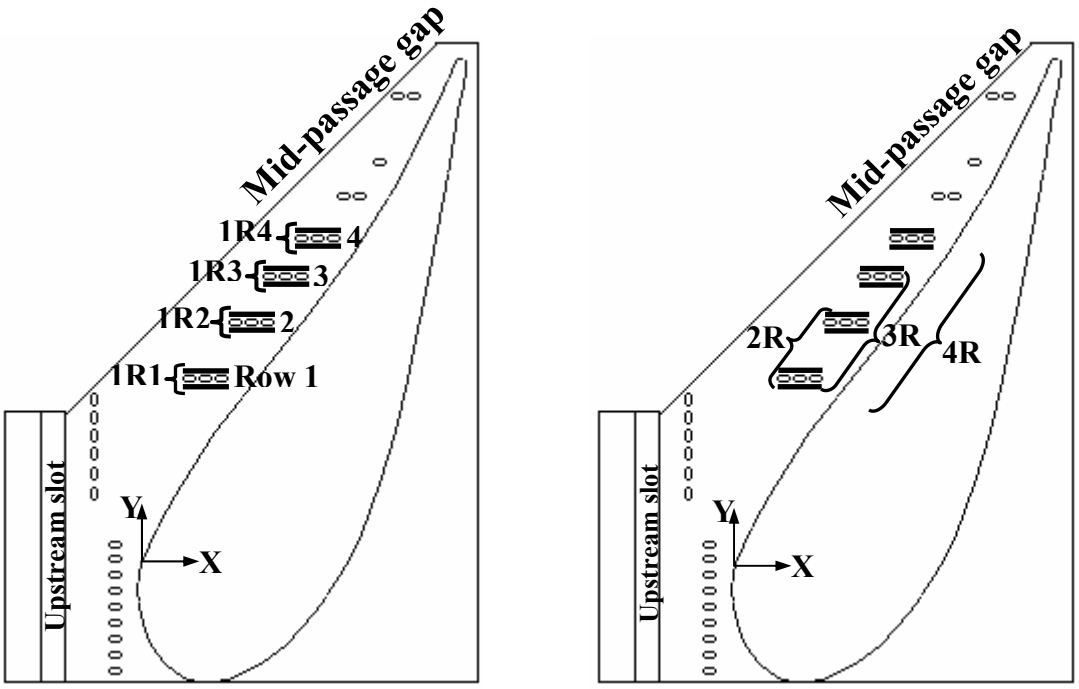

Figure 3.3. Illustrates a) single row deposition and b) multiple row deposition on the pressure side along four film cooling rows.

increase in flowrate, the adiabatic effectiveness levels increased on the pressure side. From Figure 3.4a it can be seen that at a coolant flow rate of 0.5%, the coolant spreads in the direction of the mainstream passage flow. At this coolant level, the coolant exiting the film-cooling holes follows the mainstream flow path towards the suction side in spite of the coolant injection direction being towards the pressure side. As a result, there is a formation of a thin hot band along the endwall junction. With the increase in coolant flow rate to 0.75%, there is an improved streamwise spreading of the coolant resulting in an increase in the adiabatic effectiveness levels. For the 0.75% flow rate, the width of the hot band decreases in size as the coolant extends further along the endwall towards the vane-endwall junction. Further increasing the cooling flow rate to 0.9% resulted in a very small increase in adiabatic effectiveness levels with the coolant behavior being similar to the 0.75% case.

The overall effect of the cooling mass flow rate was quantified by examining the laterally averaged adiabatic effectiveness, $\overline{\eta}$. The lateral averaging was performed across the pitch in the streamwise direction within the boxed region shown in Figure 3.4a. Figure 3.5 shows the laterally averaged effectiveness for the 0.5% baseline study along the pressure side. It can be seen that the effectiveness levels increase into the passage

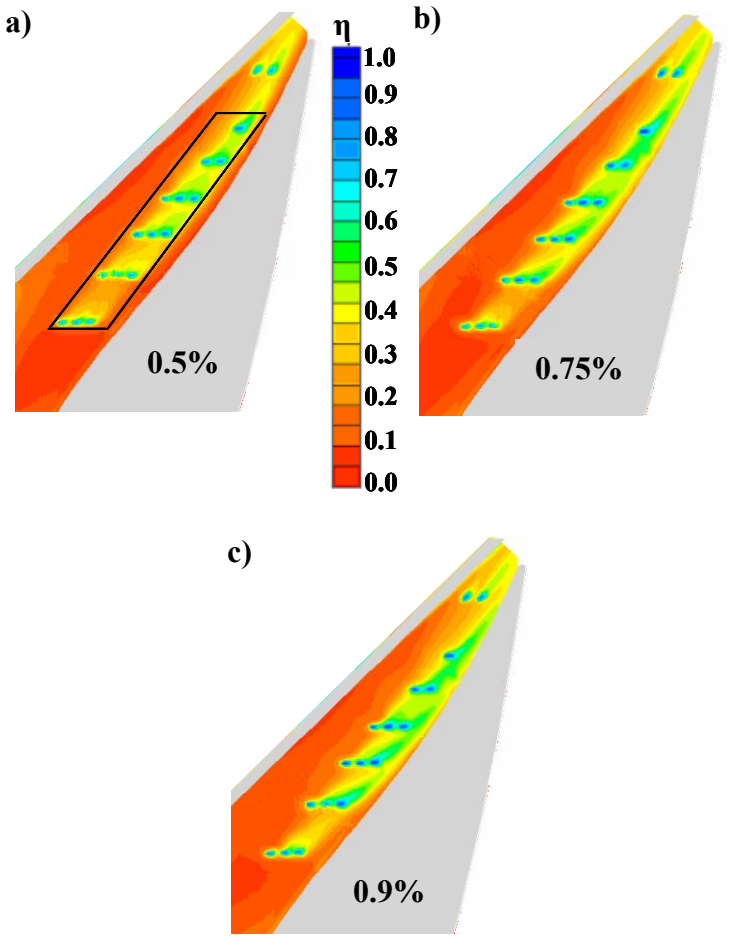

Figure 3.4. Contours of adiabatic effectiveness showing the effect of increasing the film cooling mass flow rate on the pressure side for the baseline study.

with the addition of coolant from each successive cooling row. However, downstream of row 4 there is a decrease in $\overline{\eta}$ as the number of cooling holes in each row decreases.

Also, shown in Figure 3.5 is the augmentation in $\overline{\eta}$ as a result of increasing the coolant mass flow rate from 0.5% to 0.75% and 0.9%. Note that the values less than one are reductions in effectiveness levels and values greater than one are enhancements in effectiveness levels. An overall enhancement was achieved by increasing the coolant flow to 0.75% and a further increase to 0.9% resulted in minimal change in the enhancement levels. A flow rate of 0.9% showed higher effectiveness enhancement than 0.75% downstream of rows 1 and 2, however downstream of row 3 the cooling flow rate of 0.75% showed higher effectiveness enhancement that 0.9%. This reduction in effectiveness levels downstream of row 3 at 0.9% coolant flow rate is because the jets are injected at a higher trajectory leading to more mixing with the mainstream flow.

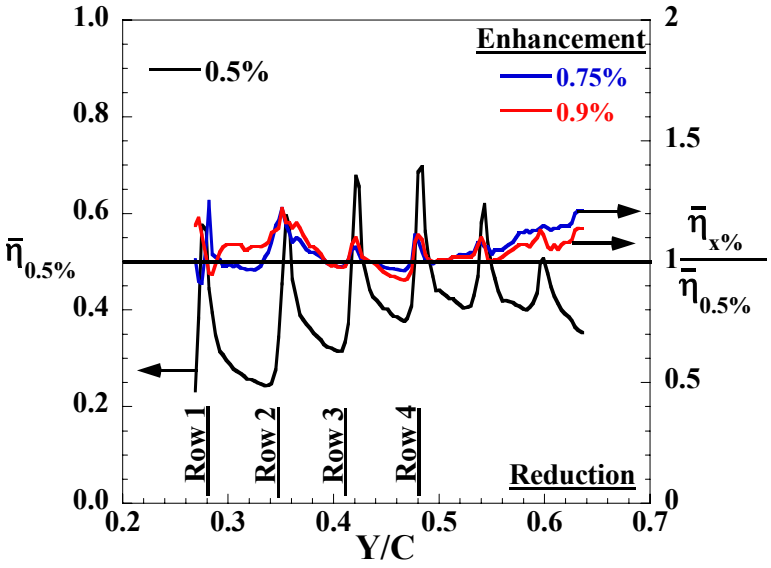

Figure 3.5. Laterally averaged effectiveness for the baseline study with 0.5% cooling flow rate, and enhancements in laterally averaged effectiveness for the 0.75% and 0.9% mass flow rates.

Effect of Simultaneous Multiple Row Deposits

Surface measurements made on a vane endwall by Bons et al. [9] revealed that deposition could occur at any location around the film-cooling hole. To study these effects, the baseline study results were compared to cases in which the deposits were placed at the upstream side, downstream side, and both upstream and downstream sides of the cooling rows.

Figures 3.6a-d compare the contours of adiabatic effectiveness levels for the three deposit configurations with the baseline study. Note that deposits were simulated for the first four rows of cooling holes with a constant coolant flow rate of 0.5% through the film-cooling holes. Comparisons were made at a constant coolant flow rate of 0.5% as it is more representative of actual engine conditions. Comparing the downstream deposition shown in Figure 3.6b to the baseline study in Figure 3.6a, it is seen that this deposit configuration causes an overall reduction in adiabatic effectiveness levels. The deposit deflects the coolant jets toward the vane-endwall junction on the pressure side, which is the designed direction of the jets. The deposit acts to locally reduce the endwall cross-passage pressure gradient near the holes that would otherwise pull the coolant towards the suction surface of the adjacent vane. As the coolant flows towards the junction, there is an overall reduction in effectiveness downstream of the cooling rows. Upstream deposition shown in Figure 3.6c results in more coolant flowing towards the

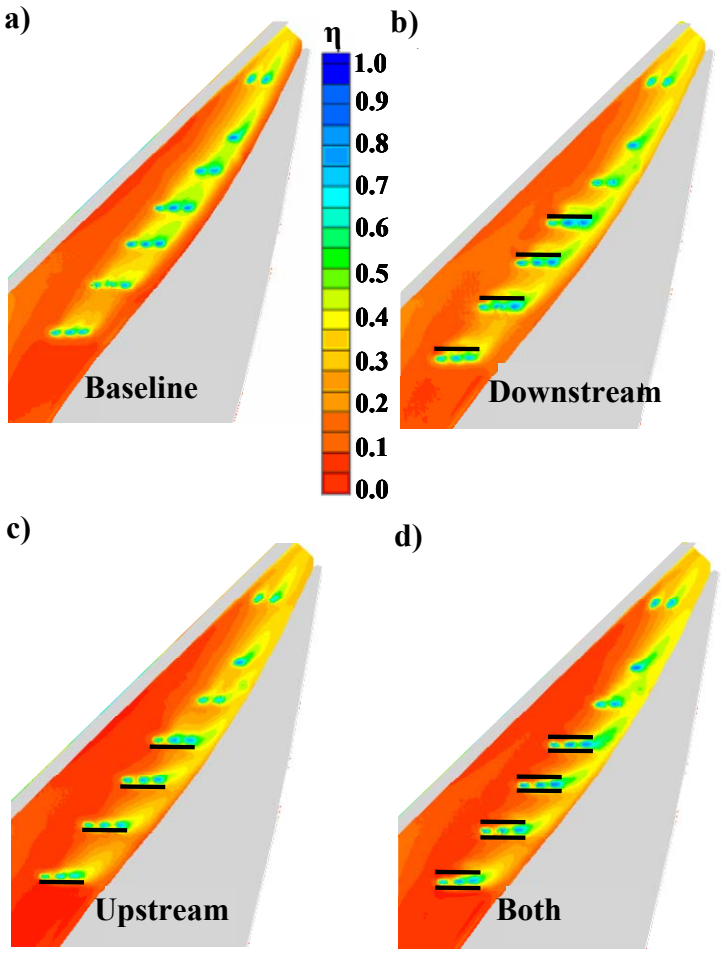

Figure 3.6. Contours of adiabatic effectiveness comparing the effect of deposition at a film cooling flow rate of 0.5%.

endwall junction and caused a higher reduction in effectiveness levels downstream of the cooling rows, relative to downstream deposition. Similar to these results, placing deposits on both upstream and downstream sides of the cooling rows (Figure 3.6d) resulted in the bulk of the coolant becoming more confined and streamlined towards the vane-endwall junction.

From Figure 3.6a it can be seen that for the baseline case, the coolant from the pressure side flowed more towards the suction side resulting in higher effectiveness downstream of the holes as compared to Figures 3.6b-d. Placing deposits along the pressure side cooling holes redirected the coolant towards the vane-endwall junction on the pressure side causing an overall reduction in the effectiveness levels downstream of the cooling rows.

The above effects can be further quantified by comparing the laterally averaged

effectiveness. Figure 3.7 shows the reduction in $\overline{\eta}$ as a result of deposits located upstream, downstream, and on both upstream and downstream sides of the cooling rows. Also shown in Figure 3.7 are the average local blowing ratios for each row of holes along the pressure side for a coolant mass flow rate of 0.5%. Computational predictions of the local static pressure (and local external velocity at each hole location) were used to quantify the local coolant blowing ratios from each cooling hole. It was seen that deposits upstream of the cooling rows and on both upstream and downstream sides of the cooling rows caused similar and higher degradation than deposits placed downstream of the cooling rows. As such it can be concluded that the upstream deposits have a more dominating effect than the downstream deposits on degrading the effectiveness when the deposits are placed on both upstream and downstream sides of the cooling rows. Note that the deposits were placed on the first four cooling hole rows, but the effects are present on all the six rows. This is because in the absence of the deposits the coolant from the upstream rows adds to the effectiveness of the downstream rows, but with deposits, the coolant gets deflected towards the vane-endwall junction. This causes a reduction in effectiveness levels downstream of the coolant rows and the effect cascades to all the six rows.

An overall effect of deposits on the adiabatic effectiveness levels can be compared by using the area averaged effectiveness. Note that the area used was that

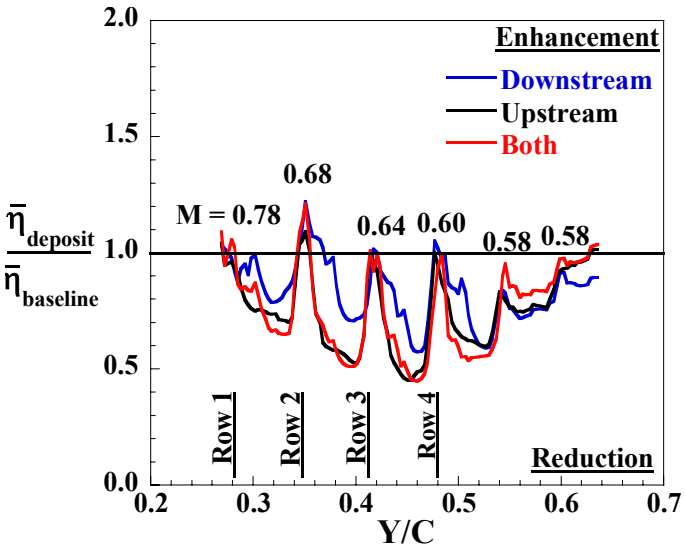

Figure 3.7. Reduction in laterally averaged adiabatic effectiveness as a result of deposition located upstream, downstream, and on both sides of the cooling rows.

shown in the box in Figure 3.4a. Figure 3.8 compares the area averaged adiabatic effectiveness levels for the different deposit configurations with the baseline study for each of the three film-cooling flow rates. At a film-cooling flow rate of 0.5% the overall effectiveness levels are the lowest for deposition on the upstream and on both sides of the cooling rows. Reduction in adiabatic effectiveness levels were seen at all the three coolant flows for the three deposit configurations, relative to the baseline study. As shown earlier, the adiabatic effectiveness levels improved with an increase in coolant flow for the baseline study. A similar trend in increased effectiveness levels with increased coolant flow was seen for the downstream deposition, but the overall levels were still lower than the baseline study. For deposition on the upstream location and on both upstream and downstream sides of the cooling row, an increase in effectiveness levels was seen from 0.5% to 0.75%, but a further increase to 0.9% reduced the effectiveness levels. The reduction in effectiveness levels for deposits on both sides was higher than the upstream deposition at a coolant flow rate of 0.9%. Deposits on both sides showed the highest reduction in effectiveness levels and showed the combined effect of upstream and downstream deposition. As such, the configuration of placing deposits on both sides of the cooling rows was used to investigate the effects of single row and multiple row deposition.

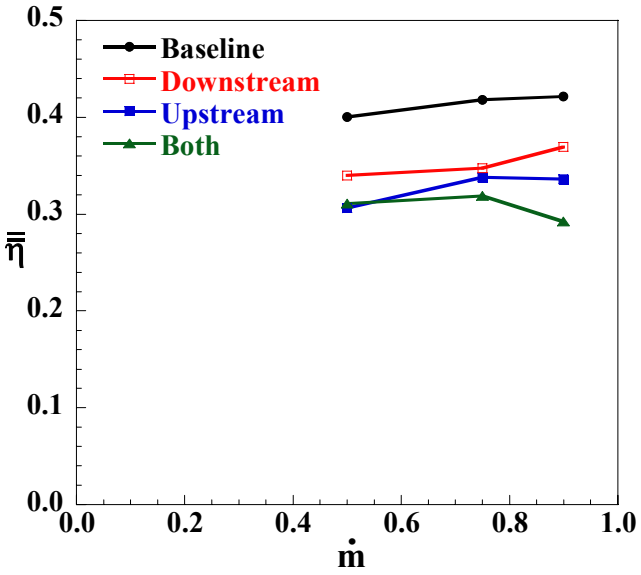

Figure 3.8. Area averaged effectiveness comparing the baseline study to the deposition located upstream, downstream, and both upstream and downstream.

Effect of Single Row Deposits

Tests were also performed by placing individual row deposits from row 1 to row 4 for film-cooling flow rates of 0.5% and 0.9%. The aim of these studies was to determine the row-to-row deposit interaction. Figure 3.9 compares the degradation in laterally averaged effectiveness as a result of single row deposition at a coolant mass flow rate of 0.5%. The smallest reduction in adiabatic effectiveness occurred at row 1 for configuration 1R1. When the deposits were placed at row 2, there was a 40% reduction caused by deposit 1R2 at that location and its effect is carried further downstream. Similarly, the local reduction in adiabatic effectiveness because of deposits 1R3 and 1R4 at location row 3 and row 4 was also found to be near 40%. It can be seen that at the location of the deposit there is a maximum reduction in adiabatic effectiveness levels.

The overall effect of single row deposits on the pressure side can be compared with the area averaged adiabatic effectiveness as shown in Figure 3.10. Adiabatic effectiveness values were averaged over the pressure side film-cooling rows for the area shown in Figure 3.5a (boxed region). Figure 3.10 compares the effect of deposits with the baseline study at a low coolant flow rate of 0.5% and a high coolant flow rate of 0.9%. Deposits placed in row 1 resulted in very little effect on the overall effectiveness at both the coolant flow rates. This is explained by the fact that at row 1 the local blowing ratio

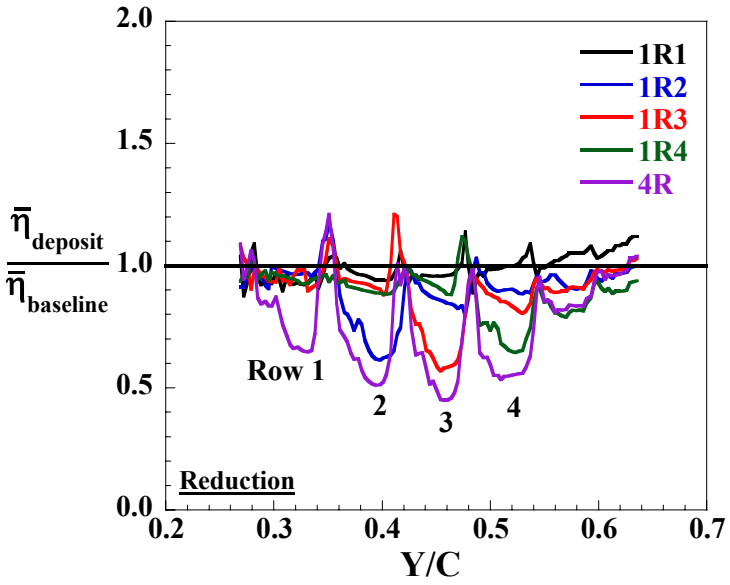

Figure 3.9. Reduction in laterally averaged effectiveness as a result of single row deposits located along the pressure side at a coolant flow rate of 0.5%.

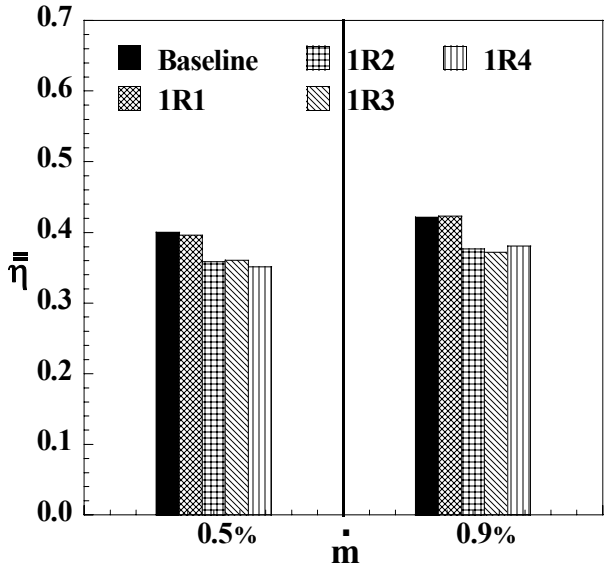

Figure 3.10. Area averaged effectiveness comparing the effect of single row deposition with the baseline for a low and high film cooling flow rate.

is higher than the succeeding cooling row within the passage which results in coolant jet lift off. As a result, the deposit at row 1 does not deflect the coolant jets and hence there is no degradation in adiabatic effectiveness levels. Whereas, the deposit configurations 1R2, 1R3, and 1R4, placed at row 2, 3, and 4 respectively, resulted in a similar overall degradation in effectiveness. It can be concluded that the individual effect of a single row deposit on the overall adiabatic effectiveness levels on the pressure side is independent of its location since it results in a similar overall reduction in effectiveness levels.

Effect of Sequentially Added Multiple Row Deposits

In addition to single row deposits a study was conducted on the effects of multiple cooling row depositions along the pressure side. This was done by sequentially increasing the number of row deposits from one row (1R) to four rows (4R) along the pressure side. Figure 3.11 compares the degradation in laterally averaged adiabatic effectiveness with deposits placed on a single film-cooling row to those with deposits placed on two, three, and four rows at a coolant mass flow rate of 0.5%. It can be seen that the deposit at location 1R (same as deposit 1R1) has very little effect on the pressure side effectiveness levels, whereas deposit configurations 2R, 3R, and 4R have a substantial effect on lowering the effectiveness levels downstream of the film-cooling

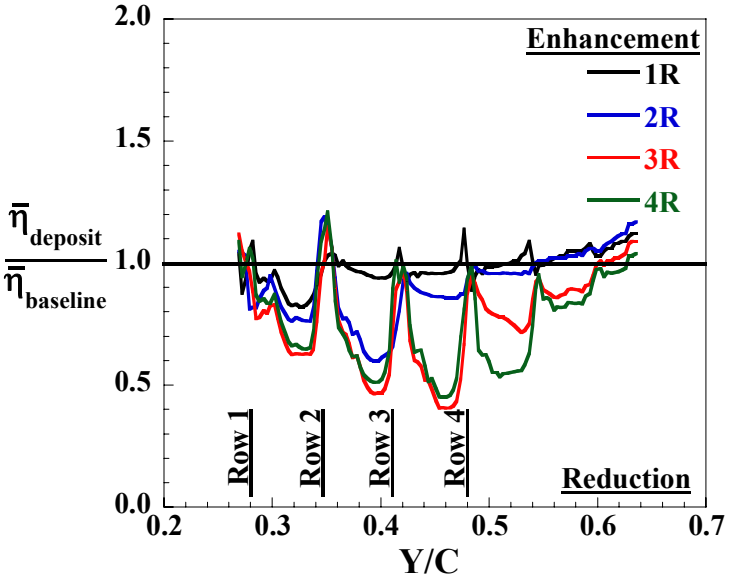

Figure 3.11. Reduction in laterally averaged effectiveness as a result of sequentially added multiple row deposits on the pressure side at a coolant flow rate of 0.5%.

holes. Sequentially increasing the number of deposits rows had a cascading effect on lowering the effectiveness levels.

The overall result of multiple row deposits was further quantified by comparing the area averaged effectiveness levels along the pressure side. Figure 3.12 compares the effect of increasing the number of deposit rows with the baseline study at coolant mass flow rates of 0.5%, 0.75%, and 0.9%. At the low mass flow rate of 0.5%, there is a reduction of 9% in effectiveness levels with the successive increase in the number of deposit rows from 1R to 3R. There was only a slight continued reduction in effectiveness levels from changing the deposit configuration from 3R to 4R. At the high flow rate of 0.9%, there was a near linear reduction of 9% in the area averaged effectiveness levels with a sequential increase in the number of row deposits. Note that the trends shown at the coolant flow rate of 0.75% were consistent with the high coolant flow rate of 0.9%. Multiple row deposits on the endwall were found to have a detrimental effect on the effectiveness levels along the pressure side. This multiple row deposition is most likely what occurs in an actual engine.

Superposition of Deposits

An overall comparison of the laterally averaged adiabatic effectiveness between

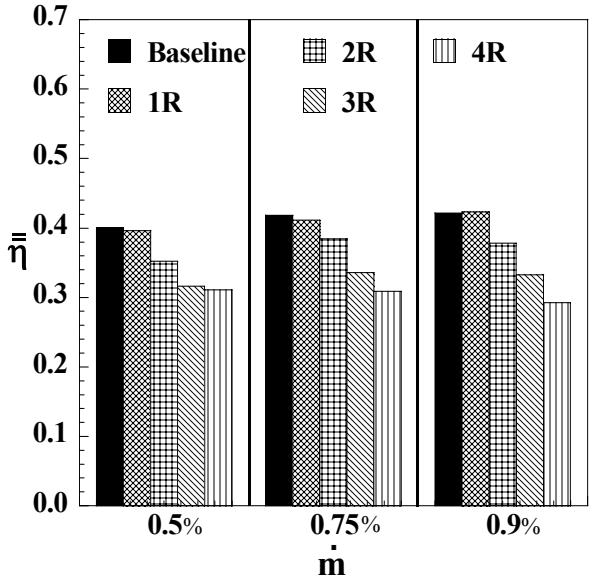

Figure 3.12. Area averaged effectiveness comparing the effect of multiple row deposition with the baseline for a low and high film cooling flow rate.

the baseline study, single row deposition study (1R1), and the multiple row deposition (4R) study is shown in Figure 3.13 at a film-cooling flow rate of 0.5%. The question of whether or not the results from the four row deposit study (4R) can be accurately predicted by superimposing the results from single rows of deposits is an important one. Two superposition approaches were considered to determine if the results from a single hole row were cumulative.

The first method involved using the superposition method developed by Sellers [23] to predict the overall reduction in $\overline{\eta}$ due to multiple row deposition. The reduction in $\overline{\eta}$ at the first film-cooling row due to a single row deposit was calculated to be $\Delta\overline{\eta}_{1R1} = \overline{\eta}_{baseline} - \overline{\eta}_{1R1}$. Similarly reductions along rows 2, 3, and 4 were calculated to be $\Delta\overline{\eta}_{1R2}$, $\Delta\overline{\eta}_{1R3}$, and $\Delta\overline{\eta}_{1R4}$ respectively. Using the above single row reductions in adiabatic effectiveness, the overall reduction in adiabatic effectiveness, $\Delta\overline{\eta}_{overall}$ was calculated by applying the method developed by the Sellers [23]. Then the predicted result was simply $\overline{\eta}_{4R} = \overline{\eta}_{baseline} - \Delta\overline{\eta}_{overall}$ and the result is shown in Figure 3.14. It can be seen that this method resulted in over predicting the degradation in $\overline{\eta}$ at each film-cooling hole row by about 40%.

The second superposition method involved using the reduction in $\overline{\eta}$ from the baseline due to adding a single row of deposits at each individual corresponding row of

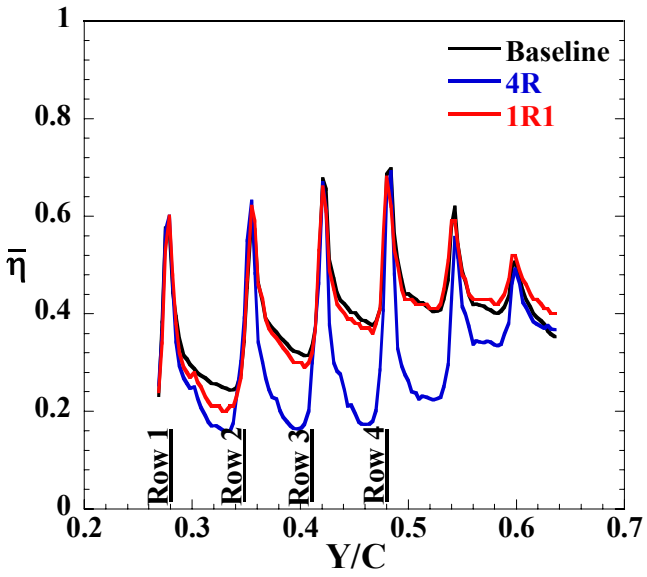

Figure 3.13. Comparison of $\overline{\eta}$ between the baseline and cases 1R1 and 4R (film cooling at 0.5%).

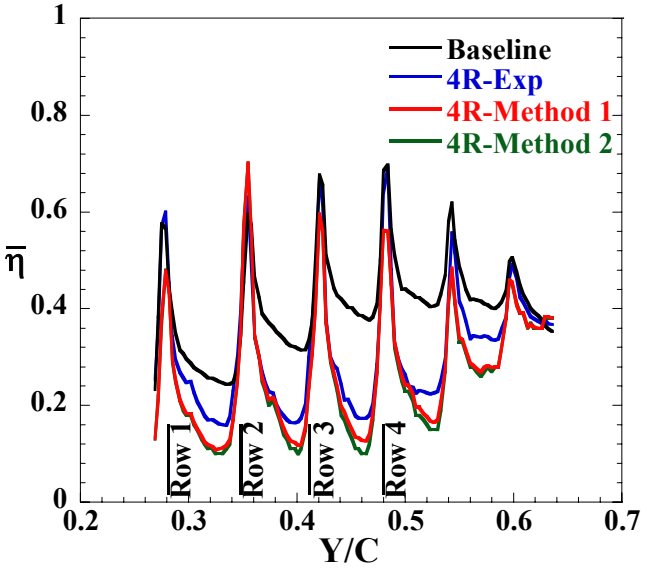

Figure 3.14. Comparison of two superposition methods in predicting the results for the four row deposition study (film cooling at 0.5%).

film-cooling holes. This resulted in a prediction of the form $\overline{\eta}_{4R} = \overline{\eta}_{baseline} - \Delta\overline{\eta}_{1R1} - \Delta\overline{\eta}_{1R2} - \Delta\overline{\eta}_{1R3} - \Delta\overline{\eta}_{1R4}$ and the results are also shown in Figure 3.14. It can be seen that this second method also resulted in over estimating the reduction in $\overline{\eta}$ and the error at each film-cooling row was about 40% similar to method 1.

This study indicates that there is not a linear cumulative effect in adding the reduction in $\overline{\eta}$ resulting from the single row of deposits in order to predict the results

when multiple rows of deposits are present. This is due to the fact that there is a varied effect that the deposits at the downstream hole row have on adiabatic effectiveness levels at the upstream hole rows. The degrading effect on the adiabatic effectiveness levels at the upstream hole row due to deposits on the downstream hole row is contingent upon the simultaneous presence of a deposit at the upstream location. This effect violates most superposition methods and hence there is a discrepancy between the predicted and measured adiabatic effectiveness levels. Another important result is that from viewing Figures 3.9, 3.11, and 3.13 it can be seen that the third row was the row that was most affected by the presence of the deposits in both the single row configurations and the multiple row configurations.

Conclusions

Measurements of adiabatic effectiveness levels were presented on a turbine vane endwall with simulated surface depositions. The depositions were studied along the pressure side of the endwall, and were placed upstream, downstream and on both sides of four rows of film-cooling holes. The focus of this paper was on evaluating the effect of single row, multiple row, and sequentially added deposits to the overall reductions that would occur for endwall film-cooling. The effect of the deposits on endwall adiabatic effectiveness levels were compared with a baseline study having no surface deposition.

It was found that deposition upstream and on both the upstream and downstream of the cooling holes resulted in similar and higher degradation in effectiveness levels than deposition located just downstream of the cooling holes. When using deposits on both the upstream and downstream regions of the cooling holes, the effect of a single row deposition was investigated. The single row deposits resulted in similar degradation of the total area averaged effectiveness that was independent of row location, with the exception of the first row which showed little degradation.

Sequentially increasing the number of deposition rows resulted in a significant decrease in the overall adiabatic effectiveness levels. The results indicate that there is a linear reduction in adiabatic effectiveness levels with the sequential increase in the number of row deposits. This effect is more prominent at the higher coolant flow rate of 0.9% than at the lower flow rate of 0.5%.

Finally, the work presented in this paper indicates that by applying superposition methods the degradation in adiabatic effectiveness can be predicted within a 40% error. The over prediction using superposition occurs because of the large effect that the downstream deposits can have on upstream rows when deposits are placed along multiple rows.

Acknowledgments

This publication was prepared with the support of the US Department of Energy, Office of Fossil Fuel, and National Energy Technology Laboratory. Any opinions, findings, conclusions, or recommendations expressed herein are solely those of the authors and do not necessarily reflect the views of the DOE. The authors thank Mike Blair (Pratt & Whitney), Ron Bunker (General Electric), and John Weaver (Rolls-Royce) for their input on the modeling of realistic turbine features.

Attribution

This paper was co-authored with Dr. Michael Barringer and Dr. Karen Thole. They had the following roles in the paper

Co-author 1 – paper 3

Name – Dr. Michael Barringer

Department – Mechanical Engineering

Degree – Ph.D

Relationship – Post-doctoral research associate

Role - Dr. barringer helped me with the superposition study which was included in this paper in addition to the adiabatic effectiveness measurements.

Co-author 2 – paper 3

Name – Dr. Karen A. Thole

Department – Mechanical Engineering

Degree – Ph.D

Relationship – Chair and primary advisor

Role - Dr. Thole served as my dissertation chair and advised me through my Ph.D and on all the work presented in this dissertation.

Nomenclature

C true chord of stator vane

D diameter of film-cooling hole

h height of the deposit

L film-cooling hole length

M blowing ratio based on inlet mainstream velocity

$M = \rho_j U_j / \rho_\infty U_\infty$

M_{in} blowing ratio based on inlet mainstream velocity

$\dot{m}$ coolant mass flow rate

P vane pitch; hole pitch

PS pressure side

Re_{in} Reynolds number defined as

$Re_{in} = CU_{in} / \nu$

S span of stator vane

T temperature

U velocity

w width of the deposit

X,Y,Z local coordinates

Greek

η_{meas} measured adiabatic effectiveness,

$\eta_{meas} = (T_\infty - T_{meas}) / (T_\infty - T_j)$

η_o correction adiabatic effectiveness

η adiabatic wall effectiveness,

$\eta = (\eta_{meas} - \eta_o) / (1 - \eta_o)$

$\overline{\eta}$ laterally averaged effectiveness

$\overline{\overline{\eta}}$ area-averaged effectiveness

ν kinematic viscosity

Subscripts

aw adiabatic wall

in inlet conditions

j coolant flow through film-cooling holes

∞ local freestream conditions

Overbar

– lateral average

= area average

References

[1] Bons, J. P., Crosby, J., Wammack, J. E., Bentley, B. I., and Fletcher, T. H., 2005, "High Pressure Turbine Deposition in Land Based Gas Turbines from Various Synfuels," GT2005-67468.

[2] Wenglarz, R. A., 1985, "Deposition, Erosion, and Corrosion Protection for Coal-Fired Gas Turbines" 85-IGT-61.

[3] Wenglarz, R. A., Nirmalan, N. V., and Daehler, T. G., 1995, "Rugged ATS Turbines for Alternate Fuels," 95-GT-63.

[4] Decorso, S. M., Newby, R. A., Anson, D., Wenglarz, R. A., and Wright, I. G., 1996, "Coal/Biomass Fuels and the gas Turbine: Utilization of Solid Fuels and their Derivatives," 96-GT-66.

[5] Moses, C. A., and Bernstein, H. L., 1996, "Fuel-Specification Considerations for Biomass Pyrolysis Liquids to be used in Stationary Gas Turbines," 96-GT-406.

[6] Wenglarz, R. A., 1992, "An Approach for Evaluation of Gas Turbine Deposition," *Journal of Engineering for Gas Turbines and Power*, Vol. 104, pp. 230 – 234.

[7] Bons, J. P., Corsby, J., Wammack, J. E., Bentley, B. I., and Fletcher, T. H., 2005, "High Pressure Turbine Deposition in Land Based Gas Turbines from Various Synfuels," GT2005-67468.

[8] Bornstein, N. S., 1996, "Reviewing Sulfidation Corrosion – Yesterday and Today," *Journal of the Minerals, Metals, and Materials Society*, 47(10), 36-38.

[9] Wright, I. G., Leyens, C., and Pint, B. A., 2000, "An Analysis of the Potential for Deposition, Erosion, or Corrosion in Gas Turbines Fueled by the Products of Biomass Gasification or Combustion," 2000-GT-0018.

[10] Bons, J. P., Taylor, R. P., McClain, S. T., and Rivir, R. B., 2001, "The Many Faces of Turbine Surface Roughness," *Journal of Turbomachinery*, Vol.112, pp. 638-647.

[11] Taylor, R. P., 1990, "Surface Roughness Measurements on Gas Turbine Blades," *Journal of Turbomachinery*, Vol.102, pp. 165-170.

[12] Tarada, F., and Suzuki, M., 1993, "External Heat Transfer Enhancement to Turbine Blading Due to Surface Roughness," 93-GT-64.

[13] Goldstein, R. J., Eckert, E. R. G., and Chiang, H. D., 1985, "Effect of Surface Roughness on Film cooling Performance," *Journal of Engineering for Gas Turbines and Power*, Vol. 96, pp. 101-106.

[14] Schmidt, D. L., Sen, B., and Bogard, D. G., 1996, "Effects of Surface Roughness on Film-Cooling," 96-GT-288.

[15] Barlow, D. N., and Kim. Y. W., 1995, "Effect of Surface Roughness on Local Heat Transfer and Film cooling Effectiveness," 95-GT-13.

[16] Cardwell N. D., Sundaram, N., and Thole, K. A., 2005, "Effects of Mid-Passage Gap, Endwall Misalignment, and Roughness on Endwall Film-Cooling," *Journal of Turbomachinery*, Vol. 117, pp. 62-60.

[17] Sundaram, N., and Thole, K. A., 2006. "Effects of Surface Deposition, Hole Blockage, and TBC Spallation on Vane Endwall Film-Cooling," accepted to *Journal of Turbomachinery*, GT2006-80368.

[18] Radomsky, R., and Thole, K. A., 2000, "Flowfield Measurements for a Highly Turbulent Flow in a Stator Vane Passage," *Journal of Turbomachinery*, Vol.112, pp. 255-262.

[19] Knost, D. G., and Thole, K. A., 2004, "Adiabatic Effectiveness Measurements of Endwall Film cooling for a First Stage Vane," *Journal of Turbomachinery*, Vol. 116, pp. 286-305.

[20] Knost, D. G., and Thole, K. A., 2003, "Computational Predictions of Endwall Film cooling for a First Stage Vane," GT2003-37252.

[21] Ethridge, M. I., Cutbirth, J. M., and Bogard, D. G., 2000, "Scaling of Performance for Varying Density Ratio Coolants on an Airfoil with Strong Curvature and Pressure Gradient Effects," *Journal of Turbomachinery*, Vol. 112, pp. 231-236.

[22] Moffat, R. J., 1988, "Describing the Uncertainties in Experimental Results," *Experimental Thermal and Fluid Science*, Vol.1, pp. 3-16.

[23] Sellers, J. P., 1963, "Gaseous Film Cooling with Multiple Injection Stations," *AIAA Journal,* 1, pp. 2144-2146.

Paper 4:
Bump and Trench Modifications to Film-Cooling Holes at the Vane Endwall Junction

Recommended for publication in the *ASME Journal of Turbomachinery* [*]

Abstract

The endwall of a first stage vane experiences high heat transfer and low adiabatic effectiveness levels because of high turbine operating temperatures and formation of leading edge vortices. These vortices lift the coolant off the endwall and pull the hot mainstream gases towards it. The region of focus for this study is the vane-endwall junction region near the stagnation location where cooling is very difficult. Two different film-cooling hole modifications, namely trenches and bumps, were evaluated to improve the cooling in the leading edge region.

This study uses a large-scale turbine vane cascade with a single row of axial film-cooling holes at the leading edge of the vane endwall. Individual hole trenches and row trenches were placed along the complete row of film-cooling holes. Two-dimensional semi-elliptically shaped bumps were also evaluated by placing the bumps upstream and downstream of the film-cooling row. Tests were carried out for different trench depths and bump heights under varying blowing ratios. The results indicated that a row trench placed along the row of film-cooling holes showed a greater enhancement in adiabatic effectiveness levels when compared to individual hole trenches and bumps. All geometries considered produced an overall improvement to adiabatic effectiveness levels.

* Co-author: Dr. Karen A. Thole, Mechanical Engineering Department, Virginia Tech

Introduction

A higher demand in power output for modern gas turbines has resulted in an increase in combustor exit temperatures. Higher temperatures in turn has resulted in flatter profiles at the combustor exit [1] warranting the need for sufficient cooling of endwall surfaces. In addition to these flat profiles, the endwall surfaces also experience high heat transfer due to the formation of leading edge vortices which tend to lift the coolant off the surface. Friedrichs et al [2-4] showed that the leading edge on the endwall is the most difficult region to cool. Studies by Thole and Knost [5] showed that even with an upstream leakage flow, the leading edge endwall junction around the stagnation region remains uncooled.

To achieve higher adiabatic effectiveness levels at the leading edge it is important to ensure that there is a uniform spread of coolant exiting the film-cooling holes. Typical film-cooling hole designs on a surface give low adiabatic effectiveness levels near and in between the hole exits causing localized regions of hot spots. This study focuses on eliminating these hot spots by improving the adiabatic effectiveness levels at the leading edge region of a vane endwall.

Since effective cooling at the leading edge is a challenge to a turbine designer, new cooling methods are desired. This study is aimed at understanding the effect of modifying the coolant jet trajectory at the cooling hole exit and how it enhances the adiabatic effectiveness levels. The work presented in this paper compares the effect of two different modifications on the adiabatic effectiveness levels at the leading edge, namely trenches and bumps.

Relevant Past Studies

Effective cooling of a turbine surface is highly important for its improved operational life and the performance of the engine as a whole. With regard to that, a number of studies have focused on developing alternate methods to cool a surface in addition to placing film-cooling holes.

An early study was carried out by Blair [6] in which he showed that coolant flow from an upstream slot resulted in higher cooling near the suction side and reduced cooling near the pressure side. This non-uniform cooling was as a result of the coolant

being swept from the pressure side to the suction side caused by the secondary flow within the vane passage. Knost and Thole [7] studied the effect of leakage flow through the combustor-vane interface on to the endwall adiabatic effectiveness levels. Similar to Blair [6] they also showed that the coolant exits the upstream slot in a non-uniform fashion. The non-uniformity was associated with the formation of a hot ring around the stagnation region towards the pressure side of the vane. Cardwell et al. [8] showed that the size of this hot ring can be reduced by decreasing the width of the upstream slot which results in a more uniform spread of coolant. Burd et al. [9] studied the effects of slot bleed injection over the contoured endwall of a nozzle guide vane. They concluded from their measurements that bleed cooling from upstream of the leading edge of the vane provides considerable thermal protection within the passage. These studies of coolant flow through a slot showed that effective cooling can be achieved by injecting a 2D layer of film-cooling over the surface.

Searching for better cooling techniques, Bunker [10] measured improved film-cooling effectiveness levels on a flat plate using discrete holes placed within a transverse slot with varying widths. Bunker [10] showed that the narrowest possible slot width relative to the interior cooling hole diameter is most desirable. As placing cooling holes in slots basically modifies the hole exit, there have been few studies that have investigated this particular effect. Lu et al. [11] investigated the effect of slot exit area and edge shape on film effectiveness measurements made on a flat plate. They found that a straight edge exit performed the best at a blowing ratio of M = 1.0, whereas a ramped exit enhanced the adiabatic effectiveness levels at lower blowing ratios. Waye and Bogard [12] applied the trench configuration on the suction side of a first stage vane with varying slot exit configurations. They tested a narrow trench where the trench wall was at the film-cooling hole exit, a wide trench where the trench wall was at a distance of one cooling hole diameter from the hole exit, and a trench with an angled exit. They also found that the narrow trench performed the best relative to a wide trench and angled exit trench and the adiabatic effectiveness levels peaked for blowing ratios beyond M = 1.0.

A recent study was carried out by Sundaram and Thole [13] to understand the effect of placing semi-elliptically shaped deposits downstream of a row of cooling holes. While their study was aimed at understanding how deposits could adversely affect

cooling levels, their results indicated improved cooling performance for some geometries. They carried out this study at the leading edge of a first stage vane endwall on a rough surface and found that smaller deposits enhanced adiabatic effectiveness levels. As the deposit height was increased, the effectiveness levels were reduced below that of the baseline with no bumps.

In summary, different modifications have been applied to film-cooling holes to enhance the adiabatic effectiveness levels. Most of these studies have been on a flat plate with no studies carried out at the leading edge of a first stage vane endwall with the exception of the authors' previous work [13].

Bump and Trench Descriptions

Previous studies by Bunker [10] and Waye and Bogard [12] showed that holes in a slot are effective in forming a layer of protective film over the surface. These studies also showed that the edges of the slot were very close to the exit of the film-cooling hole for enhanced cooling. The effect of placing cooling holes in a trench was found to show a significant enhancement in effectiveness levels. The trench on the surface can be manufactured during the TBC application process [14] and its effect can differ with varying trench depths as the thickness of the TBC can be varied. Similarly, studies by Sundaram and Thole [13] also showed that the when the edges of the semi-elliptical deposits (bumps) were close to the cooling hole exit the cooling effectiveness levels were enhanced.

Motivated from these studies, modifications were applied to the leading edge region of the first stage vane endwall as shown in Figure 4.1. The endwall of the vane was constructed of foam because of its low thermal conductivity (0.033 W/m.K). The endwall surface was covered with a thin layer of Balsa wood to simulate a smooth thermal barrier coating (TBC). All of the different configurations were tested on a smooth endwall surface. The endwall leading edge consisted of a single row of axial film-cooling holes with a hole spacing corresponding to P/D = 3. The cooling row was placed four cooling hole diameters (4D) upstream from the stagnation location. An upstream slot, representing the combustor-turbine gap, was placed 17D from the stagnation location. Note that it is important to simulate the upstream slot since this

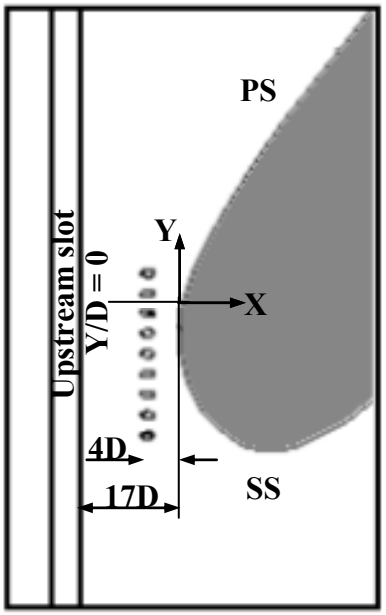

Figure 4.1. Illustrates the endwall design studied at the leading edge.

interface exists in most turbines and the exiting slot flow influences the upstream boundary condition. Figures 4.2a-b show the geometries of the two modifications studied at this leading edge location. Figure 4.2a illustrates the trench geometry and Figure 4.2b illustrates the bump geometry previously described by Sundaram and Thole [13]. For the trench configuration three different depths were studied corresponding to h/D = 0.4, 0.8, and 1.2. The trench depths were controlled by varying the thickness of the Balsa wood covering the endwall surface. Three different bump heights were also tested at the leading edge. Similar to Sundaram and Thole [13], these heights corresponded to h/D = 0.5, 0.8 and 1.2.

Based on the above two concepts, four different cooling hole configurations were tested at varying blowing ratios as shown in Figures 4.3a-d. Figure 4.3a illustrates the baseline case which simulated a smooth endwall without any surface modifications. It consisted of the axial film-cooling holes placed 30° to the endwall surface. Figure 4.3b simulates the individual hole trench configuration, where the trench surrounded each individual cooling hole. Figure 4.3c is the row trench configuration, similar to the one tested by Bunker [10] on a flat plate, where the trench runs along the entire length of the cooling row. Bunker [10] studied only a single trench depth of h/D = 0.43 for the axial hole geometry. Figure 4.3d is the bump configuration, in which two semi-elliptical bumps were placed at the upstream and downstream locations of the film-cooling hole.

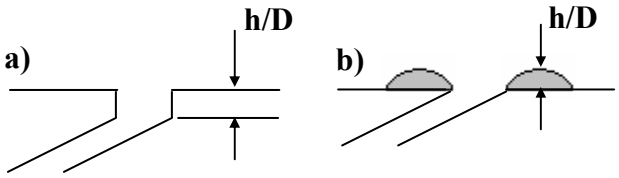

Figure 4.2. Illustrates the a) trench geometry and b) bump geometry studied at the leading edge.

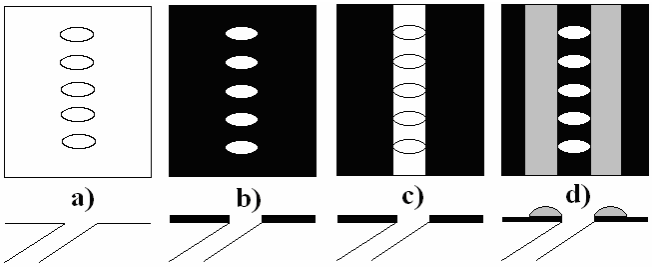

Figure 4.3. Schematic of the four configurations a) baseline, b) individual trench, c) row trench, and d) bumps tested at the leading edge.

The geometries shown in Figures 4.3b-d will be compared with the baseline case to see if these modifications result in any enhancement.

Experimental Methodology

The experimental section was placed in a closed loop wind tunnel facility, as shown in Figure 4.4. The flow encounters an elbow downstream of the fan and passes through a primary heat exchanger used to cool the bulk flow. The flow is then divided into three channels including the center passage and two cooled secondary passages located above and below the test section. Note that only the top secondary passage was used for this study. The primary core flow, located in the center passage, convects through a heater bank where the air temperature is increased to about 60°C. The secondary flow, in the outer passage, was cooled to about 20°C, thereby maintaining a temperature difference of 40°C between the primary and secondary flows. The secondary flow provided the coolant through the film-cooling holes and through the upstream slot. Also, for all the tests carried out in this study a density ratio of 1.1 was maintained between the coolant and mainstream flows. As the density ratios are not being matched to that of the engine, velocity ratios for the cooling holes will be significantly higher than those found in an engine for the same mass flux or momentum flux ratios. While there have been studies indicating that momentum flux scales jet lift-

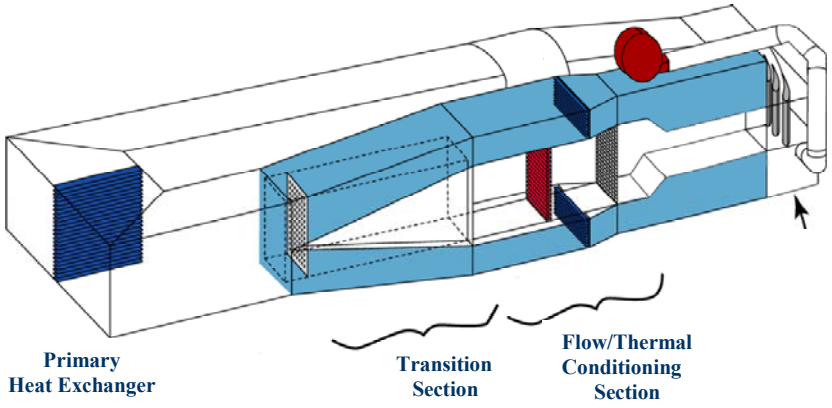

Figure 4.4. Illustration of the wind tunnel facility.

off for flat plate film-cooling, it is unknown as to whether it best scales lift-off for endwall film-cooling

Downstream of the flow/thermal conditioning section, is the test section that consists of two full passages with one center vane and two half vanes. Table 1 provides a description of the turbine vane geometry and operating conditions. Table 1 also gives the inlet boundary layer characteristics. The boundary layer approaching the vane cascade was measured at 0.63C upstream of the vane stagnation. The measurement was done far upstream from the stagnation as the upstream slot flow influences the boundary layer approaching the vane cascade. The vane geometry used in the current study is a commercial first-stage vane previously described by Radomsky and Thole [15]. The passage under study consisted of an endwall surface with film-cooling holes and leakage paths simulating the combustor-vane interface (upstream slot) and vane-to-vane interface. A detailed description of the endwall construction has been previously described by Knost and Thole [5].

The inlet turbulence intensity and length scales were measured to be 1.3 percent and 4 cm respectively. These tests were carried out at a low turbulence intensity of 1.3 percent to isolate the effects of trenches and bumps on endwall adiabatic effectiveness levels. For every test condition the dimensionless pressure coefficient distribution was verified to ensure periodic flow through the passages. Two separate plenums were used to control the coolant flowrate through the upstream slot and through the film-cooling holes, respectively. The upstream slot flow was assumed to have a discharge coefficient of 0.6 which is the assumed value for a flow through a sharp-edged orifice and the

Table 4.1. Geometric and Flow Conditions

Scaling factor	9
Scaled up chord length (C)	59.4 cm
Pitch/Chord (P/C)	0.77
Span/Chord (S/C)	0.93
Hole diameter (D)	0.46 cm
Hole L/D	8.3
Re_{in}	2.1×10^5
Inlet and exit angles	0° & 72°
Inlet &exit Mach numbers	0.017 & 0.085
Inlet mainstream velocity	6.3 m/s
Boundary layer thickness/span (δ/S)	0.18
Displacement thickness/span (δ^*/S)	0.025
Momentum thickness/span (θ/S)	0.020
Upstream slot width	0.024C

blowing ratio was calculated accordingly. The coolant flowrate through the film-cooling holes was set based on an average ideal blowing ratio. This blowing ratio was based on an inviscid calculation through the holes and the inlet mainstream velocity. It should be noted that an average discharge coefficient wasn't assumed to set the coolant flow through the film-cooling holes as it varies from hole-to-hole.

Instrumentation and Measurement Methods

A FLIR P20 infrared camera was used to spatially-resolve adiabatic wall temperatures on the endwall. Measurements were taken at six different viewing locations to ensure that the entire endwall surface was mapped. The camera was placed perpendicular to the endwall surface at a distance 55 cm from the endwall. Each picture covered an area 24 cm by 18 cm with the area being divided into 320 by 240 pixel locations. The spatial integration of the camera was 0.715 mm (0.16 hole diameters). Thermocouples were also placed on the endwall surface at different locations to directly measure the temperature to post calibrate the infrared images. For the post calibration the emissivity was set at a constant value of 0.92 and the background temperature (~ 45ºC) was adjusted until the temperatures from the infrared camera images were within 0.05ºC of the corresponding thermocouple data. Six images were taken at each of the viewing locations to obtain an averaged picture using an in-house Matlab program. The same program was also used to assemble the averaged pictures at all locations to give a

complete temperature distribution along the passage endwall.

Freestream temperatures were measured at multiple locations along the pitch and the average was determined by using a thermocouple rake consisting of three thermocouples along the span. It was found that the variations along the pitch were less than 0.2ºC and that along the span were less than 1.5ºC. Voltage outputs from the thermocouples were acquired by a 32 channel data acquisition module that was used with a 12-bit digitizing card. The temperature data was compiled after the system reached steady state.

A 1D conduction correction as described by Ethridge et al. [16] was applied to all adiabatic effectiveness measurements to account for conduction losses through the endwall surface. The conduction correction was applied by measuring the endwall surface effectiveness with no blowing through the film-cooling holes. This was done by blocking the film-cooling holes on the endwall passage under study while maintaining similar flowrates through the adjacent passage to insure the correct boundary condition under the endwall. At the entrance to the flow passage for a measured value of $\eta = 0.9$, a correction of 0.16 was typical while along the pressure side for a measured value of $\eta = 0.1$, a correction of 0.03 was applied.

Experimental Uncertainty

An uncertainty analysis was performed on the measurements of adiabatic effectiveness and blowing ratio using the partial derivative method described at length by Moffat [17].

For adiabatic effectiveness measurements the precision uncertainty was determined by taking the standard deviation of six measurement sets of IR camera images with each set consisting of six images. The precision uncertainty of the measurements was ±0.014°C. The bias uncertainty was ±1.0°C based on the uncertainty in the IR camera measurements specified by the manufacturer. The bias uncertainty of the thermocouples was ±0.5°C as specified by the manufacturer and the bias uncertainty associated with the digitizing card was ±0.35°C. Then the total bias uncertainty of the temperature measurement due to the thermocouple and the digitizing card was calculated to be ±0.61°C. The total uncertainty was then calculated as ±1.02°C for the images and

±0.62°C for the thermocouple measurements. Uncertainty in effectiveness, η, was found based on the partial derivative of η with respect to each temperature in the definition and the total uncertainty in the measurements. Uncertainties in adiabatic effectiveness were calculated to be $\partial\eta = \pm 0.032$ at a η value of 0.2 and $\partial\eta = \pm 0.033$ at a η value of 0.9.

To calculate the uncertainty in blowing ratio, the uncertainties associated with the pressure transducers, the Pitot probe and the thermocouples were taken into account. The pressure transducer had a total uncertainty of ±0.13Pa and the pitot probe which was used to measure the inlet mainstream velocity had a total uncertainty of ±0.22Pa. The total uncertainty of the thermocouples as explained earlier was ±0.62°C. The uncertainties in blowing ratio were then calculated to be $\partial M = \pm 0.045$ at a value of M = 0.5 and $\partial M = \pm 0.052$ at a value of M = 3.0.

Discussion of Results

As mentioned previously the baseline case was measured on a smooth endwall surface. Baseline tests were carried out at six film-cooling blowing ratios varying from M = 0.5 to M = 3.0 as shown in Figure 4.5. A flowrate corresponding to an inlet blowing ratio of $M_{in} = 0.3$ was set through the upstream slot for all the tests.

It can be seen from the contours in Figure 4.5 that at low blowing ratios the adiabatic effectiveness levels are higher on the suction side of the endwall than on the pressure side. This is because of the lower static pressure on the suction side, which enables more coolant to exit the cooling holes near the suction side. With an increase in blowing ratio up to M = 2.0 there is a gradual increase in effectiveness levels along the pressure and suction sides. A further increase beyond M = 2.0 results in an increase in effectiveness levels on the pressure side with subsequent decrease on the suction side when compared to the lower blowing ratio. It can also be seen that at higher blowing ratios there is a reduction in effectiveness levels just downstream of the cooling holes. At high blowing ratios, the coolant jets are associated with high momentum resulting in jet lift off from the surface. It is also seen that at these high blowing ratios the adiabatic effectiveness levels increase near the vane-endwall junction. The adiabatic effectiveness levels also increase because of the horseshoe vortex formed at the leading edge, which pulls the coolant injected into the mainstream flow back to the surface. As a result, the

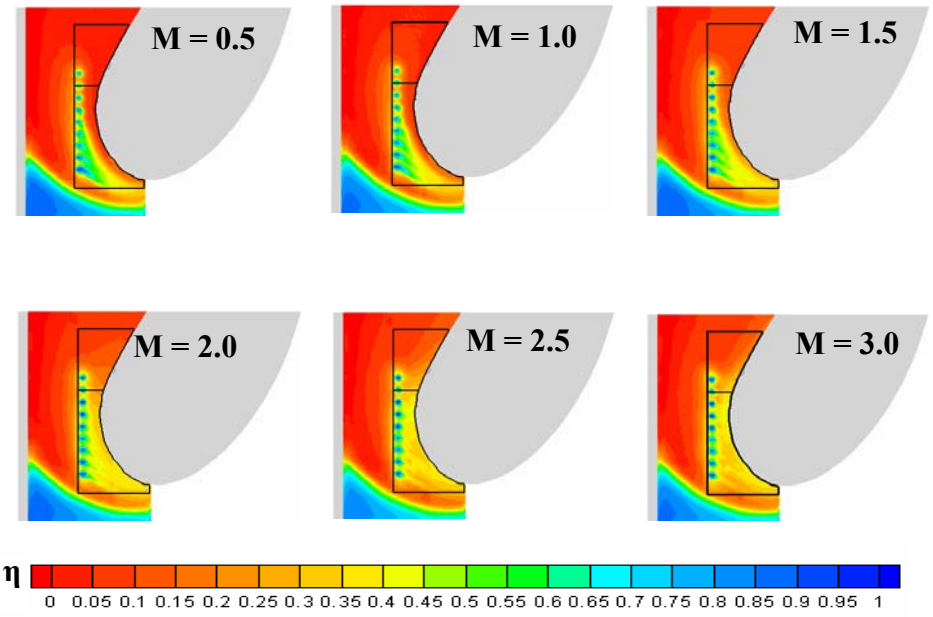

Figure 4.5. Contours of adiabatic effectiveness comparing the baseline case at different blowing ratios.

adiabatic effectiveness levels increase at the vane-endwall junction along both the pressure and suction sides.

Figure 4.6 compares the lateral average effectiveness ($\overline{\eta}$) at varying blowing ratios for the baseline case. Adiabatic effectiveness values were laterally averaged in the streamwise (X-direction) direction as shown in Figure 4.1. Figure 4.1 also shows the stagnation location along the pitch where Y/D = 0. Lateral averaging was calculated for two areas on either side of the stagnation location; suction side extending from Y/D= 0 to Y/D= -25 and pressure side extending from Y/D = 0 to Y/D = 10 (refer Figure 4.5). For calculating the lateral average, the area under consideration was divided into many small divisions starting at different pitch (Y/D) locations. The adiabatic effectiveness values were then averaged along each of these divisions to give the laterally averaged adiabatic effectiveness along the pitch. Note that lateral averaging was carried our for the same vane surface length of x/S = 0.15 along the suction and pressure sides from the vane stagnation.

From Figure 4.6 it can be seen that for blowing ratios from M = 0.5 to M = 2.0 the effectiveness levels increase on the suction side until Y/D = -10. Any subsequent increase in blowing ratio caused an increase on the pressure side and a decrease on the suction side. It is interesting to note that at a blowing ratio of M = 2.0 the effectiveness

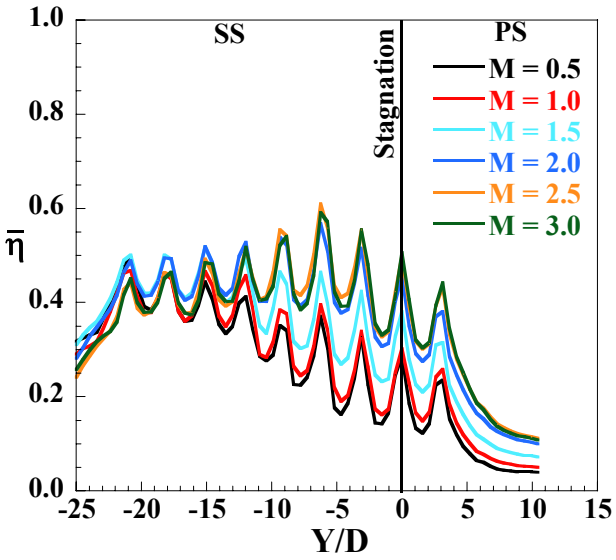

Figure 4.6. Lateral average effectiveness plots of the baseline case.

levels are the highest on the suction side as well on the pressure side when compared to other blowing ratios. The formation of peaks and valleys in the lateral average plot clearly show that at every blowing ratio, there is a variation in adiabatic effectiveness levels between the film-cooling holes. The variation in effectiveness levels is because of the formation of hot spots as a result of non-uniform coolant spread on the endwall surface.

The variation in adiabatic effectiveness levels on the suction and pressure sides can also be studied by comparing their area-averaged effectiveness ($\overline{\overline{\eta}}$). Figure 4.7 compares the area averaged effectiveness for the baseline cases at different blowing ratios. An overall area averaged effectiveness was calculated for the combined (SS+PS) region by averaging the adiabatic effectiveness values extending from the suction side to the pressure side (Y/D = -25 to Y/D = 10). Note that lateral averaging was carried our for the same vane surface length of x/S = 0.15 along the suction and pressure sides from the vane stagnation. The area averaged effectiveness of the combined region increases until a blowing ratio of M = 2.0 and then steadies out with any further increase. By looking at the individual effectiveness levels, on the suction side it peaks at M = 2.0 and then decreases and plateaus, whereas on the pressure side the effectiveness levels keep increasing with an increase in blowing ratio. So, for the baseline case with a smooth endwall surface, a blowing ratio of M = 2.0 was found to have the highest effectiveness levels.

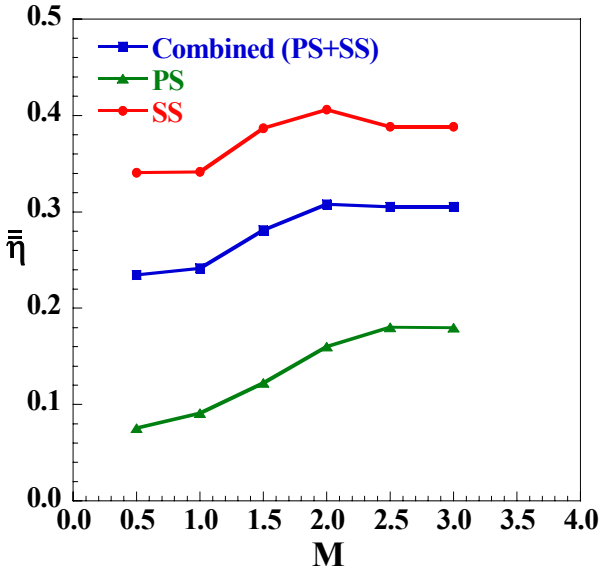

Figure 4.7. Area averaged effectiveness for the baseline geometry along suction, pressure and the whole leading edge region.

Effect of Modifying the Film-Cooling Exit

An individual hole trench, a row trench, and a bump configuration upstream and downstream of the cooling row were tested on a smooth endwall surface. These modifications were carried out at a constant coolant flowrate through the upstream slot. It was shown in Thole and Knost [5] that for a two passage study the coolant flow from the upstream slot is an important characteristic to simulate given that it provides the correct incoming boundary conditions to the vane cascade. Their study showed that due to secondary flows in the vane passage the coolant flow from the upstream slot was swept from the pressure side to the suction side creating a low adiabatic effectiveness zone around the stagnation region. They also found that in the presence of leading edge film-cooling holes, the variation in adiabatic effectiveness levels around the stagnation region was solely the result of coolant flow from the film-cooling holes. Hence it was concluded that the upstream slot did not influence the comparisons with respect to trenches and bumps. Note that for these comparisons the same pressure ratio was used to set the blowing ratio through the film-cooling holes for the baseline and the trench and bump modifications.

Figure 4.8a-d compares the contours of adiabatic effectiveness of the three modified film-cooling hole exit configurations with the baseline case at a blowing ratio of M = 2.0. In this section the baseline is compared with the smallest trench depth and

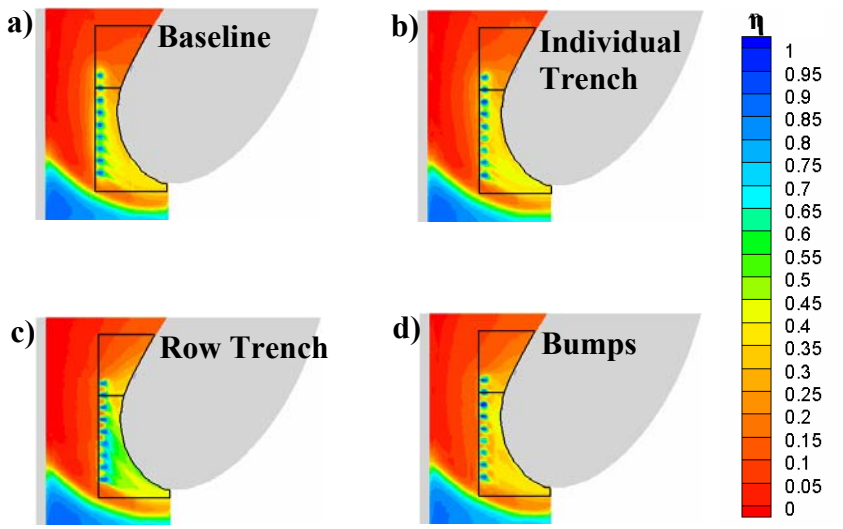

Figure 4.8. Contours of adiabatic effectiveness comparing the baseline case with the other configurations at a blowing ratio of M = 2.0.

bump height. The smallest trench depth studied corresponded to 0.4D and the smallest bump height corresponded to 0.5D. Comparing the individual hole trench (Figure 4.8b) at M = 2.0 to the baseline case (Figure 4.8a), it is seen that due to a presence of a vertical wall at the cooling hole exit, the jets are detached from the surface but reattach further downstream of the holes. Hence, the adiabatic effectiveness levels are lower at the exit of the cooling holes. The row trench in Figure 4.8c showed the maximum enhancement in effectiveness levels on the leading edge. The trench walls upstream and downstream of the holes allow the coolant to spread laterally within the trench area resulting in enhancements in adiabatic effectiveness levels. It is speculated by Bunker [10] that the trench walls reduce the typical vortex motion of the coolant jets and thereby preventing the hot gases from getting pulled underneath the coolant jets.

Placing bumps on the smooth surface caused varied results. From Figure 4.8d it can be seen that relative to the baseline case, it lowered the effectiveness levels on the suction side, whereas it increased the effectiveness levels on the pressure side. Bumps downstream of the cooling holes deflected the coolant jets off the surface thereby lowering the adiabatic effectiveness levels on the suction side, but caused an increase in effectiveness on the pressure side.

The effects of these modifications are quantified by calculating the laterally averaged effectiveness downstream of the film-cooling holes. From Figure 4.9 it can be seen that row trench performed the best on the suction and pressure sides. The individual

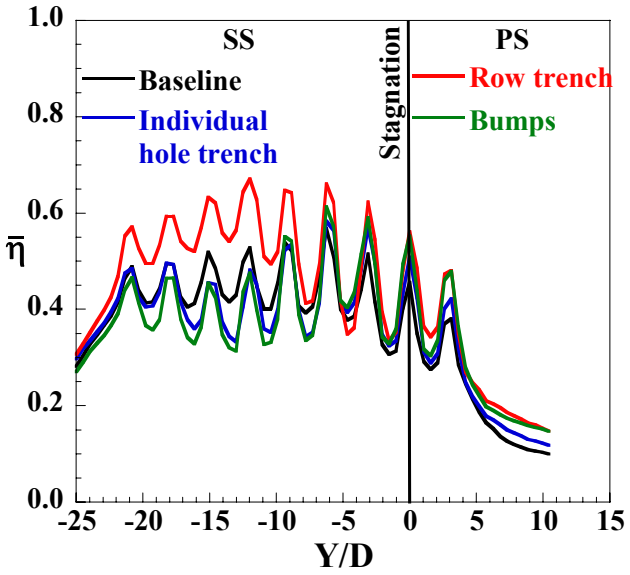

Figure 4.9. Laterally averaged adiabatic effectiveness comparing the effect of trenches and bumps at the leading edge at M = 2.0.

hole trench and the bumps showed a reduction in adiabatic effectiveness levels from Y/D = -25 to Y/D = -5 and showed an improvement in effectiveness levels from Y/D > -5. The lateral averaged effectiveness curves for the baseline and individual trench seem to coexist with little variation. Their effects at varying blowing ratios can be seen in Figure 4.10 which compares the area averaged effectiveness for the three modifications. At a blowing ratio of M = 2.0 the area averaged adiabatic effectiveness of the trenched hole, bumps, and the baseline coexist showing that their overall effectiveness levels downstream of the cooling holes are same. Trenches show an improvement over the whole range of blowing ratios tested with the maximum enhancement at a blowing ratio of M = 2.5.

This initial study was to ascertain which geometry has the maximum effect on the effectiveness levels at the leading edge. Trenches showed an overall enhancement in effectiveness levels and the bumps showed an improvement along the pressure side. The sensitivity of varied bump heights and trench depths to blowing ratios will be presented in the following sections.

Effect of Trench Depths on Adiabatic Effectiveness Levels

Three different row trench depths corresponding to 0.4D, 0.8D, and 1.2D were tested on a smooth endwall surface. This study was conducted to investigate the trench

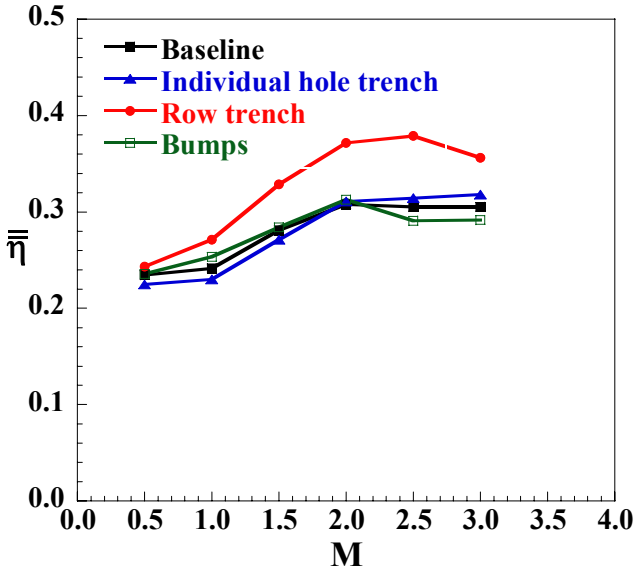

Figure 4.10. Area averaged effectiveness showing the effect of trenches and bumps on film-cooling effectiveness.

depth sensitivity to adiabatic effectiveness levels. Figure 4.11 compares the area averaged adiabatic effectiveness of the different trench depths. At the smallest trench depth of 0.4D, the enhancements in adiabatic effectiveness levels were seen for all blowing ratios. The adiabatic effectiveness levels for 0.4D trench increased with increasing blowing ratio up to a blowing ratio of M = 2.5. Upon a further increase in blowing ratio to M = 3.0, the effectiveness levels slightly dropped as a result of higher jet momentum associated with the coolant flow.

As the trench depth was further increased to 0.8D, higher enhancements in effectiveness levels were seen for all blowing ratios. Contrary to the 0.4D trench, the adiabatic effectiveness for the 0.8D trench depth increased until a blowing ratio of M = 2.5, and then stayed nearly the same with a further increase to M = 3.0. Compared to the baseline, the enhancement in effectiveness varied from $\eta = 0.24$ at M = 1.0 to a high value of almost $\eta = 0.48$ at M = 3.0.

An increase in trench depth to 1.2D also showed enhancements compared to the baseline case but the effectiveness levels were comparatively lower than the 0.8D trench as seen in Figure 4.11. Also, the effectiveness levels at 1.2D depth were similar or lower than the 0.4D depth for blowing ratios less that M = 2.5 and showed higher levels only at M = 3.0. At a higher depth and low blowing ratio, the walls of the trench prevent the coolant from exiting uniformly resulting in lower effectiveness levels. As the blowing

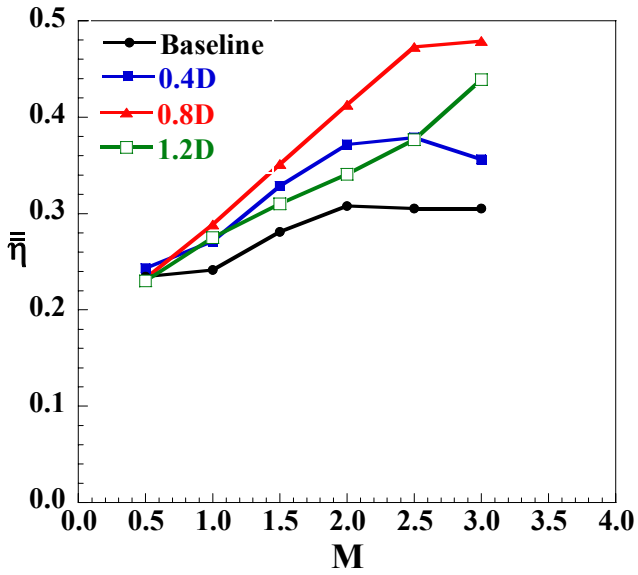

Figure 4.11. Area averaged effectiveness showing the effect of different trench depths for the row trench configuration at varying blowing ratios.

ratio is increased, the jets exit at a higher momentum making the trench more effective in the spreading of the coolant. From Figure 4.11 it can also be seen that the adiabatic effectiveness levels for the 1.2D trench follows a different pattern when compared to the 0.4D and 0.8D trench.

Figure 4.12 compares the adiabatic effectiveness levels for three blowing ratios at M = 1.0, M = 2.0, and M = 3.0 for different trench depths. The downstream edge of the trench forms a wall at the film hole exit, which forces the coolant to spread laterally within the trench before convecting over the endwall surface. At a smaller trench depth of 0.4D, it is seen that with an increase in blowing ratio the coolant spreads downstream of the cooling holes in a more uniform manner until the blowing ratio is high enough resulting in jet lift off. At a high blowing ratio of M = 3.0, there is less lateral spreading of coolant within the trench resulting in a deterioration in effectiveness levels.

An increase in trench depth to 0.8D results in a better lateral spread of coolant within the trench as there is less interaction between the mainstream gases and the coolant than when a set of axial holes are placed on a flat endwall surface. The contours of the 0.8D trench show that there are fewer hot spots between the cooling holes when compared to the 0.4D trench at the same blowing ratios. It is speculated that with an increase in trench depth the vortical nature of the flow leaving the cooling holes at the exit is less intense preventing the hot gases from getting pulled down to the surface

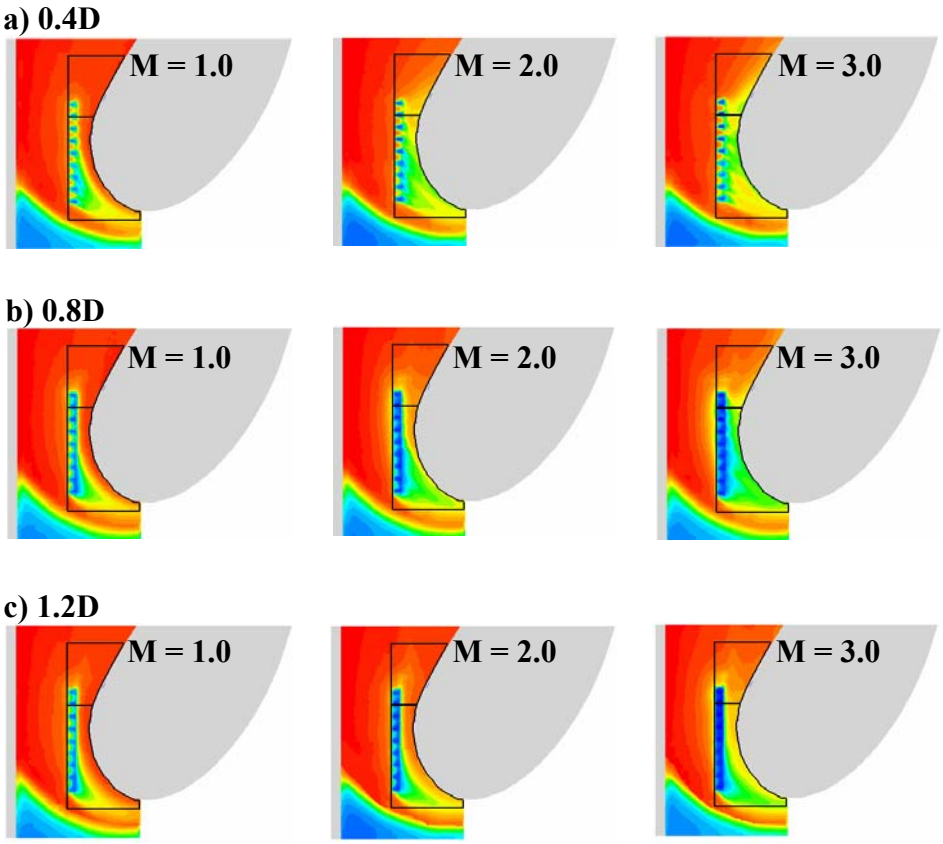

Figure 4.12. Contours of adiabatic effectiveness showing the effect of varying the trench depth for the row trench configuration at three different blowing ratios.

resulting in a better lateral spread within the trench. Lateral spreading within the trench causes the coolant to exit the trench in a more uniform manner onto the endwall surface. When the trench depth is further increased to 1.2D it is seen that at low blowing ratios there is an increase in the coolant retention within the trench. A higher depth causes a recirculation of coolant within the trench preventing it from convecting over the surface. With an increase in blowing ratio the amount of coolant spreading onto the surface increases. As this study was done only until a maximum blowing ratio of M = 3.0, it is speculated that the 1.2D trench will perform better at a blowing ratio of M = 3.0 or higher.

The uniform spread of coolant as a result of trenches can also be seen by comparing the laterally averaged effectiveness at different blowing ratios for the 0.8D trench, as shown in Figure 4.13. For the baseline cases (refer to Figure 4.6) the laterally averaged adiabatic effectiveness levels showed definite peaks and valleys indicating regions of low effectiveness between the cooling holes. With the trench it is seen from Figure 4.13 that the height between the peaks and valleys are smaller and this height

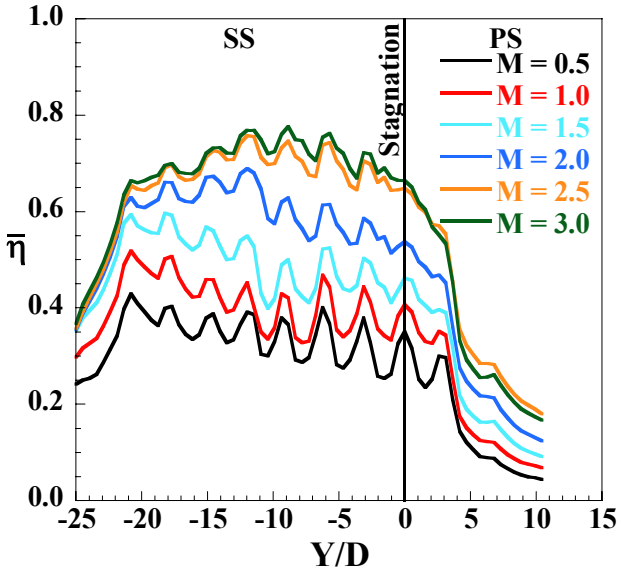

Figure 4.13. Lateral averaged effectiveness showing the effect of the 0.8D trench depth at different blowing ratios.

becomes smaller as the blowing ratio is increased, thus indicating a more uniform spread of coolant over the endwall surface. Also, the 0.8D trench was found to be the optimum depth from the three trench depths tested, and the performance is highly sensitive to blowing ratio.

Effect of Bump Heights on Adiabatic Effectiveness Levels

Three different bump heights corresponding to 0.5D, 0.8D, and 1.2D were also evaluated at the leading edge on a smooth endwall surface. Figure 4.14 compares the area averaged effectiveness for the varying bump heights with the baseline case. The 0.5D and 0.8D bumps showed little effect on modifying the adiabatic effectiveness levels downstream of the film-cooling holes. When the bump height was increased to 1.2D there was an increase in effectiveness levels up to a blowing ratio of M = 2.0 and a further increase in blowing ratio resulted in lower effectiveness levels.

The variation in effectiveness levels caused by the 1.2D bumps can be explained by the adiabatic effectiveness contours shown in Figure 4.15. The increase in blowing ratio results in an increase in coolant mass flow rate, which in turn increases the effectiveness levels. At lower blowing ratios of M = 0.5 and M = 1.0, the jets are more attached to the surface and they are obstructed by the presence of the bumps. As a result, the coolant accumulates between the cooling holes thereby preventing it from spreading

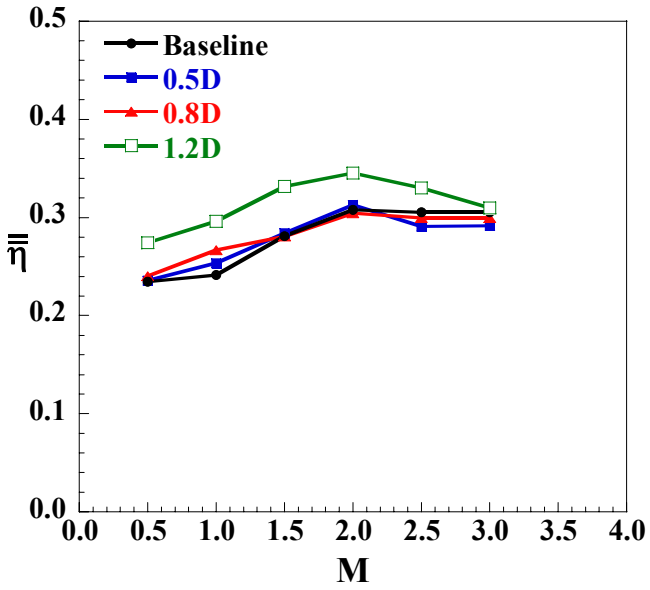

Figure 4.14. Area averaged effectiveness showing the effect of varying bump heights.

downstream. As the blowing ratio is increased it can be seen that there is less coolant accumulation between the cooling holes. With the increase in blowing ratio the coolant injects directly into the mainstream resulting in the formation of hot spots at the exit of the cooling holes. At high blowing ratios the effectiveness levels further downstream of the cooling holes are higher than at low blowing ratios as a result of jet reattachment. M = 2.0 was found to be an optimum blowing ratio where there is minimal coolant accumulation between the cooling holes and more spreading downstream of the cooling holes.

The performance of the 1.2D bumps along the pressure and suction sides at different blowing ratios can be compared using the laterally averaged effectiveness shown in Figure 4.16. Similar to the baseline study, the bumps performed better on the suction side at lower blowing ratio, whereas the effectiveness levels were higher on the pressure side at higher blowing ratios. And as mentioned previously, the bumps performed the best at a blowing ratio of M = 2.0.

Summary of Cooling Enhancements

To summarize the results, Figure 4.17 shows the percent increase in area averaged adiabatic effectiveness levels as a result of placing trenches of different depths at the leading edge. Figure 4.18 shows the enhancements in adiabatic effectiveness levels as a

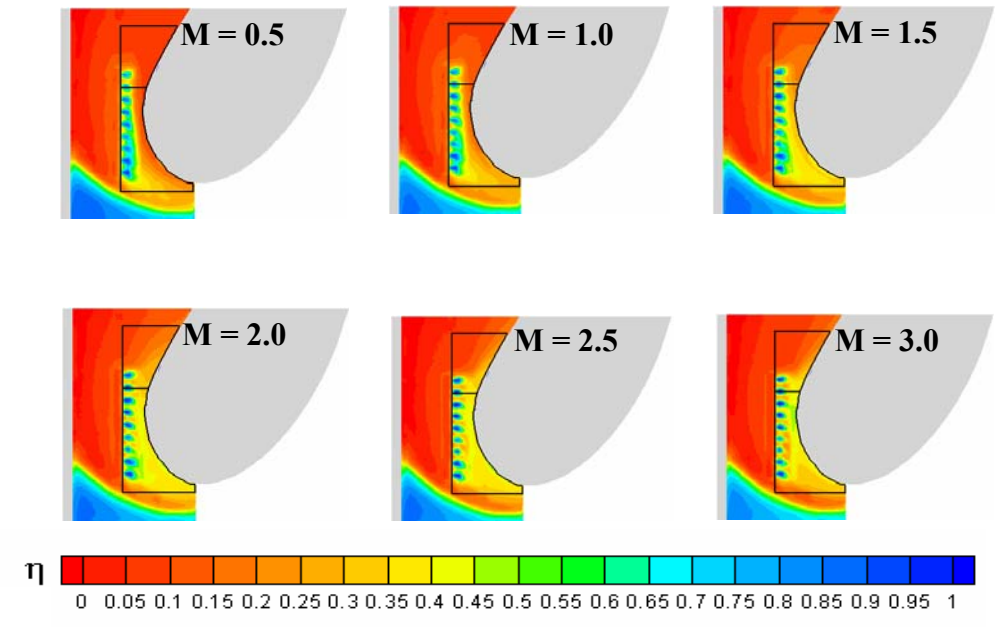

Figure 4.15. Contours of adiabatic effectiveness showing the effect of the 1.2D bumps at different blowing ratios.

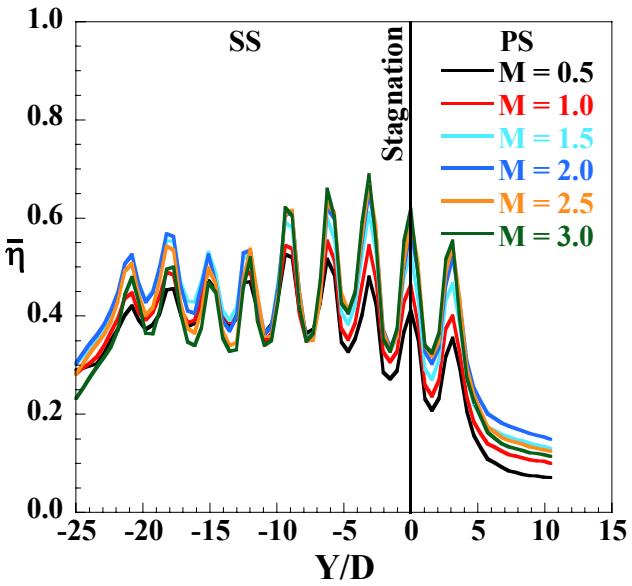

Figure 4.16. Laterally averaged effectiveness showing the effect of the 1.2D bump at different blowing ratios.

result of placing bumps of different heights at the leading edge. Trenches showed an enhancement for all depths tested whereas bumps performed better only at higher heights when compared to the baseline cases.

Trenches typically showed little effect at the lowest blowing ratio of M = 0.5. For a blowing ratio of M = 1.0 and higher, the percent enhancements ranged from 10% to

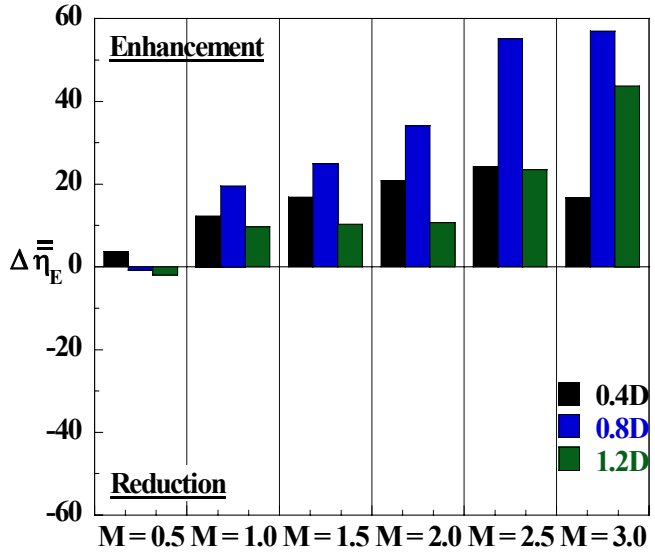

Figure 4.17. Comparison of percent enhancement on area-averaged adiabatic effectiveness as a result of placing trenches at the leading edge.

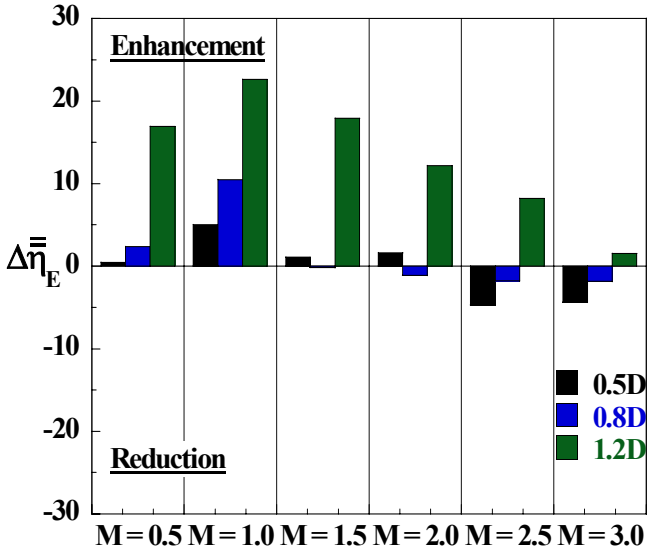

Figure 4.18. Comparison of percent enhancement on area-averaged adiabatic effectiveness as a result of placing bumps at the leading edge.

almost as high as 60%. The enhancement caused by the 0.8D trench was the highest at a blowing ratio of M = 2.5, beyond which there was a small increase in effectiveness at M = 3.0. The 1.2D trench showed a different trend compared to 0.4D and 0.8D. The cooling enhancement of the 1.2D trench was similar up to a blowing ratio of M = 2.0. At blowing ratios greater than M = 2.0 the 1.2D trench resulted in higher effectiveness levels than seen at the low blowing ratios.

Contrary to trenches, the bumps at heights of 0.5D and 0.8D showed very little

effect on adiabatic effectiveness levels. Bumps of height 1.2D showed higher enhancements at lower blowing ratios and the enhancement levels dropped with an increase in blowing ratio beyond M = 1.0. The maximum enhancement shown by the 1.2D bump was about 20%. From the baseline study it was seen that without any modification at the leading edge, the maximum effectiveness was achieved at a blowing ratio of M = 2.0. As bumps and trenches both showed an enhancement it is important to see if these modifications at lower blowing ratios can show any enhancement when directly compared to the baseline case of M = 2.0. This is important as it will ascertain if it will require less coolant which in turn will increase the efficiency of the engine.

Figure 4.19 compares the enhancements resulting from the 0.8D trench and 1.2D bump relative to a baseline case of effectiveness achieved at M = 2.0. The 0.8D trench and 1.2D bump were chosen as these were found to show the maximum enhancement for a particular geometry. For both the trenches and bumps, enhancements were only measured for $1.5 \leq M \leq 2.5$ and beyond M = 2.5 only trenches were measured to have a positive augmentation. Even in this comparison, as previously discussed, the trenches performed better than the bumps. It needs to be seen whether a reduction in blowing ratio to M = 1.5, showing an enhancement of only 10-15%, is more favorable than operating at the same blowing ratio of M = 2.0 to achieve an enhancement of 35% .

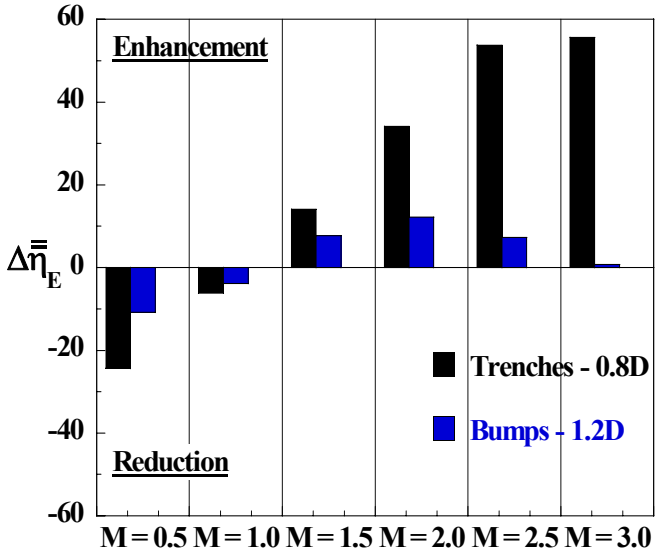

Figure 4.19. Comparison of percent enhancement on area-averaged adiabatic effectiveness on trenches and bumps when compared to the baseline case at M = 2.0.

Conclusions

Measurements of adiabatic effectiveness levels were presented at the leading edge-endwall junction where cooling is made difficult by the presence of a horseshoe vortex. In an attempt to improve cooling performance from a row of film-cooling holes placed near the junction, incorporating bumps and trenches were evaluated.

Trenches were applied in two different configurations. Individual hole trenches and row trenches were evaluated for a range of blowing ratios and trench depths. Individual hole trenches showed very little effect on adiabatic effectiveness levels, whereas the row trenches showed a considerable enhancement. The 0.8D trench depth was found to be an optimum relative to the three depths studied at different blowing ratios. It was also found that the success of the trench on improving effectiveness levels is highly sensitive to blowing ratio for a particular trench depth.

Bumps with heights of 0.4D and 0.8D did not produce a major effect on effectiveness, although a bump height of 1.2D did show an enhancement of approximately 20% at a blowing ratio of M = 1.0. Overall, this study has shown it is possible to achieve improved film-cooling at the vane-endwall junction through the use of small surface modifications near the cooling hole exits.

Acknowledgments

This publication was prepared with the support of the US Department of Energy, Office of Fossil Fuel, and National Energy Technology Laboratory. However, any opinions, findings, conclusions, or recommendations expressed herein are solely those of the authors and do not necessarily reflect the views of the DOE. The authors also thank Mike Blair (Pratt & Whitney), Ron Bunker (General Electric), and John Weaver (Rolls-Royce) for their input on the modeling of realistic turbine features.

Attribution

This paper was co-authored with Dr. Karen Thole. Her role was:

Co-author – paper 4

Name – Dr. Karen A. Thole

Department – Mechanical Engineering

Degree – Ph.D

Relationship – Chair and primary advisor

Role - Dr. Thole served as my dissertation chair and advised me through my Ph.D and on all the work presented in this dissertation.

Nomenclature

C true chord of stator vane

D diameter of film-cooling hole

h height/depth of trenches and bumps

M blowing ratio based on inlet mainstream velocity

$M = \rho_j U_j / \rho_\infty U_\infty$

P vane pitch; hole pitch

PS pressure side

Re_{in} Reynolds number defined as $Re_{in} = CU_{in} / \nu$

S span of stator vane; total vane surface length

SS suction side

T temperature

x length along the vane surface

X,Y,Z local coordinates

U velocity

Greek

η adiabatic effectiveness, $\eta = (T_\infty - T_{aw}) / (T_\infty - T_c)$

$\overline{\eta}$ laterally averaged effectiveness

$\overline{\overline{\eta}}$ area-averaged effectiveness

$\Delta\overline{\overline{\eta}}_E$ percent reduction in area-averaged effectiveness,

$\Delta\overline{\overline{\eta}}_E = [(\overline{\overline{\eta}}_{effect} - \overline{\overline{\eta}}_{baseline}) / \overline{\overline{\eta}}_{baseline}] \times 100$

ν kinematic viscosity

Subscripts

aw adiabatic wall

c coolant conditions

in inlet conditions

j coolant flow through film-cooling holes

∞ local freestream conditions

E enhancement

Overbar

– lateral average

= area average

References

[1] Chyu, M. K., 2001, "Heat Transfer near Turbine Nozzle Endwall," *Annals of the New York Academy of Sciences,* Vol. 934, pp. 27-36.

[2] Friedrichs, S., Hodson, H. P., and Daws, W. N., 1996, "Distribution of Film-Cooling Effectiveness on a Turbine Endwall Measured using Ammonia and Diazo Technique," *Journal of Turbomachinery*, Vol. 118, pp. 613-621.

[3] Friedrichs, S., Hodson, H. P. and Dawes, W. N., 1997, "Aerodynamic Aspects of Endwall Film-Cooling," *Journal of Turbomachinery*, vol. 119, pp. 786-793.

[4] Friedrichs, S., Hodson, H. P. and Dawes, W. N., 1999, "The Design of an Improved Endwall Film-Cooling Configuration," *Journal of Turbomachinery*, vol. 121, pp. 772-780.

[5] Thole, K. A., and Knost, D. G., 2005, "Heat Transfer and Film-Cooling for the Endwall of a First Stage Turbine Vane," *International Journal of Heat and Mass Transfer*, Vol. 48, pp. 5255 – 5269.

[6] Blair, M. F., 1974 “An Experimental Study of Heat Transfer and Film-Cooling on Large-Scale Turbine Endwalls,” *Journal of Heat Transfer*, Vol. 96, pp. 524-529.

[7] Knost, D. G., and Thole, K. A., “Adiabatic Effectiveness Measurements of Endwall Film-Cooling for a First Stage Vane,” *Journal of Turbomachinery*, Vol. 127, pp. 297-305.

[8] Cardwell, N. D., Sundaram, N., and Thole, K. A., 2006, “The Effects of Varying the Combustor-Turbine Gap,” *Journal of* Turbomachinery, GT2006-20089.

[9] Burd, S. W., and Simon, T. W., 2000, “Effects of Slot Bleed Injection over a Contoured Endwall on Nozzle Guide Vane Cooling Performance: Part II – Thermal Measurements,” 2000-GT-0200.

[10] Bunker, R. S., 2002 , “Film-Cooling Effectiveness due to Discrete Holes within a Transverse Surface Slot ,” GT2002-30178.

[11] Lu, Y., Nasir, H., and Ekkad, S. V., 2005, “Film-Cooling from a Row of Holes Embedded in Transverse Slots,” GT2005-68598.

[12] Waye, S. K., and Bogard. D. G., 2006, “High Resolution Film-Cooling Effectiveness Measurements of Axial Holes Embedded in a Transverse Trench with Various Trench Configurations,” *Journal of Turbomachinery*, GT2006-90226.

[13] Sundaram, N., and Thole, K. A., 2006, “Effects of Surface Deposition, Hole Blockage and TBC Spallation on Vane Endwall Film-Cooling,” *Journal of Turbomachinery*, GT2006-90379.

[14] Bunker, R. S., 2001, “A Method for Improving the Cooling Effectiveness of a Gaseous Coolant Stream,” US Patent 6,234,755.

[15] Radomsky, R., and Thole, K. A., 2002, "Flowfield Measurements for a Highly Turbulent Flow in a Stator Vane Passage," *Journal of Turbomachinery*, Vol.122, pp. 255-262.

[16] Ethridge, M. I., Cutbirth, J. M., and Bogard, D. G., 2000, "Scaling of Performance for Varying Density Ratio Coolants on an Airfoil with Strong Curvature and Pressure Gradient Effects," *Journal of Turbomachinery*, Vol. 123, pp. 231-237.

[17] Moffat, R. J., 1988, "Describing the Uncertainties in Experimental Results," *Experimental Thermal and Fluid Science*, Vol.1, pp. 3-17.

Paper 5:
Flowfield Measurements of the Endwall Leading Edge with Film-Cooling

To be submitted to the *ASME Journal of Turbomachinery* *

Abstract

In a gas turbine, the turbine section limits the overall engine performance because of the material temperature limits of the airfoils. One region, in particular, is investigated in this study, which is the interface between the combustor and first vane in the turbine. The leading edge along the endwall of the stator vane experiences high heat transfer rates resulting from a leading edge vortex. Typical turbine designs include a leakage slot at the interface between the combustor and turbine as well as film-cooling holes placed in the endwall of the first vane. While there have been some studies that have documented the horseshoe vortex at the leading edge of the vane, there have been no studies that have documented the flowfield for a realistic combustor-turbine interface with the presence of the slot and film-cooling jets. It has also been shown in the literature that film-cooling holes placed in a trench provide an effective means of improving cooling. The flowfield results presented in this paper document the influences of realistic design features such as the leakage slot and film-cooling jets on the leading edge horseshoe vortex. Moreover, measurements of the flowfield were made with the endwall film-cooling holes placed in a trench just upstream of the leading edge, which has also shown to provide improved overall cooling relative to no trench. Measurements were made using a laser Doppler velocimeter in a large-scale simulation. The results indicated the formation of a second vortex present for the case with film-cooling holes relative to the case with no film-cooling holes. In addition, turbulence levels as high as 50% were measured at the leading edge in the presence of film-cooling compared to the 30% measured with no film-cooling. For the trenched film-cooling holes, the coolant was shown to stay closer to the endwall surface.

* Co-author: Dr. Karen A. Thole, Mechanical and Nuclear Engineering Department, Penn State

Introduction

The flowfield at the leading edge of a first stage vane endwall is three-dimensional and complex due to the formation of horseshoe vortices. These vortices are associated with high turbulence levels and correlate with high heat transfer rates. As the flow in the endwall boundary layer approaches the vane stagnation, the flow decelerates as it experiences an increase in pressure. This deceleration is greater on the higher velocity fluid near the endwall causing a transverse pressure gradient along the vane. This causes the higher speed fluid to turn towards the endwall. The horseshoe vortex is formed as the inlet boundary layer separates from the endwall and combines with the downward motion of the mainstream fluid. Due to this downward motion, the less dense higher temperature fluid moves towards the endwall thereby increasing the local heat transfer coefficients. As such, it is important to locally cool this region to obtain higher endwall adiabatic effectiveness levels.

With increases in combustor exit temperatures, there is an increase in the heat load at the leading edge region. High temperatures coupled with horseshoe vortices cause high heat transfer rates making cooling imperative in the near wall region. Due to the formation of the horseshoe vortices, it is a challenge to cool the leading edge region as the coolant is swept off the surface leaving hot spots on the endwall. Studies by Friedrichs et al [1, 2] showed that the leading edge on the endwall is the most difficult region to cool. Blair [3] and Thole and Knost [4] showed that this region remained predominantly uncooled even in the presence of coolant leakage from a slot simulating the combustor-turbine interface upstream of the vane stagnation.

To understand film-cooling at the leading edge and to improve the cooling hole designs, it is important to measure the adiabatic effectiveness levels and the resulting flowfield. These measurements will help to understand the modification in the leading edge vortices caused due to coolant flow at the leading edge. To date a number of studies have been carried out that have measured the flowfield at the leading edge but none in the presence of film-cooling holes and an upstream slot. This study is unique as not only flowfield measurements with film-cooling holes are presented, but measurements with film-cooling holes placed in a two-dimensional transverse slot (trench) are also presented. Studies have shown that the adiabatic effectiveness levels on a surface are enhanced by

placing film-cooling holes in a trench. A study by Bunker [5] on a flat plate showed that placing film-cooling holes in a trench causes an increase in adiabatic effectiveness levels. Waye and Bogard [6] showed that the trench on a vane surface also enhanced the adiabatic effectiveness levels when compared to cylindrical holes. Their results indicated that the narrowest possible trench was the most desirable geometry. Studies on a vane endwall by Sundaram and Thole [7] indicated that the adiabatic effectiveness levels increased with increases in blowing ratio and higher trench depths performed better at higher blowing ratios. This study focuses on applying the trench geometry at the leading edge and measuring the adiabatic effectiveness levels and the flowfield, which will help in understanding the cause for enhancements in cooling due to a trench.

The work presented in this paper compares three different leading edge endwall configurations including an endwall with no film-cooling, endwall with a row of film-cooling holes and an upstream slot, and an endwall with row of film-cooling holes placed in a trench and an upstream slot.

Relevant Past Studies

Effective cooling of a turbine surface is highly important for its improved operational life and the performance of the engine as a whole. With regard to that, a number of studies have focused on developing alternate methods to cool a surface in addition to placing film-cooling holes.

An early study was carried out by Blair [3] in which he showed that coolant flow from an upstream slot resulted in higher cooling near the suction side and reduced cooling near the pressure side. This non-uniform cooling was as a result of the coolant being swept from the pressure side to the suction side caused by the secondary flow within the vane passage. Burd and Simon [8] studied the effects of slot bleed injection over the contoured endwall of a nozzle guide vane. They concluded from their measurements that bleed cooling from upstream of the leading edge of the vane provides considerable thermal protection within the passage. These studies of coolant flow through a slot showed that effective cooling can be achieved by injecting a 2D layer of film-cooling over the surface. Zhang and Moon [9] studied the effect of two row film-cooling at the leading edge of a contoured endwall. They carried out their endwall

studies on two inlet geometries- one with a flush endwall and the other with a backward facing step. They found that the adiabatic effectiveness levels drastically reduced with the backward facing step as the incoming boundary layer was destabilized resulting in poor film coverage. Kost and Nicklas [10] and Nicklas [11] were the first to carry out a study with a combination of an upstream slot with film-cooling holes. They found in their studies that with the slot flow alone, which was 1.3% of the passage mass flow, the horseshoe vortex became more intense. This increase in intensity resulted in the slot coolant being moved off the endwall surface and heat transfer coefficients that were over three times that measured for no slot flow injection. They attributed the strengthening of the horseshoe vortex to the fact that for the no slot injection the boundary layer was already separated with fluid being turned away from the endwall at the injection location. Given that the slot had a normal component of velocity, injection at this location promoted the separation and enhanced the vortex. Their adiabatic effectiveness measurements indicated higher values near the suction side of the vane due to the slot coolant migration. Knost and Thole [12] studied the effect of leakage flow through the combustor-vane interface in the presence of film-cooling on the endwall adiabatic effectiveness levels. They showed that the coolant exits the upstream slot in a non-uniform fashion and the non-uniformity was associated with the formation of a hot ring around the stagnation region even in the presence of leading edge endwall cooling. Cardwell et al. [13] showed that the size of this hot ring could be reduced by decreasing the width of the upstream slot, which results in a more uniform spread of coolant.

Searching for better cooling techniques, Bunker [5] measured improved film-cooling effectiveness levels on a flat plate using discrete holes placed within a trench with varying widths. Bunker [5] showed that the narrowest possible trench width relative to the interior cooling hole diameter is most desirable. As placing cooling holes in trenches basically modifies the hole exit, there have been few studies that have investigated this particular effect. Lu et al. [14] investigated the effect of slot exit area and edge shape on film effectiveness measurements made on a flat plate. They found that a straight edge exit performed the best at a blowing ratio of M = 1.0, whereas a ramped exit enhanced the adiabatic effectiveness levels at lower blowing ratios. Waye and Bogard [6] applied the trench configuration on the suction side of a first stage vane with

varying slot exit configurations. They tested a narrow trench where the trench wall was at the film-cooling hole exit, a wide trench where the trench wall was at a distance of one cooling hole diameter from the hole exit, and a trench with an angled exit. They also found that the narrow trench performed the best relative to a wide trench and angled exit trench and the adiabatic effectiveness levels peaked for blowing ratios beyond M = 1.0.

Sundaram and Thole [7] recently studied the effect of trench depth for a row of film-cooling holes at the leading edge. They measured the adiabatic effectiveness for trench depths corresponding to 0.4D, 0.8D, and 1.2D where D was the film-cooling hole diameter. They found 0.8D trench depth to be an optimum depth relative to the three depths studied at different blowing ratios. It was also found that the success of the trench on improving effectiveness levels is highly sensitive to blowing ratio for a particular trench depth.

This work focuses on measuring the adiabatic effectiveness levels and the flowfield at the leading edge in the presence of film-cooling holes and film-cooling holes placed in a trench. These measurements will also help ascertain the effect of coolant flow through the upstream slot on leading edge flowfield.

Experimental Design and Measurements

The following sections explain the experimental set up, the test section geometry and the instrumentation and techniques employed to measure the adiabatic effectiveness levels and the flowfield at the leading edge of the first stage vane endwall.

The experimental set up consisted of a large-scale, low-speed, recirculating wind tunnel facility as shown in Figure 5.1. The flow is driven by a 50HP fan and passes through a primary heat exchanger, which is used to cool the bulk flow. The flow is then split into three channels; a primary core flow through the center and two secondary channels above and below the test section. Note that only the top secondary passage was used for this study. The primary core flow simulated the mainstream gas path and the secondary flow provided the coolant through the film-cooling holes and through the upstream slot. Two different temperature settings were maintained for the core flow as this study consisted of adiabatic effectiveness and flowfield measurements. The primary core flow was heated to about 60°C through a 55kW heater bank only for the adiabatic

effectiveness measurements. Also, for the adiabatic effectiveness measurements the secondary flow in the outer passage was cooled to about 20°C, thereby maintaining a temperature difference of 40°C between the primary and secondary flows. For flowfield measurements, the temperatures through the primary and secondary channels were both maintained at 30°C.

Endwall Geometry

From Figure 5.1 it can be seen that the test section is attached downstream of the flow/thermal conditioning section. The test section consists of two full passages with one center vane and two half vanes. Table 5.1 provides a description of the turbine vane geometry and operating conditions. The vane geometry used in the current study is a commercial first-stage vane previously described by Sundaram and Thole [6].

The vane passage under study consisted of a top and bottom endwall surface. The bottom endwall surface was made of foam and consisted of film-cooling holes and an upstream slot. The top endwall was made of plexiglass to allow easy optical access. Cardwell et al. [15] have previously described in detail the construction of the endwall surface. Similar to the study carried out by Sundaram and Thole [6] this study also consisted of a single row of nine film-cooling holes (P/D = 3) at the leading edge and an upstream slot (refer Figure 5.2). The film-cooling holes were placed at a distance of 0.03C from the vane stagnation. The upstream slot was placed at a distance 0.13C from the vane stagnation and simulated the gap at the combustor-turbine interface. The coolant flow through the upstream slot simulated the leakage flow that can occur at the

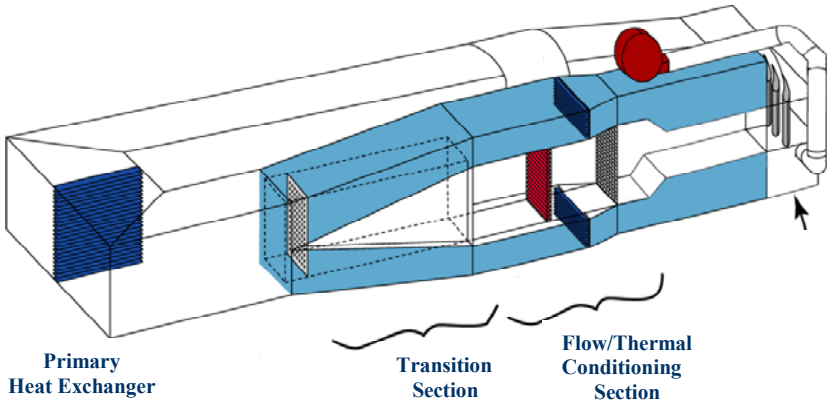

Figure 5.1. Illustration of the wind tunnel facility.

Table 5.1. Geometric and Flow Conditions

Scaling factor	9
Scaled up chord length (C)	59.4 cm
Pitch/Chord (P/C)	0.77
Span/Chord (S/C)	0.93
Hole L/D	8.3
Hole P/D	3
Re_{in}	2.1×10^5
Inlet and exit angles	0° & 72°
Inlet and exit Mach numbers	0.017 & 0.085
Inlet mainstream velocity	6.3 m/s
Upstream slot width	0.024C

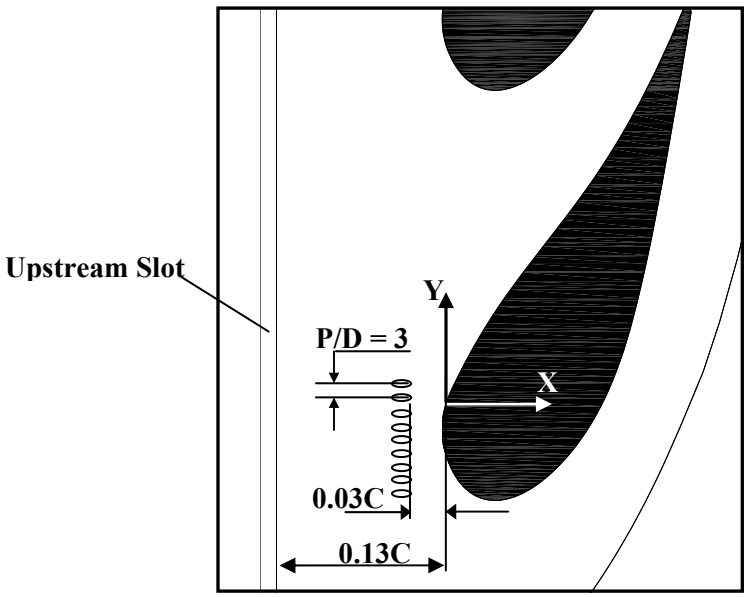

Figure 5.2. Illustrates the endwall design studied at the leading edge.

combustor-turbine interface. The film-cooling holes were placed at an angle of 30° and the upstream slot was placed at an angle of 45° to the endwall surface.

These studies were carried out on three different endwall configurations as shown in Figures 5.3a-c. Figure 5.3a shows the baseline configuration with no film-cooling holes or upstream slot. Figure 5.3b shows the hole study with film-cooling holes and the upstream slot at the leading edge. The third configuration tested was to study the effect of placing film-cooling holes inside a trench in the presence of an upstream slot, which is shown in Figure 5.3c. These trenches can have varying depths as previously described by Sundaram and Thole [7]. As suggested by Waye and Bogard [6] the trenches on a surface can be manufactured during the application of the thermal barrier coating (TBC)

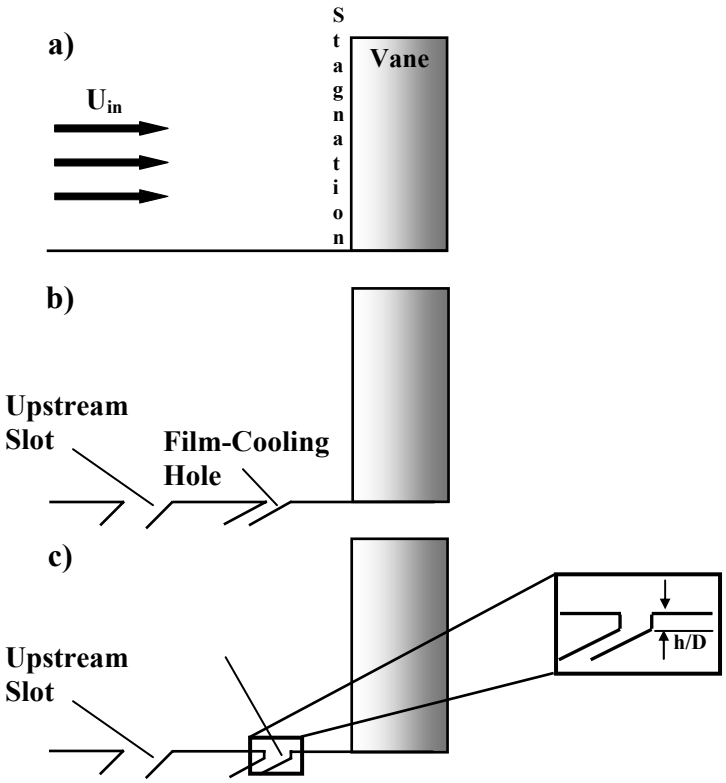

Figure 5.3. Illustrates the three endwall configurations a) baseline, b) hole, and c) trench studied at the leading edge.

and its effect can differ with varying trench depths as the thickness of the TBC can be varied. For this study, a thin piece of balsa wood was used to simulate a TBC of thickness 200μm on the engine scale. In most land based gas turbine vanes and blades the TBC thickness is on the order of 300μm. This TBC thickness corresponded to a trench depth of h = 0.4D, where D is the film-cooling hole diameter and this depth was kept constant for all studies presented in this work.

Two separate plenums were used to control the coolant flowrate through the upstream slot and through the film-cooling holes, respectively. The upstream slot flow was assumed to have a discharge coefficient of 0.6, which is the assumed value for a flow through a sharp-edged orifice, and the blowing ratio was calculated accordingly. The coolant flowrate through the film-cooling holes was set based on an average ideal blowing ratio. This blowing ratio was based on an inviscid calculation through the holes and the inlet mainstream velocity. It should be noted that an average discharge coefficient wasn't assumed to set the coolant flow through the film-cooling holes as it varies from hole-to-hole.

Endwall Adiabatic Effectiveness Measurements

A FLIR P20 infrared camera was used to spatially-resolve adiabatic wall temperatures on the endwall. Measurements were taken at six different viewing locations to ensure that the entire endwall surface was mapped. The camera was placed perpendicular to the endwall surface at a distance 55 cm from the endwall. Each picture covered an area of 24 cm by 18 cm with the area being divided into 320 by 240 pixel locations. The spatial integration of the camera was 0.715 mm (0.16 hole diameters). Thermocouples were also placed on the endwall surface at different locations to directly measure the temperature to post calibrate the infrared images. For the post calibration the emissivity was set at a constant value of 0.92 and the background temperature (~ 45ºC) was adjusted until the temperatures from the infrared camera images were within 0.05ºC of the corresponding thermocouple data. Six images were taken at each of the three viewing locations to obtain an averaged picture using an in-house Matlab program. The same program was also used to assemble the averaged pictures to obtain a complete temperature distribution around the stagnation region on the endwall surface.

Freestream temperatures were measured at multiple locations along the pitch and the average was determined by using a thermocouple rake consisting of three thermocouples along the span. It was found that the variations along the pitch were less than 0.2ºC and that along the span were less than 1.5ºC. Voltage outputs from the thermocouples were acquired by a 32 channel data acquisition module that was used with a 12-bit digitizing card. The temperature data was compiled after the system reached steady state.

A one-dimensional (1D) conduction correction as described by Ethridge et al. [16] was applied to all adiabatic effectiveness measurements to account for conduction losses through the endwall surface. The conduction correction was applied by measuring the endwall surface effectiveness with no blowing through the film-cooling holes. This was done by blocking the film-cooling holes on the endwall passage under study while maintaining similar flowrates through the adjacent passage to insure the correct boundary condition under the endwall. At the entrance to the flow passage for a measured value of $\eta = 0.9$, a correction of 0.16 was typical while along the pressure side for a measured value of $\eta = 0.1$, a correction of 0.03 was applied.

An uncertainty analysis was performed on the measurements of adiabatic effectiveness using the partial derivative method described by Moffat [17]. For adiabatic effectiveness measurements the precision uncertainty was determined by taking the standard deviation of six measurement sets of IR camera images with each set consisting of six images. The precision uncertainty of the measurements was ±0.014°C. The bias uncertainty was ±1.0°C based on the uncertainty in the IR camera measurements specified by the manufacturer. The bias uncertainty of the thermocouples was ±0.5°C as specified by the manufacturer and the bias uncertainty associated with the digitizing card was ±0.35°C. Then the total bias uncertainty of the temperature measurement due to the thermocouple and the digitizing card was calculated to be ±0.61°C. The total uncertainty was then calculated as ±1.02°C for the images and ±0.62°C for the thermocouple measurements. Uncertainty in effectiveness, η, was found based on the partial derivative of η with respect to each temperature in the definition and the total uncertainty in the measurements. Uncertainties in adiabatic effectiveness were calculated to be $\partial\eta = \pm 0.032$ at a η value of 0.2 and $\partial\eta = \pm 0.033$ at a η value of 0.9.

Endwall Flowfield Measurements

Laser Doppler velocimetry (LDV) was used to measure all the three velocity components and the root mean square (rms) velocities. Flowfield measurements were carried out at the stagnation plane (STAG) region as shown in Figure 5.4. The stagnation plane is parallel to the flow and intersects the vane at the stagnation location. The three component LDV system consisted of a 5W laser and a TSI 9201 Colorburst beam separator. Kang et al. [18] have previously described the LDV system used for this study. The measured velocity was then processed using a digital burst correlator which was controlled using the TSI FIND software. To calculate all the components of the velocity a 750 mm focusing lens with a beam expander was used. The probe volume length and diameter for the 750mm lens with beam expander were 0.85 mm and 46 μm. A total of 10,000 data points were measured to compute each of the mean and turbulent components of the velocity. To measure the three velocity components the flow was seeded with 1 μm diameter olive oil particles.

All the three components of velocity were measured, with the streamwise (U) and

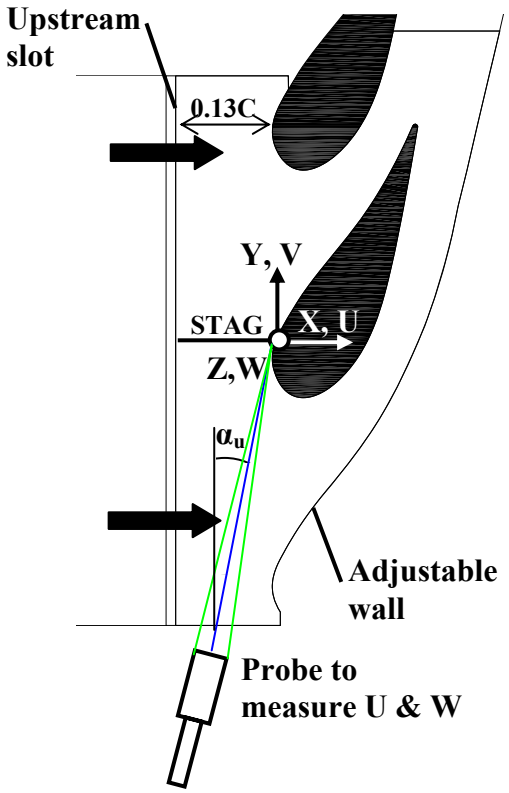

Figure 5.4. Top view of the test section showing the location of the upstream slot and the co-ordinate system to measure the velocity components.

the spanwise (W) measured from the side and the pitchwise (V) measured from the top endwall as shown in Figure 5.4. To allow measurements to be made close to the stagnation location the probe had to be turned 18° (α_u) to the right from the central axis as shown in Figure 5.4. This caused the measured streamwise velocity (U_{meas}) to be turned by an angle α_u in the U-V plane (refer Figure 5.5). The same probe was also tilted by 7° (α_w) downwards to facilitate measurements close to the endwall. The tilting of the probe resulted in transforming the measured spanwise component by an angle of 7° in the W-V plane as shown in Figure 5.5. The pitchwise (V) component was measured from the top by placing the probe perpendicular to the endwall surface. As a result of the probe turning and tilting the measured streamwise (U_{meas}) and the measured spanwise (W_{meas}) velocities had to be corrected to obtain the true velocity components U and W.

The correction scheme previously described by Kang and Thole [19] was applied to the measured velocities and is given by the following relations,

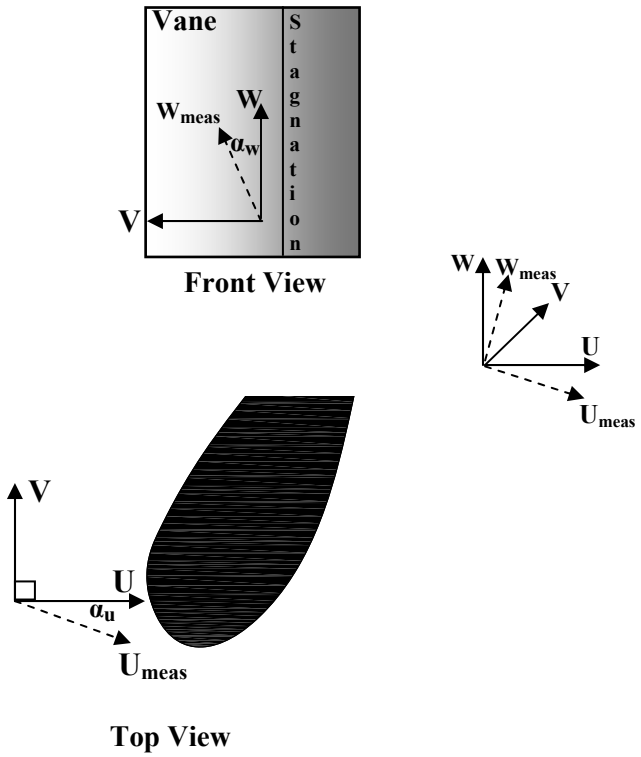

Figure 5.5. Velocity correction scheme applied for the U and W velocity components.

$$U' = \frac{U_{meas} \sin \alpha_v + V_{meas} \sin \alpha_u}{\sin(\alpha_u + \alpha_w)} \tag{1}$$

$$V' = V_{meas} \tag{2}$$

$$W' = W_{meas}. \tag{3}$$

U', V', and W' are the non-tilt corrected orthogonal velocities. As the downward tilt of θ_2 effected only the spanwise component, correction was applied only to W' and the resulting equations are given by,

$$U = U', \; V = V', \text{ and } \; W = W' \cos \alpha_w \tag{4}$$

where U, V, and W are the true mean velocities at the leading edge.

The three components of velocity were measured at the stagnation plane that is parallel the flow and intersects the vane stagnation. The measurement plane is similar to the stagnation plane measurement by Kang et al. [18]. The measurement plane extended to an axial distance of 0.25C upstream from the stagnation and 50% of the total span of the vane.

Similar to the adiabatic effectiveness measurements, an uncertainty analysis was performed based on the partial derivative method described by Moffat [17]. A 95 percent confidence interval and 10,000 data points were used to calculate the uncertainties in the mean and fluctuating velocity components. The estimate of the bias and precision uncertainties for the mean streamwise velocity in the near wall region were 1% and 0.44% respectively. In the mid-span region, the bias uncertainty was 1% and the precision uncertainty was estimated to be 0.06% for the mean streamwise velocity, and 1.0% for the mean pitchwise and spanwise velocities. In the measurements carried out at the near wall region, the precision uncertainties of the fluctuating velocities were found to be 2% for u_{rms}, 1.9% for v_{rms}, and 4.4% for w_{rms}.

Inlet Flow Conditions

For every test condition, the dimensionless pressure coefficient distribution was verified to insure a periodic flow through the vane passage. The inlet boundary layer approaching the vane was measured using the LDV system at an axial distance of 0.6C upstream from the vane stagnation. At this upstream location the incident turbulence level was measured to be 1.0% and the turbulence length scale was measured to be 4 cm (0.07C). Throughout this study the inlet turbulence level was maintained at 1.0%. Figure 5.6 shows the approaching boundary layer measured at three upstream locations. There was little variation found in the boundary layer thickness from a distance of 0.6C to 0.35C. Table 2 lists the inlet boundary layer characteristics at the 0.6C location.

The boundary layer thickness was measured at $\delta_{99}/S = 0.25$ compared to $\delta_{99}/S = 0.10$ obtained by Kang et al. [18] (refer Figure 5.6) who also used the same vane geometry. This large boundary layer thickness is because of the 45° ramp located at an axial distance of 2.3C upstream from the vane stagnation (refer Figure 5.1). Due to the

Table 5.2. Inlet Boundary Layer Characteristics

Boundary layer thickness (δ/S)	0.26
Displacement thickness/span (δ^*/S)	0.033
Momentum thickness (θ/S)	0.027
Shape factor (δ^*/θ)	1.25
Momentum thickness Reynolds number (Re_θ)	5318

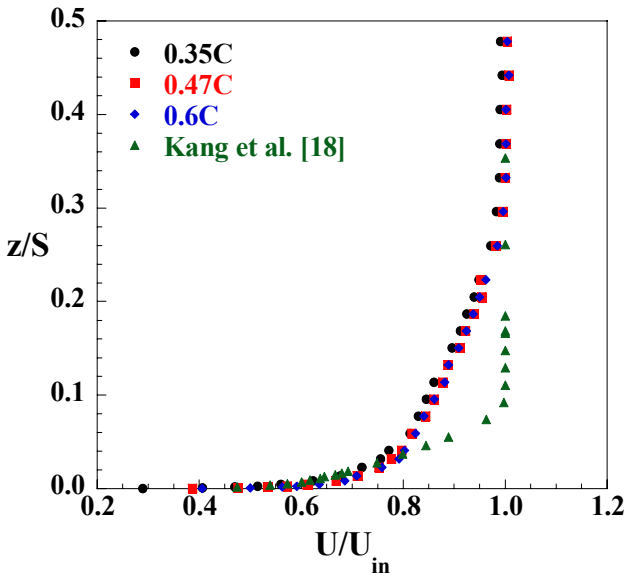

Figure 5.6 Comparison of measured streamwise boundary layer profiles at three upstream locations from the vane stagnation.

ramp the flow development length was reduced and there was a change in the inlet flow area at the location of the ramp. Figure 5.7 shows the variation of the mainstream velocity as the flow approaches the vane stagnation at different vane span locations. These measurements were made on a vane endwall having neither film-cooling holes nor an upstream slot. As expected the flow decelerated at all span locations as it approached the vane with the deceleration beginning at x/C >-0.35C at all heights. The deceleration at the mid-span is compared with the previous study by Radomsky [20], which had a longer flow development length. It is seen that in the present study the velocities are higher at the mid-span, which is caused by the reduction in the approaching flow area due to the 45° ramp upstream of the vane. The velocity variations at different span heights show that the deceleration rate is faster for the fluid near the vane endwall surface.

Adiabatic Effectiveness Measurements at the Leading Edge Endwall Junction

A study by Sundaram and Thole [21] showed that it is difficult to cool the leading edge-endwall junction due to the formation of horseshoe vortices. The temperatures around the stagnation area were found to be higher even in the presence of coolant flow through the upstream slot. The aim of this study was to understand the performance of a row of cylindrical film-cooling holes at the leading edge-endwall junction. Also, the

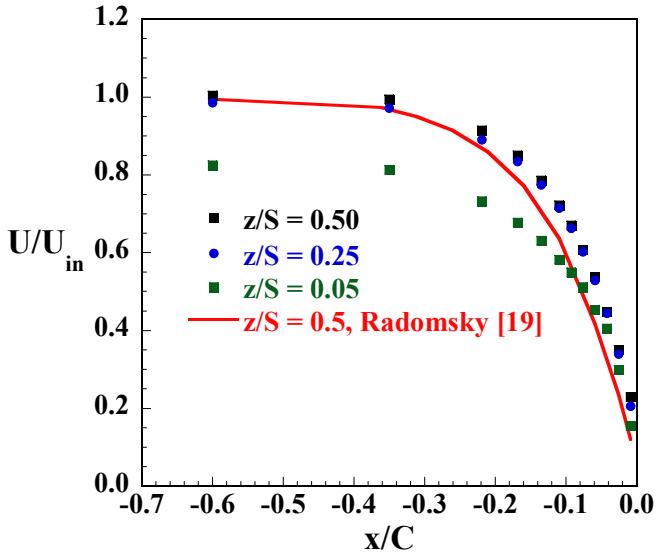

Figure 5.7 Variation of the streamwise velocity approaching the vane stagnation at different span (z/S) locations.

effect on adiabatic effectiveness by placing film-cooling holes in a trench will be studied and it's performance at higher blowing ratios.

Tests were carried out at blowing ratios varying from M = 0.5 to M = 3.0 through the film-cooling holes. A flowrate corresponding to an inlet blowing ratio of M_{in} = 0.3 was set through the upstream slot for all the tests reported in this paper. Figure 5.8a compares the contours of adiabatic effectiveness levels for coolant flow from the cooling holes at blowing ratios of M = 1.0, 2.0, and 3.0. From Figure 5.8a it can be seen that at a blowing ratio of M = 1.0, the adiabatic effectiveness levels are higher on the suction side of the endwall than on the pressure side. This is because of the lower static pressure on the suction side, which enables more coolant to exit the cooling holes near the suction side. With an increase in blowing ratio to M = 2.0 there is a gradual increase in effectiveness levels along the pressure and suction sides.

A further increase to M = 3.0 as shown in Figure 5.8a resulted in an increase in effectiveness levels on the pressure side with subsequent decrease on the suction side when compared to the lower blowing ratios. It can also be seen that at a high blowing ratio of M = 3.0, there is a reduction in effectiveness levels just downstream of the cooling holes. At high blowing ratios, the coolant jets are associated with high momentum resulting in jet lift off from the surface. In addition, at these high blowing ratios the adiabatic effectiveness levels increase near the vane-endwall junction. The

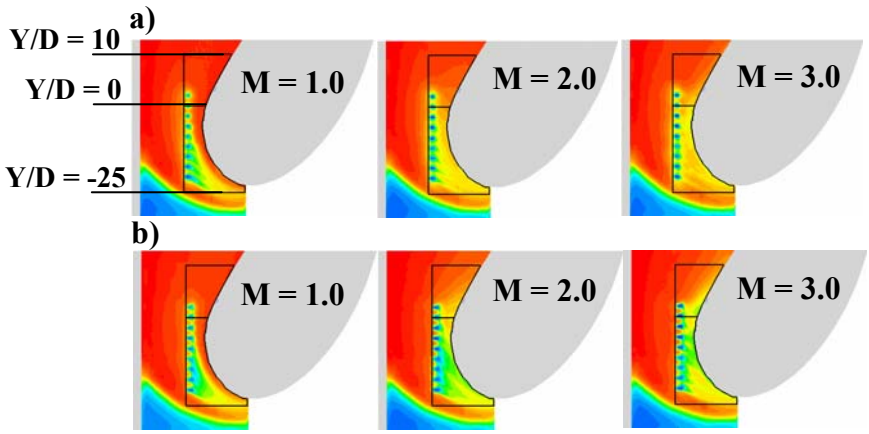

Figure 5.8. Contours of adiabatic effectiveness at varying blowing ratios comparing the a) hole study with b) the trench study at the leading edge.

adiabatic effectiveness levels increase near the junction as the horseshoe vortex formed at the leading edge pulls the coolant injected into the mainstream flow back to the surface. As a result, at high blowing ratios there is an increase in the adiabatic effectiveness levels at the vane-endwall junction but a significant decrease downstream of the film-cooling holes when compared to adiabatic effectiveness levels at low blowing ratios.

Due to the formation of the horseshoe vortex, it is difficult to achieve higher adiabatic effectiveness levels with axial cooling holes at the leading edge. As lack of cooling can be detrimental to the life of the stator vane, new cooling hole exit designs have to be implemented to achieve the required adiabatic effectiveness levels. As mentioned earlier, the study done by Waye and Bogard [6] on the vane surface showed that higher adiabatic effectiveness levels are achieved by placing film-cooling holes in a trench. Based on the study by Waye and Bogard [6], a similar trench design was applied to the leading edge film-cooling holes in this study.

Figure 5.8b compares the effect of placing film-cooling holes in a trench at varying blowing ratios. The downstream edge of the trench forms a wall at the film hole exit, which forces the coolant to spread laterally within the trench before convecting over the endwall surface. From Figure 5.8b it is seen that an increase in blowing ratio from M = 1.0 to M = 2.0 causes the coolant to spread more uniformly on the endwall surface until the blowing ratio is high enough resulting in jet lift off. At a high blowing ratio of M = 3.0, there is less lateral spreading of coolant within the trench resulting in a deterioration in effectiveness levels.

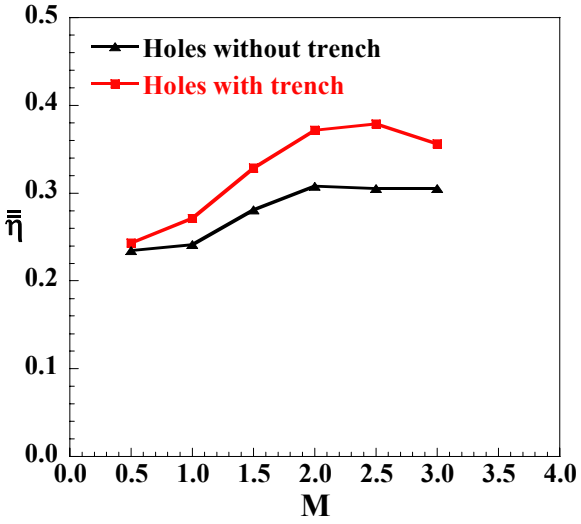

Figure 5.9. Area averaged effectiveness comparing the effect of a trench on leading edge film-cooling.

Figure 5.9 compares the area averaged effectiveness for the hole study with the trench study at different blowing ratios. An overall area averaged effectiveness was calculated for the boxed region (refer Figure 5.8) by averaging the adiabatic effectiveness values extending from the suction side to the pressure side (Y/D = -25 to Y/D = 10). The trench causes a steady increase in the adiabatic effectiveness levels as the blowing ratio is increased with the maximum enhancement at a blowing ratio of M = 2.5. At M = 3.0 there is a slight reduction in the enhancement due to possible jet lift off associated with higher momentum coolant flow. Figure 5.10 compares the laterally averaged adiabatic effectiveness levels in the boxed region at a blowing ratio of M = 2.5 to show the local enhancements downstream of each film-cooling hole. In the presence of film-cooling holes, an increase in the blowing ratio results in the reduction of effectiveness levels along the suction side. With the trench, the effectiveness levels improve on the suction side causing an overall improvement in the adiabatic effectiveness levels.

The aim of this work that followed the adiabatic effectiveness measurements was to measure the leading edge flowfield and to understand how the trench modifies the flowfield causing an increase in surface cooling. As the maximum enhancement was seen at a blowing ratio of M = 2.5, the flowfield measurements were carried out at the same blowing ratio.

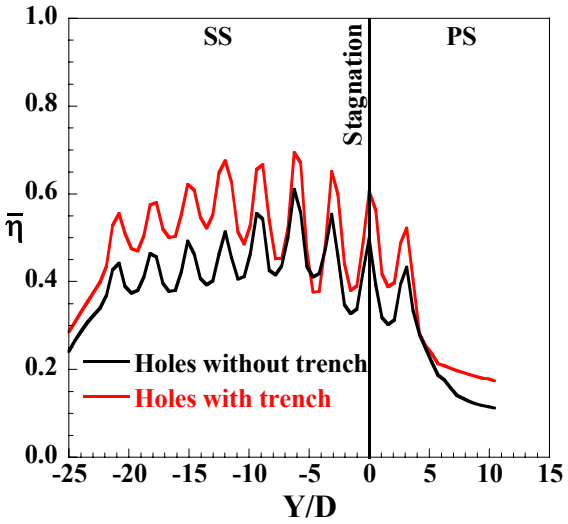

Figure 5.10. Laterally averaged effectiveness comparing the effect of trench on adiabatic effectiveness at a blowing ratio of M = 2.5.

Flowfield Measurements at the Leading Edge Endwall Junction

As described earlier, flowfield measurements were carried for the following three different endwall configurations: the baseline study - an endwall with no film-cooling holes; an endwall with a single row of film-cooling holes and an upstream slot; and an endwall with film-cooling holes placed in a trench and an upstream slot.

First the streamwise velocity contours superimposed with the secondary flow vectors are compared for each endwall configuration. Next, the variation in the turbulence components with the variation in the turbulence kinetic energy is presented and finally the effect of film-cooling and trench on the leading edge vorticity will be compared.

Flowfield Comparison at the Stagnation Plane

The flowfield was measured along a plane that is parallel to the incoming flow and intersects the vane stagnation. Figures 5.11a-c compare the secondary flow vectors along the stagnation plane for the three endwall configurations. Figure 5.11 also shows the contours of the normalized streamwise velocity (U/U_{in}) superimposed on the secondary flow vectors.

From Figure 5.11a it can be seen that there is a formation of a vortex on the endwall as the flow approaches the leading edge. The core of the vortex is located at a spanwise location of z/S = 0.015 from the endwall similar to the previous measurements

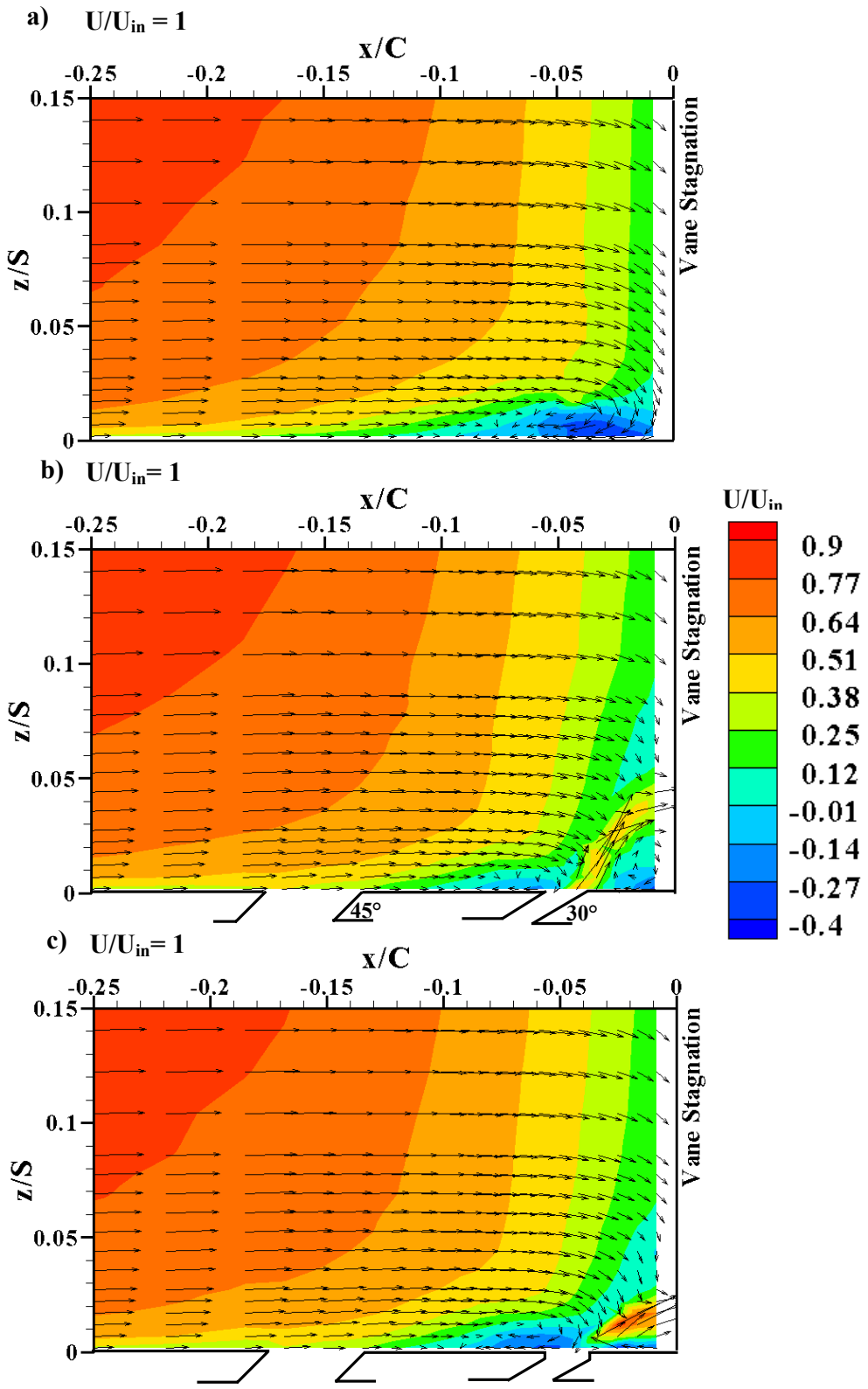

Figure 5.11. Leading edge flowfield measured at the stagnation plane superimposed with the streamwise velocity for a) baseline, b) film-cooling holes without trench, and c) film-cooling with trench.

by Kang et al. [18]. The core of the vortex is also located at a distance of x/C = 0.045 from the vane stagnation compared to the study by Kang et al. [18] where the core was located at x/C=0.08. As the 45° ramp changes the flow inlet area, the fluid velocity is faster in the near wall region thereby pushing the vortex closer to the vane surface. In the present study the location of the vortex core is similar to the study by Radomsky and Thole [22] where they showed that at high free-stream turbulence, the boundary layer flattens pushing the vortex closer to the vane surface.

Figure 5.11b shows the secondary flow vectors with coolant flow from an upstream slot and film-cooling holes without a trench. The blowing ratio through the film-cooling holes was set at M = 2.5 and the blowing ratio through the upstream slot was set at M_{in} = 0.3 which was based on the inlet mainstream velocity, U_{in}. At a blowing ratio of M = 2.5, the coolant jets are separated from the endwall surface and the coolant trajectory path reaches as high as z/S = 0.05. In the presence of the film-cooling holes there is a dual vortex formed upstream and downstream of the film-cooling holes. A stronger vortex is formed downstream of the film-cooling holes when compared to a weak vortex formed upstream of the film-cooling holes. Due to the downstream vortex and the higher trajectory of the coolant jets, the coolant exiting the film-cooling holes is lifted off the endwall surface. This prevents the coolant from spreading on to the endwall surface resulting in lower adiabatic effectiveness levels downstream of the cooling holes. The vortex formed downstream of the cooling holes also pulls the coolant injected into the mainstream flow back to the surface, thus increasing the effectiveness levels along the vane-endwall junction (refer Figure 5.8a). The temperature of the coolant also increases as the hot mainstream gases are entrained into the coolant flow thereby degrading the adiabatic effectiveness levels.

Endwall surface temperature measurements showed that by placing the film-cooling holes in a trench the adiabatic effectiveness levels downstream of the cooling holes were enhanced. Figure 5.11c shows the leading edge flowfield with the film-cooling holes placed in a trench in combination with an upstream slot. In the presence of a trench, the vortex downstream of the cooling hole disappears and the coolant jet trajectory is lower when compared to the jet trajectory in the absence of a trench. This enables better film-cooling protection on the surface at the same blowing ratio of M = 2.5

(refer Figure 5.8b). A vortex is formed upstream of the trench and is located at x/C = -0.05 similar to the baseline study. This vortex is formed as a trench results in a smaller coolant jet trajectory thereby preventing the entrainment of the mainstream flow into the coolant flow. Whereas, with just film-cooling holes, the coolant trajectory is higher causing the mainstream flow to entrain into the coolant jets thus preventing the formation of a vortex upstream of the cooling holes. Also, in the trench configuration, the coolant jets impact the leading edge of the vane in the near wall region and flow back on to the endwall surface. This aids in enhancing the adiabatic effectiveness levels in the near wall region.

Figure 5.12 compares the streamwise velocity profiles for the three endwall configurations close to the vane stagnation. These profiles were measured at an axial distance of x/C = -0.25 from the vane leading edge which is at a location downstream of the film-cooling holes. It is seen that the jets are more attached to the endwall surface in the trench study when compared to the jet trajectory in the hole study. Hence, there is less mixing between the mainstream flow and the coolant jets when film-cooling holes are placed in a trench the leading edge and thus resulting in better endwall adiabatic effectiveness levels. The magnitude of the streamwise velocity component is also higher in presence of a trench when compared to the study without a trench.

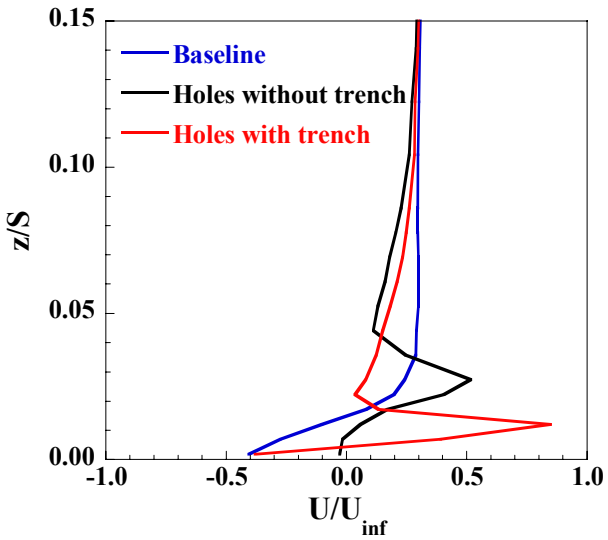

Figure 5.12. Streamwise velocity profiles at a distance of x/C = -0.025 from the vane stagnation for the three endwall configurations.

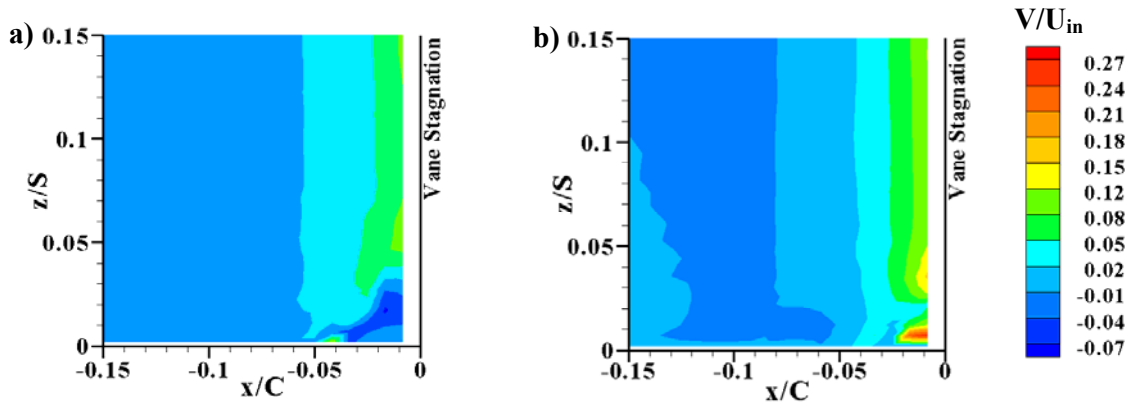

Figure 5.13. Contours of the pitchwise velocity component comparing the effect of a) film-cooling holes with no trench to b) film-cooling holes in a trench.

From the adiabatic effectiveness measurements and studies by Waye and Bogard [6], it was speculated that higher adiabatic effectiveness levels on the surface are achieved due to a lateral spreading of the coolant within and downstream of the trench. The lateral spreading in the case of a trench can be seen by comparing the contours of the pitchwise velocity components (V/U_{in}) for the hole and trench study (refer Figure 5.13). Figure 5.13a shows that at the leading edge in the near wall region, there is a very weak lateral movement as seen by the low values of pitchwise velocity. Figure 5.13b shows that in the presence of a trench there is a lateral flow at the leading edge with the peak levels occurring at the near wall region. This further confirms the ability of a trench to outperform the cylindrical holes by enhancing the adiabatic effectiveness levels at the leading edge.

In addition, it was found that the coolant leakage flow through the upstream slot did not affect the boundary layer approaching the vane stagnation. The approaching boundary layer was not disturbed as no coolant exited the slot location in front of the vane stagnation. An earlier study by Thole and Knost [4] showed that the coolant from the upstream slot is swept from the pressure side to the suction side due to the secondary flow within the vane passage. Their measurements showed that the coolant flow from the slot was mainly concentrated in the vane passage towards the suction side and not around the vane stagnation. This resulted in the formation of a hot ring around the vane stagnation resulting in low adiabatic effectiveness levels. As no coolant exited from the center of the slot, there was no flow disturbance to the approaching boundary layer.

Comparison of Turbulence Components at the Stagnation Plane

The flowfield for the different endwall configurations showed the formation of leading edge vortices at different locations each associated with different turbulence levels. Comparison of the different turbulence components for each study will reveal the location of peak turbulence levels at the leading edge for each endwall configuration.

Figures 5.14a-c compare the contours of the streamwise turbulence component u_{rms}/U_{in}, for the baseline, hole and trench studies. For the baseline study from Figure 5.14a it is seen that the peak streamwise turbulence levels of 30 percent occur in the vortex core and agree well with the previously reported measurements by Kang et al. [18]. It is also seen that the peak levels extend from the core of the vortex to the near wall region and the turbulence levels are significantly higher near the endwall surface than those occurring at the midspan. For the hole study the peak turbulence levels occur downstream of the cooling holes along the coolant jet trajectory as shown by Figure 5.14b. The turbulence levels are relatively lower in the near wall region close to the vane stagnation when compared to the levels along the coolant jet trajectory. Also, as the mainstream flow entrains into the coolant jets, the turbulence levels are higher at the jet-mainstream shear layer as seen in Figure 5.14b. The highest streamwise turbulence levels occur for the trench study as shown by Figure 5.14c. The peak turbulence levels occur along the coolant jets similar to the hole study. In the presence of a trench as the coolant jets are more attached to the surface, the peak turbulence levels are closer to the near wall region. Also, the turbulence levels inside the vortex formed upstream of the trench are similar to the turbulence levels in the horseshoe vortex formed in the baseline study.

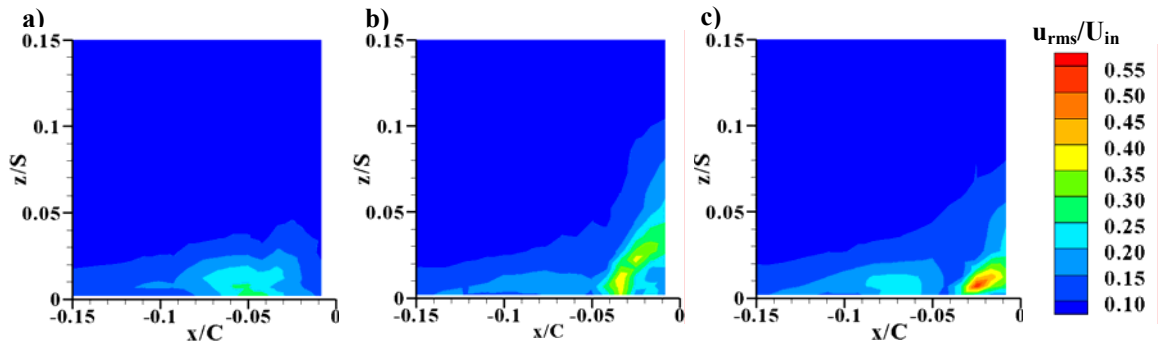

Figure 5.14. Comparison of contour levels of normalized streamwise turbulence levels for the a) baseline, b) holes without trench, and c) holes with trench.

Figures 5.15a-c compare the contours of the pitchwise turbulence levels at the stagnation plane. Figure 5.15a shows that the turbulence levels in the cross-stream direction are the lowest for the baseline study indicating that the dominant flow direction in the horseshoe vortex is in the streamwise and spanwise direction. With film-cooling injection at the leading edge, the peak pitch wise turbulence levels exist in the coolant jet trajectory as shown in Figure 5.15b. The pitchwise turbulence levels in the near wall region at the leading edge are very small indicating no lateral movement. Whereas in the trench configuration, from Figure 5.15c, it is seen that the pitchwise turbulence levels are relatively higher than the baseline or hole studies and the peak levels occur downstream of the trench.

Figures 5.16a-c compare the contours of the spanwise turbulence levels for the three endwall configurations. For the baseline study (Figure 5.16a), the spanwise turbulence levels are similar to the streamwise values and the peak turbulence levels occur in the vortex core. For the hole study as shown in Figure 5.16b, the peak spanwise

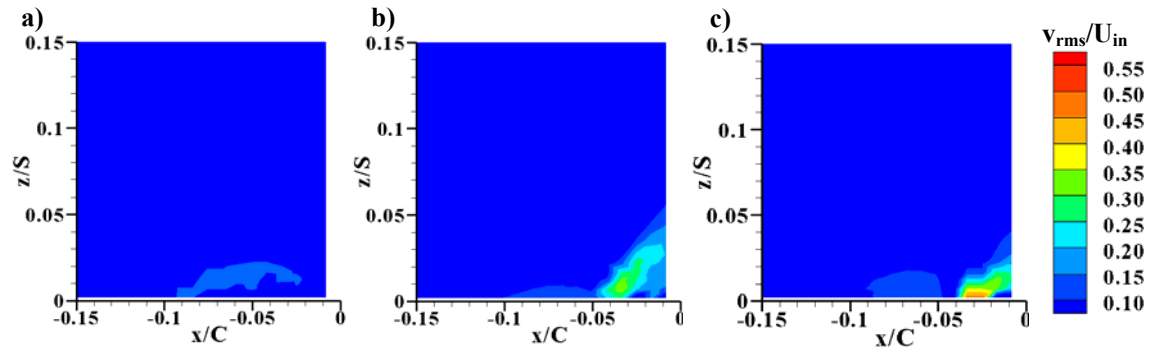

Figure 5.15. Comparison of contour levels of normalized pitchwise turbulence levels for the a) baseline, b) holes without trench, and c) holes with trench.

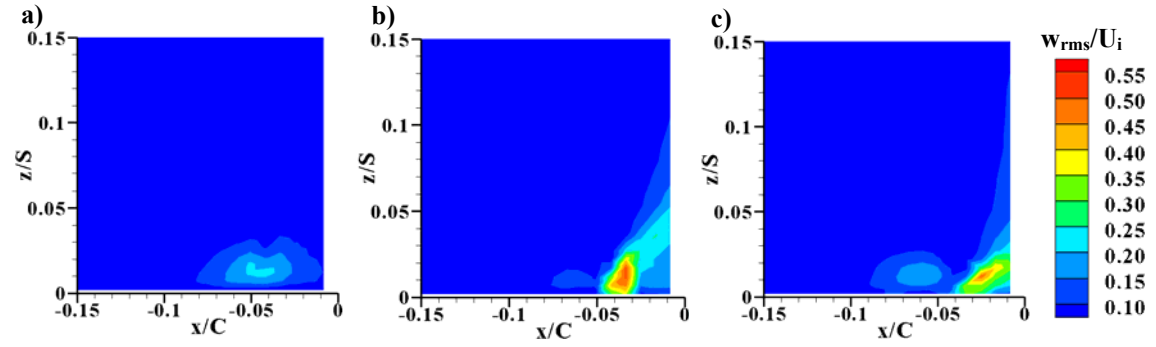

Figure 5.16. Comparison of contour levels of normalized spanwise turbulence levels for a) baseline, b) holes without trench, and c) holes with trench.

turbulence levels occur along the coolant jets and are closer to the near wall region. For the trench study as shown in Figure 5.16c, the peak levels occur downstream of the trench with relatively lower values occurring in the core of the upstream vortex. In all the studies, the peak levels of turbulence occur near the horseshoe vortex due to the unsteady motion associated with the horseshoe vortices and the peak levels of fluctuations are the highest in the vortex core.

Figures 5.17a-c compare the contours of the turbulent kinetic energy for the three endwall configurations. The contours indicate that the high turbulent kinetic energy occur in the presence of leading edge film-cooling. The peak kinetic energy levels are similar for the hole and trench studies with the peak levels occurring at the jet-mainstream shear layer. This is consistent with higher turbulence levels occurring at the shear layer which is closer to the endwall surface.

Comparison of Leading Edge Vorticity

As the leading edge vortex formed in each endwall configuration is different and at a different location along the endwall, calculation of the vorticity magnitude will help ascertain the strength of the vortex. A second order central differencing scheme was used to calculate the vorticity component normal to the stagnation plane, ω_y. Figures 5.18a-c show the normal vorticity component normalized using the vane chord and the inlet mainstream velocity. The vorticity was calculated for all the three endwall configurations and the location of the vortex was ascertained with respect to the leading edge.

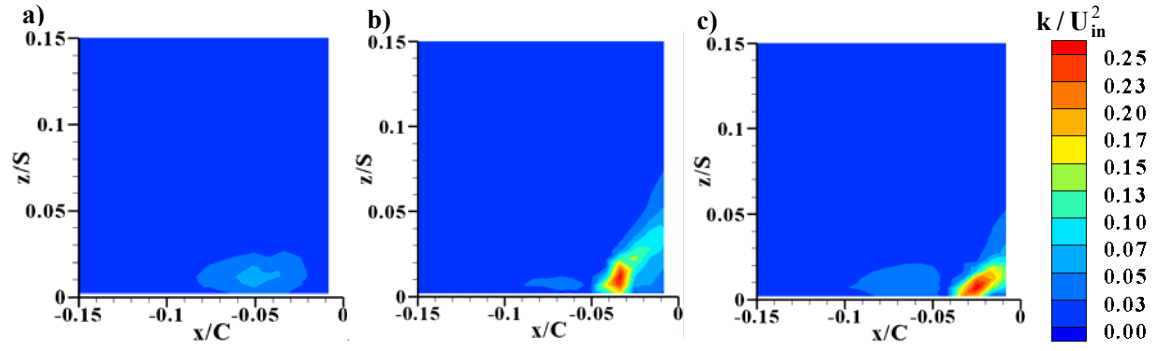

Figure 5.17. Comparison of contour levels of normalized turbulent kinetic energy for the a) baseline, b) holes without trench, and c) holes with trench.

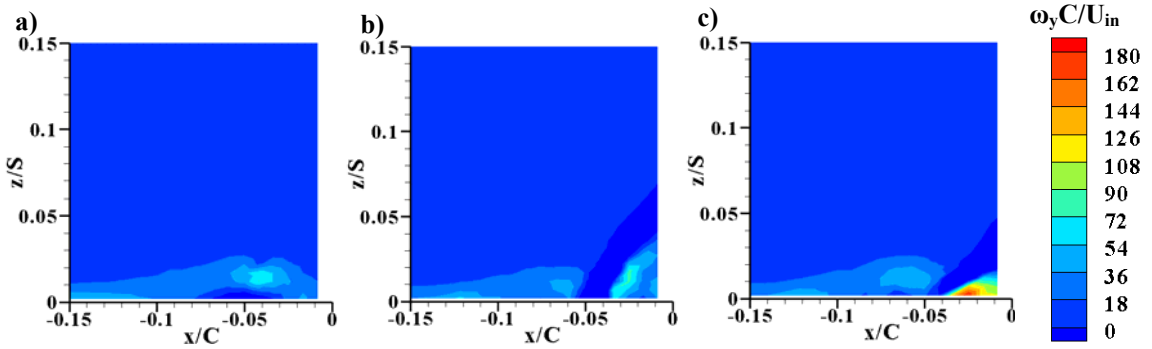

Figure 5.18. Comparison of normalized vorticity at the stagnation plane for the a) baseline, b) holes without trench, and c) holes with trench.

For the baseline study as shown in Figure 5.18a, the peak normalized vorticity with a magnitude of 70 occurs in the vortex core and is similar to the vorticity calculated by Kang et al. [18] at the leading edge. Figure 5.18b shows the leading edge vorticity in the presence of film-cooling holes and as expected, the peak vorticity levels with a magnitude of 80 occur downstream of the cooling holes with a weaker vortex formed upstream of the cooling holes. The peak vorticity magnitude of 180 occurred for the trench study as shown in Figure 5.18c. These peak values occurred in the near wall region at the location of flow reversal as shown by the secondary flow vectors. As the velocity gradients are higher in the near wall region, the vorticity magnitude is also higher for the trench configuration.

Conclusions

Measurements of adiabatic effectiveness and flowfield were presented at the vane leading edge-endwall for coolant flow through the film-cooling holes and through an upstream slot. Film-cooling holes were also placed in a trench and measurements were made on the endwall surface with and without a trench. Placing film-cooling holes in a trench resulted in enhancing the adiabatic effectiveness levels compared to a surface without a trench. A trench was found to uniformly spread the coolant downstream of the film-cooling holes thereby increasing the overall endwall effectiveness levels.

Flowfield measurements were made to investigate the cause for the superior performance of the trench at the leading edge region. Measurements indicated that in the presence of a trench the coolant jets were more attached to the endwall surface when compared to the configuration without a trench. At M = 2.5 the coolant jets injected at a

higher trajectory into the mainstream flow in the absence of a trench thereby lowering the adiabatic effectiveness levels. Also, in the case of no trench, a stronger vortex was formed downstream of the cooling holes and a weaker vortex was formed upstream of the cooling holes.

In the presence of a trench, measurements showed that there was a decreased jet separation from the endwall, which explained the higher adiabatic effectiveness levels due to a trench. Placing a trench at the leading edge region caused the vortex downstream of the cooling holes to disappear. In addition, the contours of the cross-stream velocity component indicated lateral movement of the coolant on the endwall due to a trench.

Both, the hole and trench studies showed similar and higher levels of turbulence at the jet-mainstream shear layer, though the levels in the presence of a trench were closer to the endwall. The trench configuration showed the highest vorticity in the near wall region due to a large velocity gradient near the endwall surface.

Acknowledgments

This publication was prepared with the support of the US Department of Energy, Office of Fossil Fuel, and National Energy Technology Laboratory. However, any opinions, findings, conclusions, or recommendations expressed herein are solely those of the authors and do not necessarily reflect the views of the DOE. The authors also thank Mike Blair (Pratt & Whitney), Ron Bunker (General Electric), and John Weaver (Rolls-Royce) for their input on the modeling of realistic turbine features.

Attribution

This paper was co-authored with Dr. Karen Thole. Her role was:

Co-author- paper 5

Name – Dr. Karen A. Thole

Department – Mechanical Engineering

Degree – Ph.D

Relationship – Chair and primary advisor

Role - Dr. Thole served as my dissertation chair and advised me through my Ph.D and on

all the work presented in this dissertation.

Nomenclature

C true chord of stator vane

D diameter of film-cooling hole

FC film-cooling

h height/depth of trenches and bumps

k turbulent kinetic energy, $k = 1/2(u_{rms}^2 + v_{rms}^2 + w_{rms}^2)$

M_{in} blowing ratio based on inlet mainstream velocity, $M_{in} = \rho_j U_j / \rho_{in} U_{in}$

M blowing ratio based on local mainstream conditions, $M_\infty = \rho_j U_j / \rho_\infty U_\infty$

P vane pitch; hole pitch

PS pressure side

Re_{in} Reynolds number defined as $Re_{in} = CU_{in} / \nu$

S span of stator vane; total vane surface length

SS suction side

T temperature

x length along the vane surface

X,Y,Z local coordinates

U, u streamwise mean and fluctuating velocities

V, v pitchwise mean and fluctuating velocities

W, w spanwise mean and fluctuating velocities

Greek

δ_{99} boundary layer thickness

δ^* displacement thickness

θ momentum thickness

α_u LDV turn angle on the side probe, $\alpha_u = 18°$

α_v angle between the side and top probes, $\alpha_v = 90°$

α_w LDV tilt angle on the side probe, $\alpha_w = 7°$

η adiabatic effectiveness, $\eta = (T_\infty - T_{aw}) / (T_\infty - T_c)$

$\bar{\eta}$ laterally averaged effectiveness

$\bar{\bar{\eta}}$ area-averaged effectiveness

ρ density

ν kinematic viscosity

Subscripts

aw adiabatic wall

c coolant conditions

in inlet conditions

j coolant flow through film-cooling holes

∞ local freestream conditions

Overbar

– lateral average

= area average

References

[1] Friedrichs, S., Hodson, H. P., and Daws, W. N., 1996, "Distribution of Film-Cooling Effectiveness on a Turbine Endwall Measured using Ammonia and Diazo Technique," *Journal of Turbomachinery*, Vol. 118, pp. 613-621.

[2] Friedrichs, S., Hodson, H. P. and Dawes, W. N., 1999, "The Design of an Improved Endwall Film-Cooling Configuration," *Journal of Turbomachinery*, vol. 121, pp. 772-780.

[3] Blair, M. F., 1974 "An Experimental Study of Heat Transfer and Film-Cooling on Large-Scale Turbine Endwalls," *Journal of Heat Transfer*, Vol. 96, pp. 524-529.

[4] Thole, K. A., and Knost, D. G., 2005, "Heat Transfer and Film-Cooling for the Endwall of a First Stage Turbine Vane," *International Journal of Heat and Mass Transfer*, Vol. 48, pp. 5255 – 5269.

[5] Bunker, R. S., 2002, "Film-Cooling Effectiveness due to Discrete Holes within a Transverse Surface Slot," GT2002-30178.

[6] Waye, S. K., and Bogard. D. G., 2006, "High Resolution Film-Cooling Effectiveness Measurements of Axial Holes Embedded in a Transverse Trench with Various Trench Configurations," *Journal of Turbomachinery*, GT2006-90226.

[7] Sundaram, N., and Thole. K. A., 2007, "Bump and Trench Modifications to Film-Cooling Holes as the Leading Edge," *Journal of Turbomachinery*, GT2007-27132.

[8] Burd, S. W., and Simon, T. W., 2000, "Effects of Slot Bleed Injection over a Contoured Endwall on Nozzle Guide Vane Cooling Performance: Part II – Thermal Measurements," 2000-GT-0200.

[9] Zhang, L., and Moon, H. K., 2003 "Turbine Nozzle Endwall Inlet Film Cooling-The Effect of a Backward-Facing Step," GT2003-38319.

[10] Kost, F., and Nicklas, M., 2001 "Film-Cooled Turbine Endwall in a Transonic Flowfield: Part I – Aerodynamic Measurements," 2001-GT-0145.

[11] Nicklas, M., 2001 "Film-Cooled Turbine Endwall in a Transonic Flowfield: Part II – Heat Transfer and Film Cooling Effectiveness," *ASME J of Turbomachinery*, Vol. 123, pp. 720-729.

[12] Knost, D. G., and Thole, K. A., "Adiabatic Effectiveness Measurements of Endwall Film-Cooling for a First Stage Vane," *Journal of Turbomachinery*, Vol. 127, pp. 297-305.

[13] Cardwell, N. D., Sundaram, N., and Thole, K. A., 2006, "The Effects of Varying the Combustor-Turbine Gap," *Journal of* Turbomachinery, GT2006-20089.

[14] Lu, Y., Nasir, H., and Ekkad, S. V., 2005, "Film-Cooling from a Row of Holes Embedded in Transverse Slots," GT2005-68598.

[15] Cardwell N. D., Sundaram, N., and Thole, K. A., 2005, "Effects of Mid-Passage Gap, Endwall Misalignment, and Roughness on Endwall Film-Cooling," *ASME J. of Turbomachinery*, Vol. 128, pp. 62-70.

[16] Ethridge, M. I., Cutbirth, J. M., and Bogard, D. G., 2000, "Scaling of Performance for Varying Density Ratio Coolants on an Airfoil with Strong Curvature and Pressure Gradient Effects," *Journal of Turbomachinery*, Vol. 123, pp. 231-237.

[17] Moffat, R. J., 1988, "Describing the Uncertainties in Experimental Results," *Experimental Thermal and Fluid Science*, Vol.1, pp. 3-17.

[18] Kang, M. B., Kohli, A., and Thole, K. A., 1999 "Heat Transfer and Flowfield Measurements in the Leading Edge Region of a Stator Vane Endwall," *ASME J of Turbomachinery*, Vol. 121, pp. 558-568.

[19] Kang, M. B., and Thole, K. A., 2000 "Flowfield Measurements in the Endwall Region of a Stator Vane," *ASME J of Turbomachinery*, Vol. 122, pp. 458-466.

[20] Radomsky, R. W., 2000, "High Freestream Turbulence Studies on a Scaled-Up Stator Vane," *PhD Dissertation,* University of Wisconsin.

[21] Sundaram, N., and Thole, K. A., 2007, "Effects of Surface Deposition, Hole Blockage, and TBC Spallation on Vane Endwall Film-Cooling," *Journal of Turbomachinery*, GT2006-90379.

[22] Radomsky, R. W., and Thole, K. A., 2000, "High Free-Stream Turbulence Effects on Endwall Heat Transfer for a gas Turbine Stator Vane," *Journal of Turbomachinery*, Vol. 122, pp. 699-708.

Summary of Findings and Recommendations for Future Work

This research focused on understanding the effects of realistic design features and surface conditions on endwall cooling mainly at the leading edge region. The first paper dealt with the effect of leakage flow through the combustor-vane interface slot on the endwall leading edge and along the endwall flow passage. The second and third paper focused on the effect of surface deteriorations like hole blockage, deposition and spallation on the adiabatic effectiveness levels at the endwall leading edge and along the endwall passage. The fourth paper dealt with the analysis of the effect of modifying the film-cooling hole exit by placing it in trenches and in between bumps. The final paper focused on understanding the flowfield modification in the presence of trenched holes and how enhanced cooling is achieved in the presence of a trench relative to no trench.

The first paper described in detail how the various endwall features like slot at the combustor-turbine interface and the slot at the vane-to-vane interface affects the adiabatic effectiveness levels on the endwall. Increasing the coolant mass flow rate through the slot increased the local adiabatic effectiveness levels, while increasing the momentum flux ratio for the slot leakage dictated the coverage area for the cooling. In addition, in this paper the effect of varying the slot width was also discussed, which could result due to expansion or contraction of the slot during engine operation. At a constant mass flow rate, decreasing the combustor-turbine interface width caused an increase in uniformity of coolant exiting the slot, particularly across the pressure side of the endwall surface. Whereas increasing the width of the interface had the opposite effect thereby reducing coolant coverage on the endwall surface. The coolant flow through the vane-to-vane interface slot was found to have no effect on the endwall adiabatic effectiveness levels.

The first paper focused on the effect of design features whereas the second paper focused on the effects of surface conditions on endwall adiabatic effectiveness levels. Three different surface deteriorations were studied at the leading edge namely, near hole deposition, partial film-cooling hole blockage and spallation of the thermal barrier coating. The results indicated that the semi-elliptically shaped deposits near the hole exit can sometimes improve the adiabatic effectiveness at the leading edge, but with increased deposition heights the cooling deteriorates. Partial hole blockage studies revealed that

the adiabatic effectiveness deteriorates with increases in the number of blocked holes. Spallation studies showed that for a spalled endwall surface downstream of the leading edge cooling row, adiabatic effectiveness worsened with an increase in blowing ratio.

As the deposits in the second paper showed an improvement in the adiabatic effectiveness levels, for the third paper the same was simulated along the pressure side film-cooling holes on the endwall. Results in the third paper indicated that the deposits lowered the average adiabatic effectiveness levels downstream of the film-cooling rows by deflecting the coolant jets towards the vane endwall junction on the pressure side. Results also indicated that there was a steady decrease in adiabatic effectiveness levels with a sequential increase in the number of rows with the deposits. A superposition study was also carried out as part of this work and it was found that by applying superposition methods the degradation in adiabatic effectiveness can be predicted within a 40% error.

The fourth paper dealt with applying newer film-cooling exit designs to enhance the adiabatic effectiveness levels at the leading edge as results from paper one and two showed that it is a challenge to cool this region. Film-cooling is difficult to achieve at the leading edge due to the formation of horseshoe vortices which lifts the coolant off the surface and pulls the hot mainstream gases towards it. Two different modifications, namely film-cooling holes in trenches and in between bumps were evaluated to improve the cooling in the leading edge region. Both trenches and bumps produced an overall improvement however trenches produced the maximum enhancement in adiabatic effectiveness levels relative to just placing film-cooling holes at the leading edge.

The fifth and final paper focused on understanding the superior performance of the film-cooling holes in a trench relative to no trench. Measurements of the flowfield were made just upstream of the leading edge along a plane parallel to the flow and intersecting the vane stagnation region. For the trenched film-cooling holes, the coolant was shown to stay closer to the endwall surface relative to the no trench case thus explaining the enhancements in the adiabatic effectiveness levels.

From this comprehensive study, it was possible to obtain an overall understanding of the various factors influencing endwall cooling. The adiabatic effectiveness and flowfield measurements at the leading edge revealed how the leading edge vortices effect film-cooling and how they can be modified by changing the cooling hole exit designs.

Recommendations for Future Work

Although this study offered a comprehensive examination of factors effecting endwall cooling, there is still a significant amount of work that could be done to better understand the behavior of film-cooling in the extremely complex region of endwall leading edge. There are a number or areas in which additional research could be performed, including comparison of trenched holes with shaped holes, which also shows improved adiabatic effectiveness levels.

In a study by Colban et al. [1], where they compared shaped holes with cylindrical holes on an endwall passage, the same could be done by comparing shaped holes with trenched holes in an endwall passage. A trench can be manufactured as part of the TBC application process that reduces its manufacturing cost when compared to manufacturing shaped holes. If the enhancements in effectiveness levels are comparable to shaped holes, then film-cooling holes in trenches are a more viable option than shaped holes.

The adiabatic effectiveness measurements do show that the trenches perform better than film-cooling holes with out a trench. However, it is important to understand the affect of trenches on the total pressure losses through a vane passage and its affect on the overall performance of the engine. Aerodynamic measurements need to be carried out to further understand the effects of trenched holes.

In this study detailed flowfield measurements were carried out only at the leading edge, but it will be interesting to measure the flowfield all along the vane passage. This will help in understanding the effect of trenches on endwall secondary flows relative to the secondary flows resulting from placing cylindrical holes without a trench.

References

[1] Colban, W. F., Thole, K. A., and 2007, "A Comparison of Cylindrical and Fan-Shaped Film-Cooling Holes on a Vane Endwall at Low and High Freestream Turbulence Levels," *Journal of Turbomachinery* (GT2007-90021).

Vita

Narayan (Sundar) Sundaram

Sundar was born on April 11, 1979 in Bangalore, the garden city (now the silicon valley) of India to late Wing Commander R. Narayan and Akhila Narayan. He has one older brother Gautham who has a baccalaureate degree in Mechanical Engineering and masters degree in business. As Sundar's Dad was a pilot in the Indian Air Force, he got to travel extensively covering the length and breadth of India and getting an opportunity to meet new people and learn new languages. Sundar graduated from the high school Kendriya Vidyalaya no. 1 in Banaglore in 1996 and decided to join the University of Mysore to pursue a degree in Mechanical Engineering. Sundar was placed 7^{th} in a class of 550 when he graduated with a BE degree in the year 2000.

Sundar then worked as a trainee engineer and subsequently promoted to Assistant Manager in British Physical Labs (BPL) from 2000 to 2002. In the fall of 2002 he decided to pursue a graduate degree and landed in the beautiful town of Blacksburg to get his MS. He worked on computationally developing a micro-total analysis system as part of his MS thesis. After that, Sundar took an 8-month Swiss vacation working for Alstom Power in Baden Switzerland until the end of summer 2004.

In the fall of 2004, Sundar started his PhD on gas turbine heat transfer under the able guidance of Dr. Karen A. Thole and successfully defended his dissertation on April 18, 2007 a week after he turned 28. Sundar plans to move to Penn State as a post-doctoral research associate to further enhance his research skills and to work with Dr. Thole for another year.